Mandar S. Bhagwat,Ph.D.,April 12, 2005 NUCLEAR PHYSICS

ASPECTS OF NON-PERTURBATIVE QCD FOR HADRON PHYSICS (99 pp.)

Director of Dissertation: Peter C. Tandy

Quenched lattice-QCD data on the dressed-quark Schwinger function can be correlated with dressed-gluon data via a rainbow gap equation so long as that equation's kernel possesses enhancement at infrared momenta above that exhibited by the gluon alone. The required enhancement can be ascribed to a dressing of the quark-gluon vertex. The solutions of the rainbow gap equation exhibit dynamical chiral symmetry breaking and are consistent with confinement. The gap equation and related, symmetry-preserving, ladder Bethe-Salpeter equation yield estimates for chiral and physical pion observables that suggest these quantities are materially underestimated in the quenched theory: $|\langle\bar{q}q\rangle|$ by a factor of two and f_π by 30 %.

Features of the dressed-quark-gluon vertex and their role in the gap and Bethe-Salpeter equations are explored. It is argued that quenched lattice data indicate the existence of net attraction in the colour-octet projection of the quark-antiquark scattering kernel. The study employs a vertex model whose diagrammatic content is explicitly enumerable. That enables the systematic construction of a vertex-consistent Bethe-Salpeter kernel and thereby an exploration of the consequences for the strong interaction spectrum of attraction in the colour-octet channel. With rising current-quark mass the rainbow-ladder truncation is shown to provide an increasingly accurate estimate of a bound state's mass. Moreover, the calculated splitting between vector and pseudoscalar meson masses vanishes as the current-quark mass increases, which argues for the mass of the pseudoscalar partner of the $\Upsilon(1S)$ to be above 9.4 GeV.

A model for the dressed quark-gluon vertex, at zero gluon momentum, is formed from a nonperturbative extension of the two Feynman diagrams that contribute at 1-loop in perturbation theory. The required input is an existing ladder-rainbow model Bethe-Salpeter kernel from an approach based on the Dyson-Schwinger equations; no new parameters are introduced. The model includes an Ansatz for the triple-gluon vertex. Two of the three vertex amplitudes from the model provide a point-wise description of the recent quenched lattice-QCD data. An estimate of the effects of quenching is made. To be phenomenologically tested this model has to be extended to non-zero gluon momentum. Various options for such an extension are under consideration.

ASPECTS OF NON-PERTURBATIVE QCD FOR HADRON PHYSICS

A dissertation submitted to
Kent State University Department of Physics
in partial fulfillment of the requirements
for the degree of Doctor of Philosophy

by

Mandar S. Bhagwat

April 12, 2005

A dissertation written by

Mandar S. Bhagwat

B.Sc., Shivaji University, 1984

M.Sc., Shivaji University, 1986

Ph.D., Kent State University, 2004

Approved by

Dr. Peter Tandy , Chair, Doctoral Dissertation Committee

Dr. Richard Aron , Members, Doctoral Dissertation Committee

Dr. Alfred Cavaretta ,

Dr. Declan Keane ,

Accepted by

Dr. Makis Petratos , Chair, Department of Physics

Dr. John Stavley , Dean, College of Arts and Sciences

Table of Contents

List of Figures

List of Tables

Chapter 1

Introduction

Interactions of quarks, leptons and gauge bosons are described by the Standard Model, a theory of Electromagnetic, Weak and Strong forces.

Electrically charged particles interact by exchanging chargeless photons. The theory of these electromagnetic interactions is Quantum Electrodynamics (QED). This means that physical quantities such as the anamolous magnetic moment of the electron can be calculated from first principles of QED. Also a state like positronium that does not appear in the QED Lagrangian can be understood as a relativistic bound state of elementary excitations of QED, where "elementary excitations" means those quantum fields that appear in the Lagrangian of the theory. For QED these are electrons, positrons and photons.

Strong interactions are due to the color charge carried by particles called quarks and gluons, and the theory is accordingly named Quantum Chromodynamics (QCD). QED and QCD are both gauge theories and so have structural similarities. But in detail they are very different. The main difference is that because photons are electrically neutral they cannot interact directly with each other, but gluons (the QCD equivalent of photons) carry color charge and so interact directly with each other. It is an observational fact that only colorless bound states of quarks and gluons, generically called hadrons, have been observed. It is the direct interaction of colored gluons that seems responsible for the non-existence of free colored particles. An understanding of color confinement was listed as one of the top ten problems in particle physics for the millenium. Thus unlike

positronium which can be ionized with the addition of a few (7) electron-volts into an electron and a positron, no amount of energy available presently is sufficient to break a hadron into seperate colored constituents.

A central goal of contemporary nuclear physics is then to understand the properties of hadrons in terms of the elementary excitations in QCD : quarks, gluons and ghosts. More specifically hadron physics aims at solving the quantum field theoretical bound state problem whose solution is the hadron spectrum; calculate the interactions of these hadrons between themselves and with electroweak probes; and use these interactions as incisive tools with which to identify the origins of confinement and elucidate its effects on observables.

Again, because of the structural similarity between QED and QCD, and from the relatively straight forward calculations of QED observables from first principles, it is tempting to assume that the problems in hadron physics could use the similar tools of perturbation theory in QCD. But this is not true.

The strength of particle interactions is measured in terms of the coupling $\alpha = \frac{g^2}{4\pi}$ where g is the coupling constant. The use of the word ' 'constant" is historical and a misnomer. α varies(slowly) with the momentum of interaction and so the phrase "running coupling" is the more pertinent. In QED α rises with increasing momentum (decreasing distance) and $\alpha_{\rm QED} < 1$ in the momentum range of 0 to few GeV. As a result perturbation theory yields very accurate results, eg.1 part in 10^{-10} for the electron's anamolous magnetic moment. In QCD α falls with increasing momentum (decreasing distance) and $\alpha_s < 1$ for momenta $\gtrsim$ 2 GeV and perturbative QCD (pQCD) can be applied successfully for small distance phenomena. But hadron physics requires solving QCD for momenta $\lesssim$ 2 GeV where α_s is large and the problem becomes nonperturbative. This is the reason why calculations based on QCD for observable particles are difficult: we know the theory to use, but do

not know how to solve it.

Much effort has been invested over the last thirty years in numerical simulations of QCD on a finite spacetime grid. This approach to solving QCD, called lattice-QCD is now an identifiable branch of high-energy physics with numerous large-scale collaborations, not unlike the high-energy physics experimental collaborations; even the final results of a lattice calculation are called lattice data. There are computational challenges faced by lattice-QCD. Three of the principal ones are: reducing discretization errors (grid spacing and total lattice volume), extrapolating to small quark masses and going beyond the quenched approximation. Significant efforts are being expended to develop improved algorithms so that discretization errors could be reduced. u and d quark masses are affected most by dynamical chiral symmetry breaking (DCSB) effects in QCD, and the physics of light quark mesons is dominated by these effects. As of today lattice has to extrapolate to light quark masses and seeks help from other approaches developed to study hadron physics. Quenched approximation introduces an *a priori* unquantifiable, systematic error.

In contrast to discretized lattice simulation, continuum tools in hadron physics depend on modelling. Constituent-quark models describe the baryon spectrum and decays very well using only a few parameters. But such models do not simultaneously give a satisfactory description of all the phenomena associated with light-quark mesons, which requires an accurate description of DCSB. Light-front techniques are also useful in describing many aspects of hadron physics as are effective field theories. Contemporary Dyson-Schwinger equation (DSE) studies complement these approaches.

The DSEs are coupled integral (or differential) equations which relate the Green functions (i.e. Schwinger functions) of a field theory to each other. Solving these equations provides a solution of the theory; QCD is completely defined when all of its n-point Green functions are known, where n is the number of different external legs. The Bethe-Salpeter

equation (BSE) which describes the relativistic two-body scattering and bound states is one of the DSEs. For studies based on DSEs it is inevitable that the infinite tower of coupled equations must be truncated, i.e. the tower of equations must be limited to some *n*. In this dissertation we shall discuss *2* and *3*-point functions and the Bethe-Salpeter equation. These truncations necessarily introduce a model for the omitted function. However, much can be achieved by maintaining certain properties of the theory, such as various global and local symmetries, multiplicative renormalizability, known perturbative behavior in the weak coupling limit, etc. These can provide stringent conditions on the model. In Chapter 2 the DSE formalism for QCD is introduced by deriving both the gap equation for the quark propagator and the Bethe-Salpeter equation. The relevance of maintaining the axial vector Ward-Takahashi identity is discussed. And arguments for using Euclidean metric are provided.

It is a longstanding prediction from DSE studies that the Schwinger functions which characterise the propagation of QCD's elementary excitations: gluons, ghosts and quarks, are strongly modified at infrared momentum scales, namely, spacelike momenta $k^2 \lesssim 2\,\mathrm{GeV}^2$ [1, 2, 3]. Such momentum-dependent dressing is a fundamental feature of strong QCD that is observable in hadronic phenomena [4]. For example: it is the mechanism by which the current-quark mass evolves to assume the scale of a constituent-quark mass at infrared momenta, and thereby the mechanism that exhibits dynamical chiral symmetry breaking (DCSB); and it may also provide an understanding of confinement, as we discuss in Chapter 3.

A great deal of progress in the QCD modeling of hadron physics has been achieved through the use of the ladder-rainbow truncation of the Dyson-Schwinger equations (DSEs). For two recent reviews, see Refs. [4] and [3]. Apart from 1-loop renormalization group

improvement, this truncation is built upon a bare quark-gluon vertex. Recent investigations with simple dressed vertex models have indicated that material contributions to a number of observables are possible with *a better understanding of the infrared structure of the vertex. This is the central theme of the work presented in the following chapters.* It is certain that the infrared structure of the quark-gluon vertex, a $\mathcal{3}$-point function, has a big impact on properties of the gap equation's solution, such as: multiplicative renormalisability [5, 6, 7]; gauge covariance [8, 9, 6], and the existence and realisation of confinement and DCSB [10, 11, 12, 13, 14, 15]. For example, related vertex *Ansätze*, which agree in the ultraviolet, can yield solutions for the dressed-quark propagator with completely different analytic properties and incompatible conclusions on DCSB [16, 17]. These diverse model indications include an enhancement in the quark condensate [18, 19], an increase of about 300 MeV in the b_1/h_1 axial vector meson mass [20], and about 200 MeV of attraction in the ρ/ω vector meson mass.

Numerical simulations of lattice-QCD provide direct access to QCD's Schwinger functions, and recent studies of the quenched theory yield dressed-gluon [21, 22, 23, 24] and dressed -quark [25, 26] two-point functions ("propagators") that are in semi-quantitative agreement with earlier Dyson-Schwinger equation (DSE) calculations [27, 28, 29, 30, 31, 18, 32]. However, these dressed-gluon and -quark propagators are not obviously consistent with each other in the following sense: use of the lattice dressed-gluon two-point function as the sole basis for the kernel of the QCDs gap equation cannot yield the lattice dressed-quark propagator without a material infrared contribution (enhancement) from the dressed-quark-gluon vertex [10, 11, 12]. Fortunately, just such behaviour can be understood to arise owing to multiplicative renormalisability of the gap equation [33, 34] and is observed in lattice estimates of this three-point function [35, 36, 37].

In Chapter 3, we elucidate these points using a concrete model for the gap equation's

kernel. Since the ultraviolet behaviour of this kernel is fixed by perturbative QCD and hence model-independent, our study will focus on aspects of the infrared behaviour of the Schwinger functions.

Furthermore, DCSB is encoded in the chiral-limit behavior of the dressed-quark propagator. However as mentioned above, contemporary lattice-QCD simulations are restricted to current-quark masses that are too large for unambiguous statements to be made about the magnitude of this effect. With a well-constrained model for the gap equation's kernel it is straightforward to calculate the dressed-quark propagator in the chiral limit. Hence our analysis will also provide an informed estimate of the chiral limit behaviour of the lattice results.

We consider two additional questions; namely, how do Schwinger functions obtained in simulations of quenched lattice-QCD differ from those in full QCD, and can that difference be used to estimate the effect of quenching on physical observables? Our model for the gap equation's kernel provides a foundation from which we believe these problems can fruitfully be addressed.

As seen in Chapter 3 the gap equation study provides an understanding of the circumstances in which pointwise agreement is obtained [38, 39] with the lattice-data. *This level of sophistication does not prevail with the dressed-quark-gluon vertex, however. Acquiring that is a realisable contemporary goal, and it is to aspects of this task that we address ourselves Chapter 4 and 5.*

Chapter 4 is concerned with an algebraic model for the dressed-quark-gluon vertex, $\Gamma^a_\nu(q;p)$. We are generally interested in its form, how that arises, and the way it affects strong interaction phenomena. After outlining some general properties of the dressed-quark gluon vertex, we recapitulate on a nonperturbative DSE truncation scheme [40, 41]

that has already enabled some systematic study of the connection between the dressed-quark-gluon vertex and the expression of symmetries in strong interaction observables. In doing this we are led to propose an extension of earlier work, one which facilitates an exploration of the impact that aspects of the three-gluon vertex have on hadron phenomena. To amplify the illustrative efficacy of our analysis we introduce a simple model to describe the propagation of dressed-gluons [42] that reduces the relevant DSEs to a set of coupled algebraic equations which, notwithstanding their simplicity, exhibit characteristics essential to the strong interaction.

We capitalise on the simplicity of our model and chronicle a range of qualitative features of the dressed-quark-gluon vertex and dressed-quark propagator that are common to our model and QCD. Of particular interest are the effects of net attraction in the colour-octet quark-antiquark scattering kernel which we are able to identify. We follow that with an analysis of the Bethe-Salpeter equation which can be constructed, consistent with the fully dressed-quark-gluon vertex, so that the Ward-Takahashi identities associated with strong interaction observables are automatically satisfied. This property is crucial to understanding hadron properties and interactions [43, 44, 46, 45, 47]. In addition, we describe the evolution of pseudoscalar and vector meson masses with growing current-quark mass. One outcome of that is a quantitative assessment of the accuracy for meson masses of the widely used rainbow-ladder truncation, which we determine by a comparison with the masses obtained with all terms in the vertex and kernel retained.

After investigating the effects of the quark-gluon vertex with a simple model we attempt to provide a more realistic description of the vertex. In Chapter 5 we generate a model dressed vertex, for zero gluon momentum, based on an Ansatz for non-perturbative extensions of the only two diagrams that contribute at 1-loop order in perturbation theory. An existing ladder-rainbow model kernel is the only required input. We compare to the

recent lattice-QCD data without parameter adjustment.

We first recall the vertex to 1-loop in perturbation theory and point out the structure and properties that are used to suggest the Ansatz for non-perturbative extension. The non-perturbative extension is described later and the results are presented and discussed.

Chapter 2

The Dyson-Schwinger Equation formalism

2.1 *Dyson-Schwinger equations*

The QCD action in Minkowski space of signature -2 can be written as,

$$S[\overline{\psi},\psi,\mathcal{A},\overline{\phi},\phi] = \int d^4x\,\overline{\psi}(i\partial\!\!\!/ - m_0 + g_0\mathcal{A}\!\!\!/)\psi + \mathscr{L}(\mathcal{A},\overline{\phi},\phi) \tag{2.1}$$

where ψ is the quark field, $\mathcal{A} = \mathcal{A}^a_\mu t^a$ is the gluon field and ϕ is the ghost field, $t^a, a = 1, ..., 8$ are the $SU_c(3)$ generators in the fundamental representation and $\mathscr{L}(\mathcal{A},\overline{\phi},\phi)$ contains the gluon and ghost terms. The action for N_f quark flavors is a sum of the fermionic part of $S[\overline{\psi},\psi,\mathcal{A},\overline{\phi},\phi]$ over f with $\psi \to \psi^f$ and $m_0 \to m_0^f$.

The corresponding generating functional, including the sources is ,

$$Z[\eta,\overline{\eta},\mathcal{J},\omega,\overline{\omega}] = \int \mathscr{D}(\overline{\psi},\psi,\mathcal{A},\phi,\overline{\phi})\, exp(iS[\overline{\psi},\psi,\mathcal{A},\overline{\phi},\phi]+i\int d^4x\,(\overline{\psi}\eta+\overline{\eta}\psi+\mathcal{A}\cdot\mathcal{J}+\overline{\omega}\phi+\overline{\phi}\omega)) \tag{2.2}$$

and because the integral of a derivative is zero [48], we get the following equation,

$$[(i\partial\!\!\!/ - m_0 + g_o\gamma^\mu\frac{\delta}{\delta i\mathcal{J}^\mu(y)})\frac{\delta}{\delta i\overline{\eta}(y)} + \eta(y)]Z = 0\,\cdot \tag{2.3}$$

This is the Dyson-Schwinger equation for the generating functional $Z[\eta,\overline{\eta},\mathcal{J},\omega,\overline{\omega}]$ [49].

Differentiating with respect to $i\eta(x)$ yields a relation between the quark 2-point function $\frac{\delta^2 Z}{\delta i\eta(x)\delta i\overline{\eta}(y)}$ and the quark-gluon 3-point function $\frac{\delta^3 Z}{\delta i\eta(x)\delta i\overline{\eta}(y)i\mathcal{J}_\mu(y)}$,

$$(i\partial\!\!\!/ - m_0)\frac{\delta^2 Z}{\delta i\eta(x)\delta i\overline{\eta}(y)} + g_0\gamma^\mu\frac{\delta^3 Z}{\delta i\eta(x)\delta i\overline{\eta}(y)i\mathcal{J}^\mu(y)} = -i\delta(x-y)Z + \eta(y)\frac{\delta Z}{\delta i\eta(x)} \tag{2.4}$$

.

Higher derivatives relate higher n-point functions. These equations are called DSE for n-point functions and equation (2.4) is often called *the* Dyson-Schwinger equation or the gap equation. The main point to note is that calculation of the 2-point function requires the knowledge of the 3-point function. This inter-dependence of 1, 2, ... , n, ... point functions on each other is seen in all DSEs and they form an infinite number of coupled equations, so that a nontrivial solution of even the simplest equation can only be obtained after making truncations.

In the Dyson-Schwinger approach to hadron phenomenology the choice of truncation is based on the preservation of the Ward-Takahashi identities. Also the formulation is carried out in Euclidean space [1] . The motivation for implementing field theory in Euclidean metric is briefly discussed later.

2.2 *Gap Equation*

After the sources are put to zero Eq(2.4) can schematically be written as,

$$S_0^{-1} i S + g_0^2 t_a \gamma^\mu S \Gamma^\nu_b S D^{ab}_{\mu\nu} = i \cdot \tag{2.5}$$

Here Γ^μ is the fully amputated quark-gluon 3-point function also known as the fully dressed quark-gluon vertex. Rearrangement gives,

$$S^{-1} = S_0^{-1} - i g_0^2 t_a \gamma^\mu S \Gamma^\nu_b D^{ab}_{\mu\nu} \tag{2.6}$$

which in momentum space takes the form

$$S^{-1}(p) = \not{p} - m_0 - \Sigma(p) \tag{2.7}$$

with the self-energy given by,

$$\Sigma(p) = i \int_q^\Lambda g_0^2 D^{ab}_{\mu\nu}(p-k) t^a \gamma_\mu S(k) \Gamma^b_\nu(k,p). \tag{2.8}$$

[1] We employ a Euclidean metric, with: $\{\gamma_\mu, \gamma_\nu\} = 2\delta_{\mu\nu}$; $\gamma_\mu^\dagger = \gamma_\mu$; and $a \cdot b = \sum_{i=1}^4 a_i b_i$.

This is the useful integral equation form of the gap equation. Here, $\int_q^\Lambda \doteq \int^\Lambda d^4q/(2\pi)^4$ represents mnemonically a *translationally-invariant* regularisation of the integral, with Λ the regularisation mass-scale. The final stage of any calculation is to remove the regularisation by taking the limit $\Lambda \to \infty$.

After operating with $\frac{\delta^2}{\delta i\overline{\eta}(u)\delta i\eta(v)}$ on Eq(2.4), putting the sources to zero and then rearranging the various terms gives the inhomogeneous Bethe-Salpeter equation for the 4-point function $S^{12}(u,v,x,y)$ [48]. Symbolically it can be arranged as,

$$S^{12} = S^1 S^2 - S^1 S^2 K S^{12} \tag{2.9}$$

where the kernel K is defined through the relation,

$$(i\partial\!\!\!/ - m_0 - \Sigma)(\Sigma + g_o t^a \gamma_\mu \frac{\delta}{\delta i \mathcal{J}^{\mu a}(y)})S^{12} = \int d^4x_1 d^4x_2 K(u,y;x_1,x_2) S(x_1,x_2;v,z). \tag{2.10}$$

In the vicinity of a bound state $|B\rangle, S^{12}$ can be written as [50]

$$S^{12} = \frac{i|B\rangle\langle B|}{P^2 - M^2 + i\epsilon} + \mathcal{R} \tag{2.11}$$

where $\mathcal{R}$ is regular in the vicinity $P^2 = M^2$.

$|B\rangle$ is of course an eigenstate of the QCD Hamiltonian but because we do not obtain it as such, it cannot be normalized in the usual way. As a result its normalization condition must come from the inhomogeneous Bethe-Salpeter equation as $P^2 \to M^2$. The inhomogeneous BSE can be rearranged as,

$$S^{12}((S^1 S^2)^{-1} + K)S^{12} = S^{12}. \tag{2.12}$$

Substituting for S^{12} from Eq(2.9) in this form of BSE we get the normalization condition for the bound state,

$$\langle B|\frac{\partial}{\partial P_\mu}((S^1 S^2)^{-1} + K)|B\rangle = -2iP^\mu \tag{2.13}$$

where use was made of the homogeneous BSE for $|B\rangle$,

$$|B\rangle = S^1 S^2 K |B\rangle\cdot \tag{2.14}$$

One more relation that is relevant to the present work is the axial vector-Ward Takahasi Identity. This relation can be derived by observing the invariance of the 2-point function under the following transformation,

$$\psi \to \psi' = e^{i\gamma_5 \alpha(x)}\, \psi \tag{2.15}$$

This function is invariant because the value of an integral does not change on changing the variables and the measure can also be shown to be invariant in the flavor non-singlet channel i.e. when the axial anomaly is not present. Thus we get,

$$\begin{aligned} &\partial_\mu \langle 0|T(j^5_\mu(x)\psi(y)\overline{\psi}(z))|0\rangle - 2m\langle 0|T(j^5(x)\psi(y)\overline{\psi}(z))|0\rangle = \\ &-\langle 0|T(\psi(y)\overline{\psi}(z))|0\rangle\delta(x-y) - \langle 0|T(\psi(y)\overline{\psi}(z))|0\rangle\delta(x-z) \end{aligned} \tag{2.16}$$

where m is the renormalized quark mass and $j^5(x) = \overline{\psi}\gamma_5\lambda^\alpha\psi$ and $j^5_\mu(x) = \overline{\psi}\gamma_\mu\gamma_5\lambda^\alpha\psi$

Since 2-legs can be extracted from $\langle 0|T(j^5_\mu(x)\psi(y)\overline{\psi}(z))|0\rangle$ and $\langle 0|T(j^5(x)\psi(y)\overline{\psi}(z))|0\rangle$ we are led to the amputated form of the AV-WTI identity which in momentum space is,

$$iP_\mu\Gamma^5_\mu(P,k) = \gamma_5 S^{-1}(k-P/2) + S^{-1}(k+P/2)\gamma_5 - 2m\Gamma^5(P,k) \tag{2.17}$$

.

2.3 *n-point functions*

In Minkowski spacetime after a Pauli-Villars regularization, the time integral can be evaluated either directly [51] or after Wick rotation[52]. In either case the positon and nature of all singularities in the complex plane have to be known. In nonperturbative studies these are not known because the singularities are dynamical and thus a part of

the final solution. Nonperturbative studies of DSEs in Euclidean space for QED and QCD in the last 2 decades indicate that the singular behavior of 2-point functions of electrons and quarks in the timelike region is quite different from the perturbative one, due to the presence of complex conjugate poles or branch cuts. Thus the simple Minkowski $\rightarrow$ Euclidean Wick rotation that works so well in perturbation calculations is not firmly established in nonpertubative formulations. n-point functions can be regularized and renormalized in Euclidean theory as there are no dynamical singularities in the Euclidean region. As a result one of the approaches to buiding field theoretic models is to start in Euclidean space, obtain the regularized and renormalized n-point functions and then analytically continue these functions into the timelike domain for calculating observables. That this procedure is mathematically valid is discussed in [1] and references therein. .

The generating functional of Euclidean space QED or QCD is obtained from the one in Minkowski space through the following transcription rules:

$$\begin{aligned} Minkowski &\rightarrow Euclidean, \\ \int d^4x &\rightarrow -i \int d^4x, \\ \gamma.\partial &\rightarrow -i\gamma.\partial, \\ \gamma.A &\rightarrow -i\gamma.A, \\ A.B &\rightarrow -A.B \end{aligned} \tag{2.18}$$

where the Minkowski metric has been chosen to have signature = -2. These rules follow from the analytic continuation in the time variable $x^0 \rightarrow -ix_4$ with $\vec{x} \rightarrow \vec{x}$

This method of analytic continuation of Schwinger functions is also used by the practitioners of lattice gauge theory allowing, as will be seen later, a pointwise comparison of the n-point functions computed in these two independent approaches.

2.4 *Quark Dyson-Schwinger Equation*

The Euclidean space renormalised action is,

$$S[\overline{\psi},\psi,\mathcal{A},\overline{\phi},\phi] = \int d^4x \overline{\psi}(Z_2\partial\!\!\!/ + Z_4 m + Z_1 ig\mathcal{A}\!\!\!/)\psi + \mathscr{L}(\mathcal{A},\overline{\phi},\phi) \tag{2.19}$$

where $Z_1(\zeta,\Lambda)$, $Z_2(\zeta,\Lambda)$ and $Z_4(\zeta,\Lambda)$ are, respectively, Lagrangian renormalisation constants for the quark-gluon vertex, quark wave function and mass. m and g are the renormalized mass and renormalized coupling constant. Here, $\{\gamma_\mu,\gamma_\nu\} = 2\delta_{\mu\nu}$, $\gamma_\mu^\dagger = \gamma_\mu$ and $a\cdot b = \sum_{i=1}^4 a_i b_i$. Then the DSE for the renormalised dressed-quark propagator can be derived as before. It is

$$S(p)^{-1} \;=\; Z_2(i\gamma\cdot p + m_0) + Z_1 \int_q^\Lambda g^2 D_{\mu\nu}(p-q)\frac{\lambda^a}{2}\gamma_\mu S(q)\Gamma^a_\nu(q,p)\,, \tag{2.20}$$

where $D_{\mu\nu}(k)$ is the renormalised dressed-gluon propagator, $\Gamma^a_\nu(q;p)$ is the renormalised dressed-quark-gluon vertex, m_0 is the Λ-dependent current-quark bare mass that appears in the Lagrangian and $\int_q^\Lambda \doteq \int^\Lambda d^4q/(2\pi)^4$ represents mnemonically a *translationally-invariant* regularisation of the integral, with Λ the regularisation mass-scale. The final stage of any calculation is to remove the regularisation by taking the limit $\Lambda\to\infty$. The quark-gluon vertex and quark wave function renormalisation constants, $Z_1(\mu^2,\Lambda^2)$ and $Z_2(\mu^2,\Lambda^2)$ respectively, depend on the renormalisation point and the regularisation mass-scale, as does the mass renormalisation constant $Z_m(\mu^2,\Lambda^2) \doteq Z_2(\mu^2,\Lambda^2)^{-1} Z_4(\mu^2,\Lambda^2)$. In Eq. (2.20), S, Γ^a_μ and m_0 depend on the quark flavour, although we have not indicated this explicitly. However, in our analysis we assume, and employ, a flavour-independent renormalisation scheme and hence all the renormalisation constants are flavour-independent.

2.4.1 *Dressed-quark propagator*

The solution of Eq. (2.20) has the general form

$$S(p)^{-1} = i\gamma\cdot p A(p^2,\mu^2) + B(p^2,\mu^2) = \frac{1}{Z(p^2,\mu^2)}\left[i\gamma\cdot p + M(p^2,\mu^2)\right]\,, \tag{2.21}$$

renormalised such that at some large spacelike momenta μ

$$S(p)^{-1}\big|_{p^2=\mu^2} = i\gamma\cdot p + m(\mu)\,, \tag{2.22}$$

where $m(\mu)$ is the renormalised quark mass at the scale μ. In the presence of an explicit chiral symmetry breaking current-quark mass, one has $Z_4 m(\mu) = Z_2 m_0$, neglecting $\mathrm{O}(1/\mu^2)$ corrections associated with dynamical chiral symmetry breaking that are intrinsically nonperturbative in origin.

Multiplicative renormalisability in QCD entails that

$$\frac{A(p^2,\mu^2)}{A(p^2,\bar\mu^2)} = \frac{Z_2(\mu^2,\Lambda^2)}{Z_2(\bar\mu^2,\Lambda^2)} = A(\bar\mu^2,\mu^2) = \frac{1}{A(\mu^2,\bar\mu^2)}\,. \tag{2.23}$$

Such relations can be used as constraints on model studies of Eq. (2.20). Explicitly, at one-loop order in perturbation theory,

$$Z_2(\mu^2,\Lambda^2) = \left[\frac{\alpha(\Lambda^2)}{\alpha(\mu^2)}\right]^{-\frac{\gamma_F}{\beta_1}}\,, \tag{2.24}$$

where $\gamma_F = \frac{2}{3}\xi$ and $\beta_1 = N_f/3 - 11/2$, with ξ the gauge parameter and N_f the number of active quark flavours. At this order,

$$\alpha(Q^2) = \frac{\pi}{-\frac{1}{2}\beta_1 \ln\left[\frac{Q^2}{\Lambda^2_{\mathrm{QCD}}}\right]}\,. \tag{2.25}$$

Clearly, at one-loop in Landau gauge [$\xi = 0$], $A(p^2,\mu^2) \equiv 1$, and a deviation from this result in a solution of Eq. (2.20) is a higher-loop effect. Such effects are always present in the self-consistent solution of Eq. (2.20).

The ratio $M(p^2,\mu^2) = B(p^2,\mu^2)/A(p^2,\mu^2)$ is independent of the renormalisation point in perturbation theory; i.e., with $\mu \neq \bar\mu$,

$$M(p^2,\mu^2) = M(p^2,\bar\mu^2) \doteq M(p^2)\,,\ \forall\, p^2\,. \tag{2.26}$$

At one-loop order:

$$m(\mu) \doteq M(\mu^2) = \frac{\hat{m}}{\left(\frac{1}{2}\ln\left[\frac{\mu^2}{\Lambda^2_{\rm QCD}}\right]\right)^{\gamma_m}}\,, \tag{2.27}$$

where $\hat{m}$ is a renormalisation-point-independent current-quark mass and $\gamma_m = 12/(33 - 2N_f)$ is the anomalous dimension at this order; and

$$Z_m(\mu^2,\Lambda^2) = \left[\frac{\alpha(\Lambda^2)}{\alpha(\mu^2)}\right]^{\gamma_m}\,. \tag{2.28}$$

In QCD, γ_m is independent of the gauge parameter to all orders in perturbation theory and the chiral limit is defined by $\hat{m} = 0$. Dynamical chiral symmetry breaking is manifest when, for $\hat{m} = 0$, one obtains $m(\mu) \sim {\rm O}(1/\mu^2) \neq 0$ in solving Eq. (2.20), which is impossible at any finite order in perturbation theory.

2.4.2 *Dressed-gluon propagator*

In a general covariant gauge the renormalised dressed-gluon propagator in Eq. (2.20) has the general form

$$D_{\mu\nu}(k) = \left(\delta_{\mu\nu} - \frac{k_\mu k_\nu}{k^2}\right)\frac{d(k^2,\mu^2)}{k^2} + \xi\,\frac{k_\mu k_\nu}{k^4}\,, \tag{2.29}$$

where $d(k^2,\mu^2) = 1/[1+\Pi(k^2,\mu^2)]$, with $\Pi(k^2,\mu^2)$ the renormalised gluon vacuum polarisation. The fact that the longitudinal [ξ-dependent] part of $D_{\mu\nu}(k)$ is not modified by interactions is the result of a Slavnov-Taylor identity in QCD: $k_\mu D_{\mu\nu}(k) = \xi\, k_\nu/k^2$. We note that Landau gauge is a fixed point of the renormalisation group; i.e., in Landau gauge the renormalisation-group-invariant gauge parameter is zero to all orders in perturbation theory; hence we employ this gauge in all numerical studies herein.

Multiplicative renormalisability entails that

$$\frac{d(k^2,\mu^2)}{d(k^2,\bar{\mu}^2)} = \frac{Z_3(\bar{\mu}^2,\Lambda^2)}{Z_3(\mu^2,\Lambda^2)} = d(\bar{\mu}^2,\mu^2) = \frac{1}{d(\mu^2,\bar{\mu}^2)}\,. \tag{2.30}$$

At one-loop order in perturbation theory

$$Z_3(\mu^2,\Lambda^2) = \left[\frac{\alpha(\Lambda^2)}{\alpha(\mu^2)}\right]^{-\frac{\gamma_1}{\beta_1}} , \tag{2.31}$$

where $\gamma_1 = \frac{1}{3}N_f - \frac{1}{4}(13-3\xi)$.

2.4.3 *Dressed-quark-gluon vertex*

The renormalised dressed-quark-gluon vertex in Eq. (2.20) is of the form

$$\Gamma^a_\nu(k,p) = \frac{\lambda^a}{2}\Gamma_\nu(k,p)\,. \tag{2.32}$$

As a fully amputated vertex, it is free of kinematic singularities. The general Lorentz structure of $\Gamma_\nu(k,p)$ is straightforward but lengthy, involving 12 distinct scalar form factors, and here we do not reproduce it fully:

$$\Gamma_\nu(k,p) = \gamma_\nu F_1(k,p,\mu) + \ldots\,; \tag{2.33}$$

but remark that Ref. [53], pp. 80-83, and Refs. [95] provide an elucidation of its structure, evaluation and properties.

Renormalisability entails that only the form factor F_1, associated with the γ_ν tensor, is ultraviolet-divergent. By convention, and defining: $f_1(k^2,\mu^2) \doteq F_1(k,-k,\mu)$, $\Gamma_\nu(k,p)$ is renormalised such that at some large spacelike μ^2

$$f_1(\mu^2,\mu^2) = 1\,. \tag{2.34}$$

Since the renormalisation is multiplicative, one has

$$\frac{f_1(k^2,\mu^2)}{f_1(k^2,\bar{\mu}^2)} = \frac{Z_1(\mu^2,\Lambda^2)}{Z_1(\bar{\mu}^2,\Lambda^2)} = f_1(\bar{\mu}^2,\mu^2) = \frac{1}{f_1(\mu^2,\bar{\mu}^2)}\,. \tag{2.35}$$

At one-loop in perturbation theory the vertex renormalisation constant is

$$Z_1(\mu^2,\Lambda^2) = \left[\frac{\alpha(\Lambda^2)}{\alpha(\mu^2)}\right]^{-\frac{\gamma_\Gamma}{\beta_1}} , \tag{2.36}$$

where $\gamma_\Gamma = \frac{1}{2}[\frac{3}{4}(3+\xi) + \frac{4}{3}\xi]$.

2.5 *Model for the quark DSE*

As noted earlier, even the simplest DSE, the gap equation, can be solved only in an approximate form. The approximation scheme used in our formulation is such that it preserves the Axial Vector Ward Takashi Identity.

Consider the 2-flavor QCD Lagrangian in the chiral limit. Then it is invariant under $SU_L(2) \otimes SU_R(2)$, besides other symmetries. As such, the currents with these symmetries j_L^μ and j_R^μ, are conserved. The sum of these chiral currents corresponds to isospin currents and its conservation to the conservation of isospin.

The difference is an axial vector current and does not correspond to any known conservation law of strong interactions. In 1960 Nambu and Jona-Lasinio hypothesized that the symmetry corresponding to the conservation of this current is spontaneously broken. Goldstone's theorem states that every spontaneously broken continuous symmetry of a quantum field theory leads to a massless particle with the quantum numbers of the broken symmetry generator. Thus in this case there would be a particle of negative parity, zero spin, unit isospin and zero baryon number. The pion fits the description quite well, except that it is not exactly massless. But its mass is much lower than other hadrons and so can be blamed on the u and d quarks having a tiny mass. The question then is how to incorporate this Goldstone boson character of the pion in our formulation?

We obtain the amplitudes for the mesons as solutions of the homogeneous Bethe-Salpeter equation (BSE), which has 2 inputs: 1) Solution of the quark propagator equation and 2) Approximate form for the kernel K. To preserve the consequences of spontaneous chiral symmetry breaking in this program, it has been shown in ref() that the truncation of the gap equation and of the BSE must be consistent in the sense that the meson amplitudes must satisfy the AVWTI.

To introduce an approximation, we use Eqs. (2.24), (2.31) and (2.36) and observe that

$$\frac{2\gamma_F}{\beta_1} + \frac{\gamma_1}{\beta_1} - \frac{2\gamma_\Gamma}{\beta_1} = 1\,. \tag{2.37}$$

Hence, on the kinematic domain for which $Q^2 \doteq (p-q)^2 \sim p^2 \sim q^2$ is large and space-like, the renormalised dressed-ladder kernel in the Bethe-Salpeter equation for the (fully-amputated) Bethe-Salpeter amplitude behaves as follows:

$$\begin{aligned} & g^2(\mu^2)\, D_{\mu\nu}(p-q)\, \left[\Gamma^a_\mu(p_+,q_+) S\,(q_+)\right] \times \left[S(q_-)\,\Gamma^a_\nu(q_-,p_-)\right] \\ & \quad = 4\pi\,\alpha(Q^2)\, D^{\rm free}_{\mu\nu}(p-q)\, \left[\frac{\lambda^a}{2}\gamma_\mu\, S^{\rm free}(q_+)\right] \times \left[S^{\rm free}(q_-)\,\frac{\lambda^a}{2}\gamma_\nu\right]\,, \end{aligned} \tag{2.38}$$

as can be seen ffrom the renormalised, homogeneous, pseudoscalar Bethe-Salpeter Equation (BSE)

$$[\Gamma_H(k;P)]_{tu} \;\; = \;\; \int_q^\Lambda [\chi_H(q;P)]_{sr}\, K^{rs}_{tu}(q,k;P)\,, \tag{2.39}$$

where: $H = \pi$ or K specifies the flavour-matrix structure of the amplitude; $\chi_H(q;P) \doteq \mathcal{S}(q_+)\Gamma_H(q;P)\mathcal{S}(q_-)$, with $\mathcal{S}(q) = {\rm diag}(S_u(q), S_d(q), S_s(q))$; $q_+ = q + \eta_P\, P$, $q_- = q - (1-\eta_P)\, P$, with P the total momentum of the bound state; and r,...,u represent colour-, Dirac- and flavour-matrix indices.This observation, and the intimate relation between the kernel of the pseudoscalar BSE and the integrand in Eq. (2.20) [40], provides a means of understanding the origin of an often used Ansatz for $D_{\mu\nu}(k)$; i.e., in Landau gauge, making the replacement

$$g^2 D_{\mu\nu}(k) \to 4\pi\,\alpha(k^2)\, D^{\rm free}_{\mu\nu}(k) \tag{2.40}$$

in Eq. (2.20), and using the "rainbow approximation":

$$\Gamma_\nu(q,p) = \gamma_\nu\,. \tag{2.41}$$

The Ansatz expressed in Eq. (2.40) is often described as the "Abelian approximation" because the left- and right-hand-sides are *equal* in QED. In QCD, equality between the

two sides of Eq. (2.40) cannot be obtained easily by a selective resummation of diagrams. As reviewed in Ref. [1], Eqs. (5.1) to (5.8), it can only be achieved by enforcing equality between the renormalisation constants for the ghost-gluon vertex and ghost wave function: $\tilde{Z}_1 = \tilde{Z}_3$.

A mutually consistent constraint, which follows from $\tilde{Z}_1 = \tilde{Z}_3$ at a formal level, is to enforce the Abelian Ward identity $Z_1 = Z_2$. At one-loop this corresponds to neglecting the contribution of the 3-gluon vertex to Γ_ν, in which case $\gamma_\Gamma \to \frac{2}{3}\xi = \gamma_F$. This additional constraint provides the basis for extensions of Eq. (2.41); i.e., using Ansätze for Γ_ν that are consistent with the vector Ward-Takahashi identity in QED, such as Refs. [14, 17, 10].

The combination of Abelian and rainbow approximations [with $Z_1 = 1 = Z_2$] yields a mass function, $M(p^2)$, with the "correct" one-loop anomalous dimension; i.e., γ_m in Eq. (2.27) in the case of explicit chiral symmetry breaking or $(1 - \gamma_m)$ in its absence [54]. However, other often used Ansätze for Γ_ν [95, 5] yield different and incorrect anomalous dimensions for $M(p^2)$ [55]. This illustrates and emphasises that the anomalous dimension of the solution of Eq. (2.20) is sensitive to the details of the asymptotic behaviour of the Ansätze for the elements in the integrand. One role of the multiplicative renormalisation constant Z_1 is to compensate for this.

An extensively studied model for the kernel of Eq. (2.20) is based on the Abelian approximation [29, 30],:

$$Z_1 \int_q^\Lambda g^2 D_{\mu\nu}(p-q)\frac{\lambda^a}{2}\gamma_\mu S(q)\Gamma^a_\nu(q,p) \to \int_q^\Lambda \mathcal{G}((p-q)^2)\, D^{\rm free}_{\mu\nu}(p-q)\frac{\lambda^a}{2}\gamma_\mu S(q)\frac{\lambda^a}{2}\gamma_\nu\,, \tag{2.42}$$

with the specification of the model complete once a form is chosen for the "effective coupling" $\mathcal{G}(k^2)$.

One consideration underlying this Ansatz is that while carrying out subtractive renormalisation in a DSE-model of QCD it is not possible to determine Z_1 without analysing

the DSE for the dressed-quark-gluon vertex. In [29] various Ansätze for Γ_ν have been explored to show that, with $\mathcal{G}(k^2) = 4\pi\alpha(k^2)$ for large-k^2, there is always at least one Ansatz for Z_1 that leads to the correct anomalous dimension for $M(p^2)$. This interplay between the the renormalisation constant and the integral is manifest in QCD and Eq. (2.42) is a simple means of implementing it.

Using Eqs. (2.20) and (2.42) our model quark DSE is

$$S(p,\mu)^{-1} \;=\; Z_2\, i\gamma\cdot p + Z_4\, m(\mu) + \Sigma'(p,\Lambda)\,, \tag{2.43}$$

with the regularised quark self energy

$$\Sigma'(p,\Lambda) \;\doteq\; \int_q^\Lambda \mathcal{G}((p-q)^2)\, D^{\rm free}_{\mu\nu}(p-q)\frac{\lambda^a}{2}\gamma_\mu S(q)\frac{\lambda^a}{2}\gamma_\nu\,, \tag{2.44}$$

Equation (2.43) is a pair of coupled integral equations for the functions $A(p^2,\mu^2)$ and $B(p^2,\mu^2)$ defined in Eq. (2.21).

In the case of explicit chiral symmetry breaking, $\hat{m} \neq 0$, the renormalisation boundary condition of Eq. (2.22) is straightforward to implement. With

$$\Sigma'(p,\Lambda) \doteq i\gamma\cdot p\, \left(A'(p^2,\Lambda^2) - 1\right) + B'(p^2,\Lambda^2)\,, \tag{2.45}$$

Eq. (2.22) entails

$$Z_2(\mu^2,\Lambda^2) = 2 - A'(\mu^2,\Lambda^2) \;\text{ and }\; m(\mu) = Z_2(\mu^2,\Lambda^2)\, m_0(\Lambda^2) + B'(\mu^2,\Lambda^2) \tag{2.46}$$

and hence

$$A(p^2,\mu^2) \;=\; 1 + A'(p^2,\Lambda^2) - A'(\mu^2,\Lambda^2)\,, \tag{2.47}$$

$$B(p^2,\mu^2) \;=\; m(\mu) + B'(p^2,\Lambda^2) - B'(\mu^2,\Lambda^2)\,. \tag{2.48}$$

From Sec. 2.4.1, having fixed the solutions at a single renormalisation point, μ, their form at another point, $\bar{\mu}$, is given by

$$S^{-1}(p,\bar{\mu}) = i\gamma\cdot p\, A(p^2,\bar{\mu}^2) + B(p^2,\bar{\mu}^2) = \frac{Z_2(\bar{\mu}^2,\Lambda^2)}{Z_2(\mu^2,\Lambda^2)} S^{-1}(p,\mu)\,. \tag{2.49}$$

[Recall that $M(p^2)$ is independent of the renormalisation point.] This feature is manifest in our solutions. It means that, in evolving the renormalisation point to $\bar{\mu}$, the "1" in Eq. (2.47) is replaced by $Z_2(\bar{\mu}^2,\Lambda^2)/Z_2(\bar{\mu}^2,\Lambda^2)$, and the "$m(\mu)$" in Eq. (2.48) by $m(\bar{\mu})$; i.e., the "seeds" in the integral equation evolve according to the QCD renormalisation group.

As also remarked in Sec. 2.4.1, the chiral limit in QCD is unambiguously defined by $\hat{m} = 0$. In this case there is no perturbative contribution to the scalar piece of the quark self energy, $B(p^2,\mu^2)$, and, in fact, there is no scalar, mass-like divergence in the perturbative calculation of the self energy. It follows that

$$Z_2(\mu^2,\Lambda^2)m_0(\Lambda^2) = Z_4(\mu^2,\Lambda^2)m(\mu^2) = 0\,,\ \forall\ \Lambda \gg \mu, \tag{2.50}$$

and, from Eqs. (2.46) and (2.48), that there is no subtraction in the equation for $B(p^2,\mu^2)$; i.e., Eq. (2.48) becomes

$$B(p^2,\mu^2) = B'(p^2,\Lambda^2)\,, \tag{2.51}$$

with $\lim_{\Lambda\to\infty} B'(p^2,\Lambda^2) < \infty$.[1] In terms of the renormalised current-quark mass the existence of DCSB means that, in the chiral limit, $M(\mu^2) \sim \mathrm{O}(1/\mu^2)$, up to $\ln\mu^2$-corrections.

An "Abelian approxiamtion" model for the "effective coupling" $\mathcal{G}(k^2)$ that has been successful in describing physical properties of ground state pseudoscalar and vector mesons is the Maris-Tandy (MT) model [30]. The Ansatz is

$$\frac{\mathcal{G}(k^2)}{k^2} = \frac{4\pi^2\,D\,k^2}{\omega^6}\,\mathrm{e}^{-k^2/\omega^2} + \frac{4\pi^2\,\gamma_m\,\mathcal{F}(k^2)}{\frac{1}{2}\ln\left[\tau + \left(1 + k^2/\Lambda_{\mathrm{QCD}}^2\right)^2\right]}\,, \tag{2.52}$$

with $\gamma_m = \frac{12}{33-2N_f}$ and $\mathcal{F}(s) = (1-\exp(\frac{-s}{4m_t^2}))/s$. The first term implements the strong infrared enhancement in the region $0 < k^2 < 1\,\mathrm{GeV}^2$ required for sufficient dynamical chiral symmetry breaking. The second term serves to preserve the one-loop renormalization

[1] This is a model-independent statement; i.e., it is true in any study that preserves at least the one-loop renormalisation group behaviour of QCD.

group behavior of QCD. Here $m_t = 0.5\,\mathrm{GeV}$, $\tau = \mathrm{e}^2 - 1$, $N_f = 4$, and $\Lambda_{\mathrm{QCD}} = 0.234\,\mathrm{GeV}$. The remaining parameters, $\omega = 0.4\,\mathrm{GeV}$ and $D = 0.93\ \mathrm{GeV}^2$ along with the quark masses, are fitted to give a good description of $\langle \bar{q}q \rangle$, $m_{\pi/K}$ and f_π. The subsequent values for f_K and the masses and decay constants of the vector mesons $\rho, \phi, K^\star$ are found to be within 10% of the experimental data [30].

Chapter 3

Quenched lattice-QCD dressed-quark propagator

Results from numerical simulations of lattice-QCD are available from recent studies of the quenched theory for dressed-gluon [21, 22, 23, 24] and -quark [25, 26] two-point functions ("propagators"). Use of the lattice dressed-gluon two-point function as the sole basis for the kernel of QCD's gap equation does not yield the lattice dressed-quark propagator without a material infrared enhancement of the dressed-quark-gluon vertex [10, 11, 12]. Here we elucidate this using a concrete model for the gap equation's kernel. Our analysis will also provide an informed estimate of the chiral limit behaviour of the extrapolated lattice results.

3.1 *Lattice gluon propagator*

The dressed gluon propagator in Landau gauge ($\zeta = 0$) is seen from Eq. (2.29)to have the form,

$$D_{\mu\nu}(k) = T_{\mu\nu}(k)\, D(k^2) \tag{3.1}$$

where $D(k^2) = \frac{d(k^2,\mu^2)}{k^2}$ and $T_{\mu\nu} = (\delta_{\mu\nu} - \frac{k_\mu k_\nu}{k^2})$

In Ref. [21] the Landau gauge dressed gluon propagator was computed using quenched lattice-QCD configurations and the result was parametrised as:

$$D(k^2) = Z_g \left[\frac{A\Lambda_g^{2\alpha}}{(k^2+\Lambda_g^2)^{1+\alpha}} + \frac{L(k^2,\Lambda_g)}{k^2+\Lambda_g^2} \right], \tag{3.2}$$

with

$$\begin{array}{rclcrcl} A &=& 9.8^{+0.1}_{-0.9}, & & \Lambda_g &=& 1.020 \pm 0.1 \pm 0.025\,\mathrm{GeV}, \\ \alpha &=& 2.2^{+0.1+0.2}_{-0.2-0.3}, & & Z_g &=& 2.01^{+0.04}_{-0.05}, \end{array} \tag{3.3}$$

where the first pair of errors are statistical and the second, when present, denote systematic errors associated with finite lattice spacing and volume. In the simulation the lattice spacing $a = 1/[1.885\,\mathrm{GeV}]$. The numerator in the second term of Eq. (3.2) is

$$L(k^2, \Lambda_g) = \left(\frac{1}{2} \ln \left[(k^2 + \Lambda_g^2)(\frac{1}{k^2} + \frac{1}{\Lambda_g^2}) \right] \right)^{-d_D}, \tag{3.4}$$

with $d_D = [39 - 9\,\xi - 4N_f]/[2(33 - 2N_f)]$, an expression which ensures the parametrisation expresses the correct one-loop behaviour at ultraviolet momenta. In the quenched, Landau-gauge study, $N_f = 0$, $\xi = 0$, so

$$d_D = 13/22\,. \tag{3.5}$$

3.2 *Effective quark-gluon vertex*

To reiterate, asymptotic freedom entails that the "effective coupling" $\mathcal{G}(Q^2)$ is proportional to the strong running coupling in the ultraviolet i.e.

$$\mathcal{G}(k^2) = 4\pi\alpha(k^2), \;\; Q^2 \gtrsim 2\,GeV^2; \tag{3.6}$$

and so for $Q^2 \gtrsim 2\,GeV^2$ (recall Eq. (2.25),

$$\mathcal{G}(Q^2) = \frac{4\pi^2\gamma_m}{\ln(Q^2/\Lambda^2_{\mathrm{QCD}})}, \tag{3.7}$$

where $\gamma_m = 12/(33 - 2N_f)$ is the anomalous mass dimension. To proceed we therefore write

$$\frac{1}{Q^2}\,\mathcal{G}(Q^2) = D(Q^2)\,\Gamma_1(Q^2)\,, \tag{3.8}$$

with $D(Q^2)$ given in Eq. (3.2) and

$$\Gamma_1(Q^2) = 4\pi^2\gamma_m\,\frac{1}{Z_g}\,\frac{[\frac{1}{2}\ln(\tau + Q^2/\Lambda_g^2)]^{d_D}}{[\ln(\tau + Q^2/\Lambda^2_{\mathrm{QCD}})]}\,v(Q^2)\,, \tag{3.9}$$

where $\tau = e^2 - 1 > 1$ is an infrared cutoff. Equation (3.8) factorises the effective interaction into a contribution from the lattice dressed-gluon propagator multiplied by a contribution from the vertex, which we shall subsequently determine phenomenologically.

We remark that the renormalisation-group-improved rainbow truncation retains only that single element of the dressed-quark-gluon vertex which is ultraviolet divergent at one-loop level and this explains the simple form of Eq. (3.9). Systematic analyses of corrections to the rainbow truncation show Γ_1 to be the dominant amplitude of the dressed vertex: the remaining amplitudes do not significantly affect observables [41]. In proceeding phenomenologically solely with Γ_1, we force $v(Q^2)$ to assume the role of the omitted amplitudes to the maximum extent possible.

In Eq. (3.9), so long as $v(Q^2) \simeq 1$ for $Q^2 \gtrsim 2\,\mathrm{GeV}^2$, Eq. (3.7) is satisfied and consequently the rainbow gap equation preserves the renormalisation group flow of QCD at one-loop. We therefore consider a simple *Ansatz* with this property:

$$v(Q^2) = \frac{a_v(m) + Q^2/\Lambda_g^2}{b + Q^2/\Lambda_g^2}\,, \tag{3.10}$$

where

$$a_v(m) = \frac{a_1}{1 + a_2\,[m(\zeta)/\Lambda_g] + a_3\,[m(\zeta)/\Lambda_g]^2} \tag{3.11}$$

and $a_{1,2,3}$ and b are dimensionless parameters, which are fitted by requiring that the gap equation yield a solution for the dressed-quark propagator that agrees well pointwise with the results obtained in numerical simulations of quenched lattice-QCD [25, 26]. It is important to note that a good fit to lattice data is impossible unless $a_v(m)$ depends on the current-quark mass. While more complicated forms are clearly possible, the *Ansatz* of Eq. (3.11) is adequate.

3.3 *Fit to lattice results*

Now, to be explicit, the parameters in Eqs. (3.10), (3.11) were determined by the following procedure. The rainbow gap equation; viz., Eq. (2.43) simplified via Eq. (2.44), was solved using the effective interaction specified by Eqs. (3.8)–(3.11), with $D(Q^2)$ exactly as given in Eq. (3.2).

The ultraviolet behaviour of the mass function, $M(p^2)$, is determined by perturbative QCD and is therefore model independent. Hence the current-quark mass, $m(\zeta)$, was fixed by requiring agreement between the DSE and lattice results for $M(p^2)$ on $p^2 \gtrsim 1\,\mathrm{GeV}^2$. We selected three lattice data sets from Ref. [26] and, for consistency with Refs. [29, 30], used a renormalisation point $\zeta = 19\,\mathrm{GeV}$, which is well into the perturbative domain. This gave

$a\,m_{\mathrm{lattice}}$	0.018	0.036	0.072
$m(\zeta)(\mathrm{GeV})$	0.030	0.055	0.110

. (3.12)

The dimensionless parameters $a_{1,2,3}$ and b were subsequently determined in a simultaneous least-squares fit of DSE solutions for $M(p^2)$ at these current-quark masses to all the lattice data. This necessarily required the gap equation to be solved repeatedly. Nevertheless, the fit required only hours on a modern workstation, and yielded:

a_1	a_2	a_3	b
1.5	7.35	63.0	0.005

. (3.13)

These parameters completely determine the "best-fit effective-interaction" and hence our lattice-constrained model for the gap equation's kernel.

We emphasise that because the comparison is with simulations of quenched lattice-QCD, we used $N_f = 0$ throughout and [35, 36, 37, 60]

$$\Lambda_{\mathrm{qu-QCD}} = 0.234\,\mathrm{GeV}. \tag{3.14}$$

The strength of the running strong coupling is underestimated in simulations of quenched lattice-QCD [61]. (NB. Halving or doubling $\Lambda_{\mathrm{qu-QCD}}$ has no material quantitative impact on our results, nor does it qualitatively affect our conclusions.)

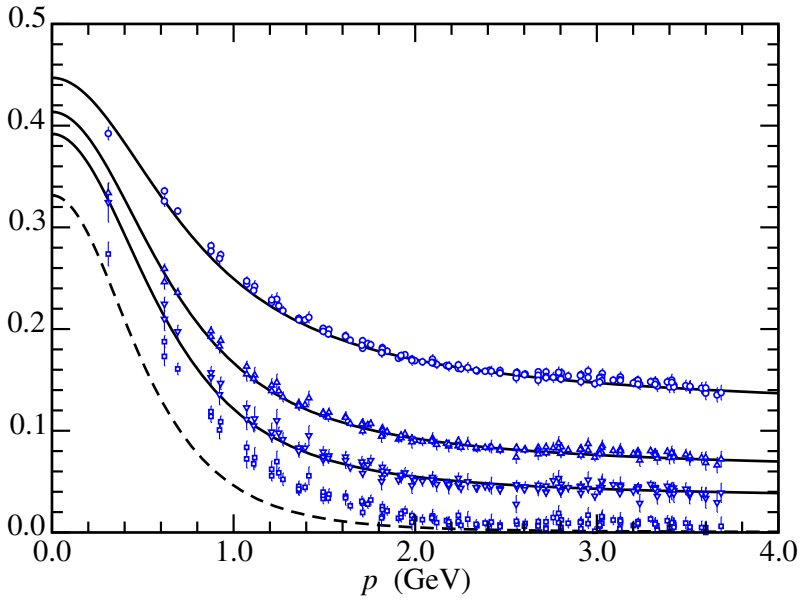

Figure 1: Data, upper three sets: lattice results for $M(p^2)$ in GeV at am values in Eq. (3.12); lower points (boxes): linear extrapolation of lattice results [26] to $am = 0$. Solid curves: best-fit-interaction gap equation solutions for $M(p^2)$ obtained using the current-quark masses in Eq. (3.12); dashed-curve: gap equation's solution in the chiral limit, Eq. (2.50).

3.4 *Fidelity and quiddity of the procedure*

In Fig. 1 we compare DSE solutions for $M(p^2)$, obtained using the optimised effective interaction, with lattice results. In addition, we depict the DSE solution for $M(p^2)$ calculated in the chiral limit along with the linear extrapolation of the lattice data to $am = 0$, as described in Ref. [25]. It is apparent that the lattice-gluon and lattice-quark propagators can be correlated via the renormalisation-group-improved gap equation. That was achieved via $v(Q^2)$ in Eq. (3.10), and the required form is depicted in Fig. 2. Plainly, consistency between the propagators via this gap equation requires an infrared enhancement of the vertex, as anticipated in Refs. [10, 11, 33, 34]. Our inferred form is in semi-quantitative agreement with the result of recent, exploratory lattice-QCD simulations of the dressed-quark-gluon vertex [35, 36, 37].

Dynamical chiral symmetry breaking is another important feature evident in Fig. 1;

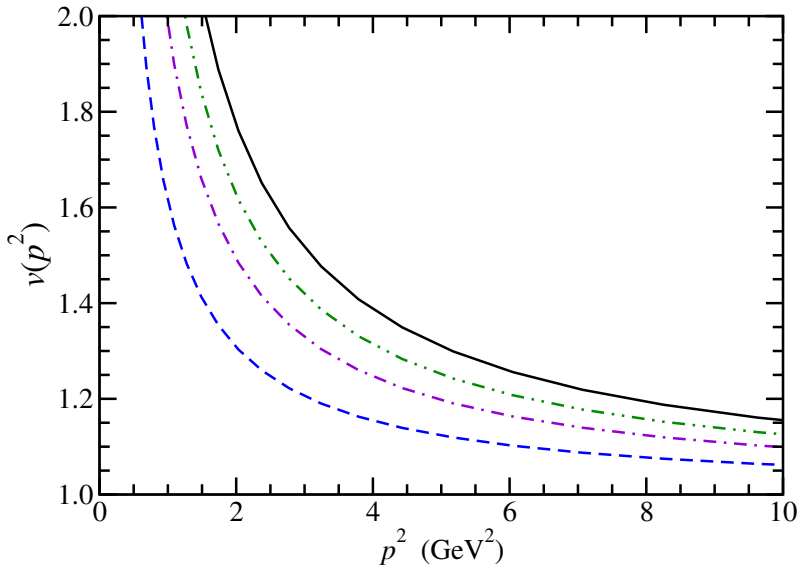

Figure 2: Dimensionless vertex dressing factor: $v(Q^2)$, defined via Eqs. (3.10), (3.11), (3.13), obtained in the chiral limit (*solid curve*) and with the current-quark masses in Eq. (3.12). $v(Q^2)$ is finite at $Q^2 = 0$ and decreases with increasing $m(\zeta)$.

viz., the existence of a $M(p^2) \neq 0$ solution of the gap equation in the chiral limit. We deduce that DCSB is manifest in quenched-QCD and, in the following, quantify the magnitude of that effect. It should be observed that a linear extrapolation to $am = 0$ of the lattice data obtained with nonzero current-quark masses overestimates the mass function calculated directly as the solution of the gap equation.

Figure 3 focuses on the lattice simulations for the intermediate value of the current-quark mass; namely, $am = 0.036$, and compares lattice output for both $M(p^2)$ and the quark wave function renormalisation, $Z(p^2)$, with our results. We emphasise that the form of $Z(p^2)$ was not used in fitting $v(Q^2)$. Hence the pointwise agreement between the gap equation's solution and the lattice result indicates that our simple expression for the effective interaction captures the dominant dynamical content and, in particular, that omitting the subdominant amplitudes in the dressed-quark-gluon vertex is not a serious flaw in this study.

3.5 *Spectral properties*

In a quantum field theory defined by a Euclidean measure [62] the Osterwalder-Schrader axioms [63, 64] are five conditions which any moment of this measure (n-point Schwinger function) must satisfy if it is to have an analytic continuation to Minkowski space and hence an association with observable quantities. One of these is "OS3": the axiom of *reflection positivity*, which is violated if the Schwinger function's Fourier transform to configuration space is not positive definite. The space of observable asymptotic states is spanned by eigenvectors of the theory's infrared Hamiltonian and no Schwinger function that breaches OS3 has a correspondent in this space. Consequently, the violation of OS3 is a sufficient condition for confinement.

This connection has long been of interest [65, 42], and is discussed at length in Refs. [66, 67, 68], and reviewed in Sec. 6.2 of Ref. [1], Sec. 2.2 of Ref. [2] and Sec. 2.4 of Ref. [3]. It suggests and admits a practical test [10] that has been exploited in Refs. [18, 10, 11, 69, 70, 71, 72, 73, 74, 75] and which for the quark 2-point function is based on the behaviour of

$$\Delta_S(T) = \int d^3x \int \frac{d^4p}{(2\pi)^4}\, \mathrm{e}^{ip\cdot x}\, \sigma_S(p^2) \tag{3.15}$$

$$= \frac{1}{\pi}\int_0^\infty d\varepsilon\, \cos(\varepsilon\, T)\, \sigma_S(\varepsilon^2)\,, \tag{3.16}$$

where σ_S is the Dirac-scalar projection of the dressed-quark propagator. For a noninteracting fermion with mass μ,

$$\Delta_S^{\mathrm{free}}(T) = \frac{1}{\pi}\int_0^\infty d\varepsilon\ \cos(\varepsilon\, T)\, \frac{\mu}{\varepsilon^2+\mu^2} = \frac{1}{2}\,\mathrm{e}^{-\mu T}. \tag{3.17}$$

The r.h.s. is positive definite. It is also plainly related via analytic continuation ($T \to it$) to the free-particle solution of the Minkowski space Dirac equation. The existence of an associated asymptotic state is indubitable.

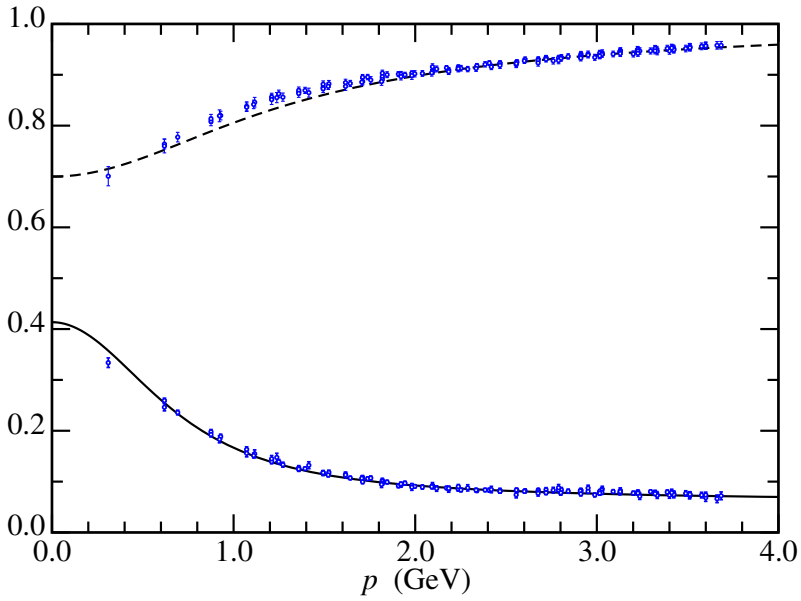

Figure 3: Data, quenched lattice-QCD results for $M(p^2)$ and $Z(p^2)$ obtained with $am = 0.036$ [26]; dashed curve, $Z(p^2)$, and solid curve, $M(p^2)$ calculated from the gap equation with our optimised effective interaction and $m(\zeta) = 55\,\mathrm{MeV}$. (NB. $Z(p^2)$ is dimensionless and $M(p^2)$ is measured in GeV.)

If instead one encountered a theory in which [67, 68, 75]

$$\sigma_S(p^2) = \frac{\mu}{2}\left[\frac{1}{p^2+\mu^2-i\rho^2} + \frac{1}{p^2+\mu^2+i\rho^2}\right], \tag{3.18}$$

a function with a pair of complex conjugate poles at $p^2 + \sigma^2 \exp(\pm i\theta) = 0$, where

$$\sigma^4 = \mu^4 + \rho^4\,,\ \tan\theta = \rho^2/\mu^2, \tag{3.19}$$

then

$$\Delta_S(T) = \frac{\mu}{2\sigma}\,\mathrm{e}^{-\sigma T\cos\frac{\theta}{2}}\,\cos\left(\sigma T\sin\frac{\theta}{2} + \frac{\theta}{2}\right). \tag{3.20}$$

This Fourier transform has infinitely many, regularly spaced zeros and hence OS3 is violated. Thus the fermion described by this Schwinger function has no correspondent in the space of observable asymptotic states.

It is readily apparent that Eq. (3.18) evolves to a free particle propagator when $\rho \to 0$. This limit is expressed in Eq. (3.20) via $\theta \to 0$, $\sigma \to \mu$, wherewith Eq. (3.17) is recovered;

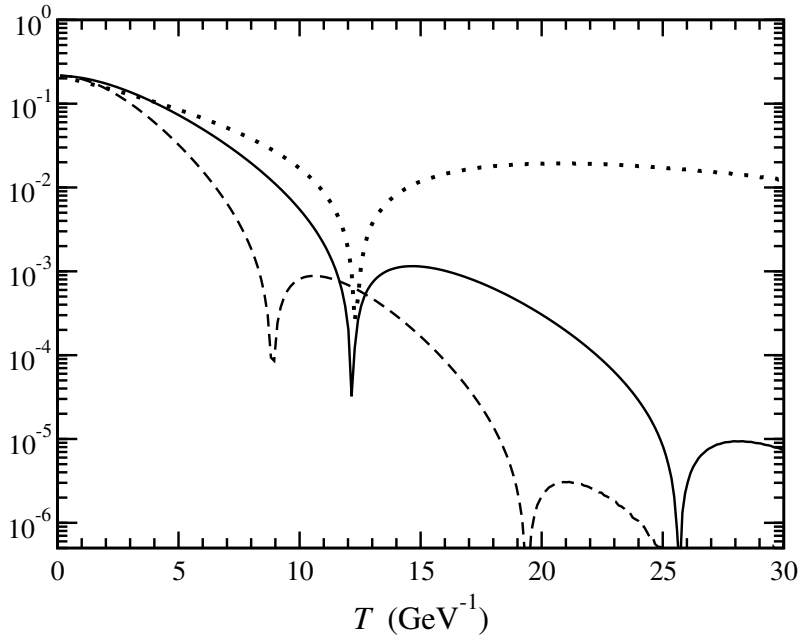

Figure 4: $|\Delta_S(T)|$ obtained from: the chiral limit gap equation solution calculated using our lattice-constrained kernel, solid curve; Eq. (3.18) with $\sigma = 0.13\,\mathrm{GeV}$, $\theta = \pi/2.46$, dotted curve; the model of Ref. [30], dashed curve.

a result that is tied to the feature that the first zero of $\Delta_S(T)$ in Eq. (3.20) occurs at

$$z_1 = \frac{\pi - \theta}{2\,\sigma}\,\csc\frac{\theta}{2} \tag{3.21}$$

and hence $z_1 \to \infty$ for $\rho \to 0$ [69, 70].

We calculated $\Delta_S(T)$ using the gap equation solutions discussed above and the form of $|\Delta_S(T)|$ obtained with the chiral limit solution is depicted in Fig. 4. The violation of OS3 is manifest in the appearance of cusps: $\ln|\Delta_S(T)|$ is negative and infinite in magnitude at zeros of $\Delta_S(T)$. The differences evident in a comparison with the result obtained from Eq. (3.20) indicate that the singularity structure of the dressed-quark 2-point Schwinger function obtained from the lattice-constrained kernel is more complicated than just a single pair of complex conjugate poles. However, the similarities suggest that this picture may serve well as an idealisation [75]. (NB. Qualitatively identical results are obtained using $\sigma_V(p^2)$, the Dirac-vector projection of the dressed-quark propagator, instead of $\sigma_S(p^2)$.)

Figure 4 also portrays the result obtained with the effective interaction proposed in Ref. [30] and used efficaciously in studies of meson properties [4]. Significantly, the first zero appears at a smaller value of T in this case. Using the model of Eq. (3.18) as a guide, that shift indicates a larger value of σ. This sits well with the fact that the mass-scale generated dynamically by the interaction of Ref. [30] is larger than that produced by the interaction used herein, which is only required to correlate quenched lattice data for the gluon and quark two-point functions.

From the results and analysis reported in this subsection, we deduce that light-quarks do not appear in the space of observable asymptotic states associated with quenched-QCD; an outcome anticipated in Ref. [34].

3.6 *Chiral limit*

The scale of DCSB is measured by the value of the renormalisation-point dependent vacuum quark condensate, which is obtained directly from the chiral limit dressed-quark propagator [43, 29]:

$$-\langle\bar{q}q\rangle^0_\zeta = \lim_{\Lambda\to\infty} Z_4(\zeta,\Lambda)\, N_c\, \mathrm{tr}\int_q^\Lambda S_0(q), \tag{3.22}$$

where "tr" denotes a trace only over Dirac indices and the index "0" labels a quantity calculated in the chiral limit, Eq. (2.50). In Eq. (3.22) the gauge parameter dependence of the renormalisation constant Z_4 is precisely that required to ensure the vacuum quark condensate is gauge independent. This constant is fixed by the renormalisation condition, Eq. (2.22), which entails

$$Z_4(\zeta,\Lambda) = -\frac{1}{m(\zeta)}\,\frac{1}{4}\,\mathrm{tr}\,\Sigma'(\zeta,\Lambda) \tag{3.23}$$

wherein the right hand side is well-defined in the chiral limit [29]. (It may also be determined by studying the fully amputated pseudoscalar-quark-antiquark 3-point function

[43].) A straightforward calculation using our chiral limit result; i.e, the propagator corresponding to the dashed-curve in Fig. 1, yields

$$-\langle\bar{q}q\rangle^0_{\zeta=19\ \mathrm{GeV}} = (0.22\,\mathrm{GeV})^3. \tag{3.24}$$

To evolve the condensate to a "typical hadronic scale," e.g., $\zeta = 1\,\mathrm{GeV}$, one may use [84]

$$\langle\bar{q}q\rangle^0_{\zeta'} = Z_4(\zeta',\zeta) Z_2^{-1}(\zeta',\zeta)\,\langle\bar{q}q\rangle^0_{\zeta} =: Z_m(\zeta',\zeta)\langle\bar{q}q\rangle^0_{\zeta}, \tag{3.25}$$

where Z_m is the gauge invariant mass renormalisation constant. Contemporary phenomenological approaches employ the one-loop expression for Z_m and following this expedient we obtain, practically as a matter of definition,

$$\begin{aligned} -\langle\bar{q}q\rangle^0_{1\,\mathrm{GeV}} &= \left(\frac{\ln[1/\Lambda_{\mathrm{qu-QCD}}]}{\ln[19/\Lambda_{\mathrm{qu-QCD}}]}\right)^{\gamma_m} (-\langle\bar{q}q\rangle^0_{19\,\mathrm{GeV}}) \\ &= (0.19\,\mathrm{GeV})^2, \end{aligned} \tag{3.26}$$

which may be compared with a best-fit phenomenological value [76]: $(0.24 \pm 0.01\,\mathrm{GeV})^3$. It is notable that DSE models which efficaciously describe light-meson physics; e.g., Refs. [29, 30], give $\langle\bar{q}q\rangle^0_{1\,\mathrm{GeV}} = -(0.24\,\mathrm{GeV})^3$.

Our gap equation assisted estimate therefore indicates that the chiral condensate in quenched-QCD is a factor of two smaller than that which is obtained from analyses of strong interaction observables. These results are in quantitative agreement with Ref. [34].

A fit to the linear extrapolation of the lattice data; viz., to the boxes in Fig. 1, gives a significantly larger value [26]: $-\langle\bar{q}q\rangle^0_{1\,\mathrm{GeV}} = (0.270 \pm 0.027\,\mathrm{GeV})^3$. However, the error is purely statistical. The systematic error, to which the linear extrapolation must contribute, was not estimated. That may be important given the discrepancy, conspicuous in Fig. 1, between our direct evaluation of the chiral limit mass function and the linear extrapolation of the lattice data to $am = 0$: the linear extrapolation lies well above the result of our chiral limit calculation.

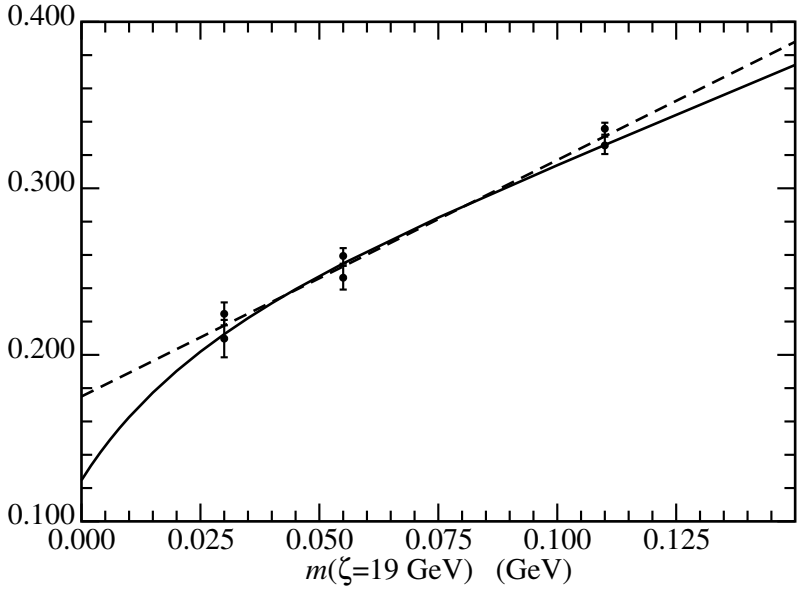

Figure 5: $M(p^2_{\rm IR} = 0.38\,{\rm GeV}^2)$, in GeV, as a function of the current-quark mass. Solid curve, our result; circles, lattice data for am in Eq. (amvalues) [26]; dashed-line, linear fit to the lattice data, Eq. (3.27).

This point may be illustrated further. In Fig. 5 we plot $M(p^2 = p^2_{\rm IR})$, where $p_{\rm IR} = 0.62\,{\rm GeV}$, as a function of the current-quark mass (*solid curve*). This value of the argument was chosen because it is the smallest p^2 for which there are two lattice results for $M(p^2)$ at each current-quark mass in Eq. (3.12). Those results are also plotted in the figure. It is evident that on the domain of current-quark masses directly accessible in lattice simulations, the lattice and DSE results lie on the same linear trajectory, of which

$$M(p^2_{\rm IR} = 0.38\,{\rm GeV}^2, m(\zeta)) = 0.18 + 1.42\,m(\zeta) \tag{3.27}$$

provides an adequate interpolation. However, as apparent in the figure, this fit on $am \in [0.018, 0.072]$ provides a poor extrapolation to $m(\zeta) = 0$, giving a result 40% too large.

In Fig. 6 we repeat this procedure, focusing solely on our value of $M(p^2 = 0)$ because directly calculated lattice data are unavailable at this extreme infrared point and published estimates obtained by extrapolating functions fitted to the lattice-p^2-dependence

are inconsistent [25]. The pattern observed in Fig. 5 is again visible. On the domain of current-quark masses for which lattice data are available, the mass-dependence of $M(p^2)$ is well-approximated by a straight line; namely,

$$M(p^2 = 0, m(\zeta)) = 0.37 + 0.68\, m(\zeta)\,, \tag{3.28}$$

but the value of $M(0)$ determined via extrapolation to $m(\zeta) = 0$ is 14% too large.

In all cases our calculated result possesses significant curvature. At fixed p^2, $M(p^2, m(\zeta))$ is a monotonically increasing function of $m(\zeta)$ but, while it is concave-down for $m(\zeta) \lesssim 0.1\,\mathrm{GeV}$, it inflects thereafter to become concave-up. In addition, at fixed $m(\zeta)$, $M(p^2)$ is a monotonically decreasing function of p^2. It follows that a linear extrapolation determined by data on $am \in [0.018, 0.072]$ will necessarily overestimate $M(p^2)$ at all positive values of p^2. The figures illustrate that the error owing to extrapolation increases with increasing p^2 and hence a significant overestimate can be anticipated on the domain in which the condensate was inferred from lattice data.

It is straightforward to understand the behaviour evident in Figs. 5, 6 qualitatively. The existence of DCSB means that in the neighbourhood of the chiral limit a mass-scale other than the current-quark mass determines the magnitude of $M(p^2)$. As the current-quark mass increases from zero, its magnitude will come to affect that of the mass function. The gap equation is a nonlinear integral equation and hence this evolution of the mass-dependence of $M(p^2)$ will in general be nonlinear. Only at very large values of the current-quark mass will this scale dominate the behaviour of the mass function, as seen in studies of heavy-quark systems [44], and the evolution become linear.

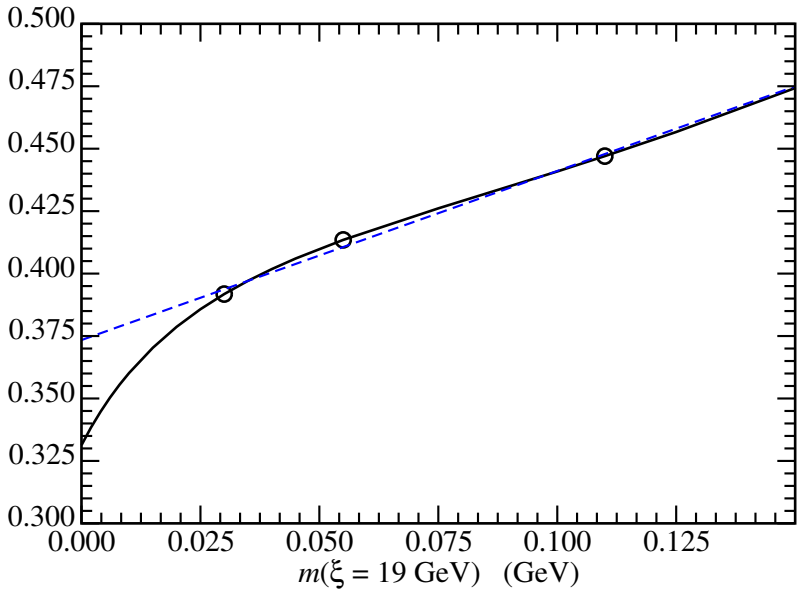

Figure 6: Solid curve, calculated $M(p^2 = 0)$, in GeV, as a function of the current-quark mass $m(\zeta)$. The circles mark the current-quark masses in Eq. (3.12). Dashed-line, linear interpolation of our result for $M(p^2 = 0)$ on this mass domain.

3.7 *Pion properties*

The renormalised homogeneous Bethe-Salpeter equation (BSE) for the isovector-pseudoscalar channel; i.e., the pion, is

$$\left[\Gamma^j_\pi(k;P)\right]_{tu} = \int_q^\Lambda [\chi^j_\pi(q;P)]_{sr}\, K^{rs}_{tu}(q,k;P)\,, \tag{3.29}$$

where k is the relative momentum of the quark-antiquark pair, P is their total momentum; and

$$\chi^j_\pi(q;P) = S(q_+)\Gamma^j_\pi(q;P)S(q_-)\,, \tag{3.30}$$

with $\Gamma^j_\pi(k;P)$ the pion's Bethe-Salpeter amplitude, which has the general form

$$\begin{aligned}\Gamma^j_\pi(k;P) = \tau^j\gamma_5 \Big[& iE_\pi(k;P) + \gamma\cdot P F_\pi(k;P) \\ + \quad & \gamma\cdot k\, k\cdot P\, G_\pi(k;P) + \sigma_{\mu\nu}\, k_\mu P_\nu\, H_\pi(k;P)\Big].\end{aligned} \tag{3.31}$$

In Eq. (3.29), $K(q,k;P)$ is the fully-amputated quark-antiquark scattering kernel, and the axial-vector Ward-Takahashi identity requires that this kernel and that of the gap

equation must be intimately related. The consequences of this are elucidated in Refs. [40, 41] and in the present case they entail

$$K^{rs}_{tu}(q,k;P) = -\mathcal{G}((k-q)^2) \\ \times D^{\rm free}_{\mu\nu}(q-k)\, \left[\frac{\lambda^a}{2}\gamma_\mu\right]_{ts} \left[\frac{\lambda^a}{2}\gamma_\nu\right]_{ru}, \tag{3.32}$$

which provides the renormalisation-group-improved ladder-truncation of the BSE. The efficacy of combining the renormalisation-group-improved rainbow-DSE and ladder-BSE truncations is exhibited in Ref. [4]. In particular, it guarantees that in the chiral limit the pion is both a Goldstone mode and a bound state of a strongly dressed quark and antiquark, and ensures consistency with chiral low energy theorems [45, 77].

All the elements involved in building the kernel of the pion's BSE were determined in the last section and hence one can solve for the pion's mass and Bethe-Salpeter amplitude. To complete this exercise practically we consider

$$[1-\ell(P^2)]\, \left[\Gamma^j_5(k;P)\right]_{tu} = \int_q^\Lambda [\chi^j_5(q;P)]_{sr}\, K^{rs}_{tu}(q,k;P)\,. \tag{3.33}$$

This equation has a solution for arbitrary P^2 and solving it one obtains a trajectory $\ell(P^2)$ whose first zero coincides with the bound state's mass, at which point $\Gamma^j_5(k;P)$ is the true bound state amplitude. In general, solving for $\ell(P^2)$ in the physical domain: $P^2 < 0$, requires that the integrand be evaluated at complex values of its argument. However, as $m_\pi^2 \ll M^2(0)$; i.e., the magnitude of the zero is much smaller than the characteristic dynamically-generated scale in this problem, we avoid complex arguments by adopting the simple expedient of calculating $\ell(P^2 > 0)$ and extrapolating to locate its timelike zero. The Bethe-Salpeter amplitude is identified with the $\ell(P^2 = 0)$ solution. Naturally, this expedient yields the exact solution in the chiral limit; and in cases where a comparison with the exact solution has been made for realistic, nonzero light-quark masses, the error is negligible [78], as we shall subsequently illustrate.

	Calc. (quenched)	Experiment
m_π	0.1385	0.1385
f_π	0.066	0.0924
f_π^0	0.063	

Table 1: Pion-related observables calculated using our lattice-constrained effective interaction. $m(\zeta = 19\,\mathrm{GeV}) = 3.3\,\mathrm{MeV}$ was chosen to give $m_\pi = 0.1395\,\mathrm{GeV}$. The index "0" indicates a quantity obtained in the chiral limit.

Once its mass and bound state amplitude are known, it is straightforward to calculate the pion's leptonic decay constant [43]:

$$f_\pi\,\delta^{ij}\,2\,P_\mu = Z_2\,\mathrm{tr}\int_q^\Lambda \tau^i\gamma_5\gamma_\mu\chi_\pi^j(q;P)\,. \tag{3.34}$$

In this expression, the factor of Z_2 is crucial: it ensures the result is gauge invariant, and cutoff and renormalisation-point independent. (The Bethe-Salpeter amplitude is normalised canonically [79].)

Table 1 lists values of pion observables calculated using the effective interaction obtained by fitting the quenched-QCD lattice data. (The nonzero current-quark mass in the table corresponds to a one-loop evolved value of $m(1\,\mathrm{GeV}) = 5.0\,\mathrm{MeV}$.) To aid with the consideration of these results we note that unquenched chiral-limit DSE calculations that accurately describe hadron observables give [30] $f_\pi^0 = 0.090\,\mathrm{GeV}$. We infer from these results that the pion decay constant in quenched lattice-QCD is underestimated by 30%. Quantitatively equivalent results were found in Ref. [34].

The rainbow-ladder truncation of the gap and Bethe-Salpeter equations is chiral symmetry preserving: without fine-tuning it properly represents the consequences of chiral symmetry and its dynamical breaking. The truncation expresses the model-independent mass formula for flavor-nonsinglet pseudoscalar mesons [43] a corollary of which, at small current-quark masses, is the Gell–Mann–Oakes–Renner relation:

$$(f_\pi^0)^2\,m_\pi^2 = -2\,m(\zeta)\,\langle\bar{q}q\rangle_\zeta^0 + O(m^2(\zeta))\,. \tag{3.35}$$

Inserting our calculated values on the l.h.s. and r.h.s. of Eq. (3.35), we have

$$(0.093\,\mathrm{GeV})^4 \text{ cf. } (0.091\,\mathrm{GeV})^4; \tag{3.36}$$

viz, the same accuracy seen in exemplary coupled DSE-BSE calculations; e.g., Ref. [29]. This establishes the fidelity of our expedient for solving the BSE.

Chapter 4

Algebraic model for the dressed quark-gluon vertex

Dyson-Schwinger equation predictions for the behaviour of dressed-gluon [27, 85, 86] and dressed-quark propagators [29] have been confirmed in recent numerical simulations of lattice-regularised QCD [87, 88]. Indeed, detailed study provides an understanding of the circumstances in which pointwise agreement is obtained [38, 39]. This level of sophistication does not prevail with the dressed-quark-gluon vertex, however. Acquiring that is a realisable contemporary goal, and it is to aspects of this task that we address ourselves herein.

4.1 *Dressed quark-gluon vertex and the gap equation*

This three-point Schwinger function can be calculated in perturbation theory but, since we are interested in the role it plays in connection with confinement, DCSB and bound state properties, that is inadequate for our purposes: these phenomena are essentially nonperturbative.

Instead we begin by observing that the dressed vertex can be written

$$i\Gamma^a_\mu(p,q) = \frac{i}{2}\lambda^a\,\Gamma_\mu(p,q) =: l^a\,\Gamma_\mu(p,q)\,; \tag{4.1}$$

viz., the colour structure factorises, and that twelve Lorentz invariant functions are required to completely specify the remaining Dirac-matrix-valued function; i.e.,

$$\begin{aligned}\Gamma_\mu(p,q) &= \gamma_\mu\,\hat{\Gamma}_1(p,q) + \gamma\cdot(p+q)\,(p+q)_\mu\,\hat{\Gamma}_2(p,q)\\ &\quad -i(p+q)_\mu\,\hat{\Gamma}_3(p,q) + [\ldots],\end{aligned} \tag{4.2}$$

where the ellipsis denotes contributions from additional Dirac matrix structures that play no part herein. Since QCD is renormalisable, the bare amplitude associated with γ_μ is the only function in Eq. (4.2) that exhibits an ultraviolet divergence at one-loop in perturbation theory.

The requirement that QCD's action be invariant under local colour gauge transformations entails[2] [89]

$$\begin{aligned} & k_\mu \, i\Gamma_\mu(p,q) = \\ & \quad \mathcal{F}^g(k^2) \, \left\{ [1 - B(p,q)] \, S(p)^{-1} - S(q)^{-1} \, [1 - B(p,q)] \right\}, \end{aligned} \tag{4.3}$$

wherein $\mathcal{F}^g(k^2)$, $k = p - q$, is the dressing function that appears in the renormalised covariant-gauge ghost propagator:

$$D^g(k^2,\zeta^2) = - \frac{\mathcal{F}^g(k^2,\zeta^2)}{k^2}, \tag{4.4}$$

and $B(p,q)$ is the renormalised ghost-quark scattering kernel. At one-loop order on the domain in which perturbation theory is a valid tool

$$\mathcal{F}^g(k^2,\zeta^2) = \left[\frac{\alpha(k^2)}{\alpha(\zeta^2)} \right]^{\gamma_g/\beta_1}, \tag{4.5}$$

with the anomalous dimensions $\gamma_g = -(3/8)\, C_2(G)$ in Landau gauge, which we use throughout, and $\beta_1 = -(11/6)\, C_2(G) + (1/3)\, N_f$, where $C_2(G) = N_c$ and N_f is the number of active quark flavours. This result may be summarised as $\mathcal{F}^g(k^2) \approx 1$ on the perturbative domain, up to $\ln p^2/\Lambda^2_{\rm QCD}$-corrections. In a similar sense, $B(p,q) \approx 0$ in Landau gauge on this domain.[3]

[2] NB. Equation (4.3) is equally valid when expressed consistently in terms of bare Schwinger functions.

[3] An even closer analogy is a kindred result for $Z(p^2)$ in Eq. (2.21); viz., in Landau gauge $[1 - Z(p^2,\zeta^2)] \equiv 0$ at one loop in perturbation theory and hence, on the perturbative domain, corrections to this result are modulated by $\ln\ln p^2/\Lambda^2_{\rm QCD}$. This very slow evolution is exhibited, e.g., in the numerical results of Ref. [14].

Equation (4.3) is a Slavnov-Taylor identity, one of a countable infinity of such relations in QCD, and it is plainly an extension of the Ward-Takahashi identity that applies to the fermion-photon vertex. The Ward-Takahashi identity entails that in the vertex describing the coupling of a photon to a dressed-quark:

$$\hat{\Gamma}^{\gamma}_1(p,p) = A(p^2,\zeta^2)\,, \tag{4.6}$$

$$\hat{\Gamma}^{\gamma}_2(p,p) = 2\,\frac{d}{dp^2}\,A(p^2,\zeta^2)\,, \tag{4.7}$$

$$\hat{\Gamma}^{\gamma}_3(p,p) = 2\,\frac{d}{dp^2}\,B(p^2,\zeta^2)\,. \tag{4.8}$$

Identifying and understanding this nontrivial structure of the dressed-quark-photon vertex has been crucial in describing the electromagnetic properties of mesons [90, 92, 91, 93].

The similarity between the Slavnov-Taylor and Ward-Takahashi identities has immediate, important consequences. For example, if the result

$$0 < \mathcal{F}^g(k^2)\,[1 - B(p,q)] < \infty \tag{4.9}$$

also prevails on the nonperturbative domain then, because of the known behaviour of the dressed-quark propagator, Eq. (4.9) is sufficient grounds for Eq. (4.3) to forecast that in the renormalised dressed-quark-gluon vertex

$$1 < \hat{\Gamma}_1(p,p) < \infty \tag{4.10}$$

at infrared spacelike momenta. This result, an echo of Eq. (4.6), signals that the complete kernel in the DSE satisfied by $\Gamma^a_\mu(p,q)$ is attractive on the nonperturbative domain. The ability to use the gap equation to make robust statements about DCSB rests on the existence of a systematic nonperturbative and chiral symmetry preserving truncation scheme. One such scheme was introduced in Ref. [40]. It may be described as a dressed-loop expansion of the dressed-quark-gluon vertex wherever it appears in the half amputated

dressed-quark-antiquark (or -quark-quark) scattering matrix: S^2K, a renormalisation-group invariant, where K is the dressed-quark-antiquark (or -quark-quark) scattering kernel. Thereafter, all n-point functions involved in connecting two particular quark-gluon vertices are *fully dressed*.

The effect of this truncation in the gap equation, Eq. (2.20), is realised through the following representation of the dressed-quark-gluon vertex [41]

$$Z_1\,\Gamma_\mu(k,p) = \gamma_\mu + \mathcal{L}_2^-(k,p) + \mathcal{L}_2^+(k,p) + [\ldots]\,, \tag{4.11}$$

with

$$\begin{aligned}\mathcal{L}_2^-(k,p) &= \frac{1}{2N_c}\int_\ell^\Lambda g^2 D_{\rho\sigma}(p-\ell) \\ &\quad\times\gamma_\rho S(\ell+k-p)\gamma_\mu S(\ell)\gamma_\sigma\,, \qquad (4.12)\\ \mathcal{L}_2^+(k,p) &= \frac{N_c}{2}\int_\ell^\Lambda g^2\, D_{\sigma'\sigma}(\ell)\, D_{\tau'\tau}(\ell+k-p) \\ &\quad\times\gamma_{\tau'}\, S(p-\ell)\,\gamma_{\sigma'}\,\Gamma^{3g}_{\sigma\tau\mu}(\ell,-k,k-p)\,, \qquad (4.13)\end{aligned}$$

wherein Γ^{3g} is the dressed-three-gluon vertex. It is apparent that the lowest order contribution to each term written explicitly is $\mathrm{O}(g^2)$. The ellipsis in Eq. (4.11) represents terms whose leading contribution is $\mathrm{O}(g^4)$; e.g., crossed-box and two-rung dressed-gluon ladder diagrams, and also terms of higher leading-order.

The $\mathcal{L}_2^-$ term in Eq. (4.11) only differs from a kindred term in QED by the colour factor. However, that factor is significant because it flips the sign of the interaction in this channel with respect to QED; i.e., since

$$\begin{aligned} l^a\, l^b\, l^a &= \left\{\frac{1}{2}\,C_2(G) - \,C_2(R)\right\} l^b = \frac{1}{2N_c}\, l^b \\ \text{cf.}\qquad l^a\,\mathbf{1}_c\, l^a &= -\,C_2(R)\,\mathbf{1}_c = -\frac{N_c^2-1}{2N_c}\,\mathbf{1}_c\,, \end{aligned} \tag{4.14}$$

then single gluon exchange between a quark and antiquark is repulsive in the colour-octet channel. Attraction in the octet channel is provided by the $\mathcal{L}_2^+$ term in Eq. (4.11),

which involves the three-gluon vertex. These observations emphasise that Eq. (4.3) cannot be satisfied if the contribution from the three gluon vertex is neglected because the Slavnov-Taylor identity signals unambiguously that on the perturbative domain there is net attraction in the octet channel.

It is apparent, too, that the term involving the three gluon vertex is numerically amplified by a factor of N_c^2 cf. the $\mathcal{L}_2^-$ (Abelian-like) vertex correction. Hence, if the integrals are of similar magnitude then the N_c^2-enhanced three-gluon term must dominate in the octet channel. This expectation is borne out by the one-loop perturbative calculation of the two integrals exhibited in Eqs. (4.12), (4.13) and, moreover, the sum of both terms is precisely that combination necessary to satisfy the Slavnov-Taylor identity at this order [94].

4.2 *Vertex and interaction model*

In illustrating features of the nonperturbative and symmetry preserving DSE truncation scheme introduced in Ref. [40] in connection, for example, with DCSB, confinement and bound state structure, Ref. [41] employed a dressed-quark-gluon vertex obtained by resumming a subclass of diagrams based on $\mathcal{L}_2^-$ alone; namely, the vertex obtained as a solution of

$$\begin{aligned}\Gamma^-_\mu(k_+,k_-) &= Z_1^{-1}\gamma_\mu + \frac{1}{2N_c}\int_\ell^\Lambda g^2 D_{\rho\sigma}(p-\ell) \\ &\quad \times \gamma_\rho S(\ell_+)\Gamma^-_\mu(\ell_+,\ell_-)S(\ell_-)\gamma_\sigma\,. \end{aligned} \tag{4.15}$$

It was acknowledged that this subclass of diagrams is $1/N_c$-suppressed but, in the absence of nonperturbative information about $\mathcal{L}_2^+$ in general, and the dressed-three-gluon vertex in particular, this limitation was accepted.

Herein we explore a model that qualitatively ameliorates this defect while preserving characteristics that make calculations tractable and results transparent; viz., in Eq. (4.11)

we write

$$\mathcal{L}_2^- + \mathcal{L}_2^+ \approx \mathcal{L}_2^{\mathcal{C}}\,, \tag{4.16}$$

where

$$\begin{aligned}\mathcal{L}_2^{\mathcal{C}}(k,p) := &-\mathcal{C}\,C_2(R)\int_\ell^\Lambda g^2 D_{\rho\sigma}(p-\ell)\\ &\times\,\gamma_\rho S(\ell+k-p)\gamma_\mu S(\ell)\gamma_\sigma\,,\end{aligned} \tag{4.17}$$

and work with the vertex obtained as the solution of

$$\begin{aligned}\Gamma_\mu^{\mathcal{C}}(k_+,k_-) = Z_1^{-1}\gamma_\mu - &\,\mathcal{C}\,C_2(R)\int_\ell^\Lambda g^2 D_{\rho\sigma}(p-\ell)\\ &\times\,\gamma_\rho S(\ell_+)\Gamma_\mu^{\mathcal{C}}(\ell_+,\ell_-)S(\ell_-)\gamma_\sigma\,.\end{aligned} \tag{4.18}$$

To explain this model we remark that the parameter $\mathcal{C}$ is a global coupling strength modifier. (NB. The value $\mathcal{C} = -(1/8)$ reproduces the vertex resummed in Ref. [41].) It is introduced so that our *Ansatz* may *mimic* the effects of attraction in the colour-octet channel without specifying a detailed form for the three-gluon vertex. This expedient will give a faithful model so long as the integrals over the momentum dependence of $\mathcal{L}_2^-$ and $\mathcal{L}_2^+$ that appear in our calculations are not too dissimilar. This is plausible because: they are both one-loop integrals projected onto the same Dirac and Lorentz structure and hence are pointwise similar at this order in perturbation theory; and their direct sum must conspire to give the simple momentum dependence in Eq. (4.3). Moreover, as we shall demonstrate, the model has material illustrative capacity and that alone is sufficient justification for proceeding.

As we have already noted, the value $\mathcal{C} = -(1/8)$ corresponds to completely neglecting the three-gluon vertex term. There is also another particular reference case; namely, $\mathcal{C} = 1$. In this case a dressed-quark propagator obtained as the solution of the rainbow truncation

of the gap equation:

$$S_R(p)^{-1} = Z_2\,(i\gamma\cdot p + m^{\rm bm}) + \int_q^\Lambda g^2 D_{\mu\nu}(p-q)\,\frac{\lambda^a}{2}\gamma_\mu\,S_R(q)\,\frac{\lambda^a}{2}\gamma_\nu\,, \tag{4.19}$$

when inserted in Eq. (4.18), yields a vertex $\Gamma^{\mathcal{C}R}_\mu(k,p)$ that satisfies

$$(k-p)_\mu\,i\Gamma^{\mathcal{C}R}_\mu(k,p) = S_R(k)^{-1} - S_R(p)^{-1}\,; \tag{4.20}$$

viz., a Ward-Takahashi identity. This is not materially useful, however, because herein we will seek and work with a dressed-quark propagator that is not a solution of Eq. (4.19) but rather a solution of Eq. (2.20) with a fully dressed vertex, and that vertex, determined self consistently, will not in general satisfy Eq. (4.20).

4.2.1 Interaction model

A simplification, important to our further analysis, is a confining model of the dressed-gluon interaction in Eq. (4.18). We use [42]

$$\mathcal{D}_{\mu\nu}(k) := g^2\,D_{\mu\nu}(k) = \left(\delta_{\mu\nu} - \frac{k_\mu k_\nu}{k^2}\right)(2\pi)^4\,\mathcal{G}^2\,\delta^4(k)\,. \tag{4.21}$$

The constant $\mathcal{G}$ sets the model's mass-scale and henceforth we mainly set $\mathcal{G}=1$ so that all mass-dimensioned quantities are measured in units of $\mathcal{G}$. Furthermore, since the model is ultraviolet-finite, we will usually remove the regularisation mass-scale to infinity and set the renormalisation constants equal to one.

In these things we follow Ref. [41]. In addition, we reiterate that the model defined by Eq. (4.21) is a precursor to an efficacious class of models that employ a renormalisation-group-improved effective interaction and whose contemporary application is reviewed in Refs. [2, 3, 4]. It has many features in common with that class and, in addition, its distinctive momentum-dependence works to advantage in reducing integral equations to

algebraic equations that preserve the character of the original. There is naturally a drawback: the simple momentum dependence also leads to some model-dependent artefacts, but they are easily identified and hence not cause for concern.

4.3 *Algebraic vertex and gap equations*

If Eq. (4.21) is used in Eq. (4.18) then that part of the vertex which acts in the gap equation has no dependence on the total momentum of the quark -antiquark pair; i.e., only $\Gamma^{\mathcal{C}}_\mu(p) := \Gamma^{\mathcal{C}}_\mu(p,p)$ contributes. In this case just the terms written explicitly in Eq. (4.2) are supported in our model for the dressed vertex, which can be expressed

$$\Gamma^{\mathcal{C}}_\mu(p) = \gamma_\mu\, \alpha^{\mathcal{C}}_1(p^2) + \gamma\cdot p\, p_\mu\, \alpha^{\mathcal{C}}_2(p^2) - i p_\mu\, \alpha^{\mathcal{C}}_3(p^2)\,. \tag{4.22}$$

This is not a severe handicap because these Dirac structures are precisely those which dominate in Eq. (4.3) if $B(p,q)$ is not materially enhanced nonperturbatively. The vertex equation is

$$\Gamma^{\mathcal{C}}_\mu(p) = \gamma_\mu - \mathcal{C}\,\gamma_\rho\, S(p)\,\Gamma^{\mathcal{C}}_\mu(p)\, S(p)\,\gamma_\rho\,, \tag{4.23}$$

where we have used the fact that $C_2(R) = 4/3$ when $N_c = 3$.

Our analysis now mirrors that of Ref. [41]. The solution of Eq. (4.23) is:

$$\Gamma^{\mathcal{C}}_\mu(p) = \sum_{i=0}^{\infty} \Gamma^{\mathcal{C}}_{\mu,i}(p) \tag{4.24}$$

$$= \sum_{i=0}^{\infty} \left[\gamma_\mu\, \alpha^{\mathcal{C}}_{1,i}(p^2) \,+\, \gamma\cdot p\, p_\mu\, \alpha^{\mathcal{C}}_{2,i}(p^2) - \, i\, p_\mu\, \alpha^{\mathcal{C}}_{3,i}(p^2)\right], \tag{4.25}$$

where $\Gamma^{\mathcal{C}}_{\mu,i}(p)$ satisfies a recursion relation:

$$\Gamma^{\mathcal{C}}_{\rho,i+1}(p) = -\mathcal{C}\,\gamma_\mu\, S(p)\,\Gamma^{\mathcal{C}}_{\rho,i}(p)\, S(p)\,\gamma_\mu\,, \tag{4.26}$$

with $\Gamma^{\mathcal{C}}_{\mu,i=0} = \gamma_\mu$, the bare vertex, so that

$$\alpha^{\mathcal{C}}_{1,0} = 1\,,\ \alpha^{\mathcal{C}}_{2,0} = 0 = \alpha^{\mathcal{C}}_{3,0}\,. \tag{4.27}$$

In concert with Eq. (4.25), Eq. (4.26) yields an algebraic matrix equation ($s = p^2$)

$$\boldsymbol{\alpha}^{\mathcal{C}}_{i+1}(s) := \begin{pmatrix} \alpha^{\mathcal{C}}_{1,i+1}(s) \\ \alpha^{\mathcal{C}}_{2,i+1}(s) \\ \alpha^{\mathcal{C}}_{3,i+1}(s) \end{pmatrix} = \mathcal{O}^{\mathcal{C}}(s;A,B)\,\boldsymbol{\alpha}^{\mathcal{C}}_{i}(s)\,, \tag{4.28}$$

where ($\Delta(s) = sA^2(s) + B^2(s)$)

$$\mathcal{O}^{\mathcal{C}}(s;A,B) = \\ -\frac{2\mathcal{C}}{\Delta^2}\begin{pmatrix} -\Delta & 0 & 0 \\ 2A^2 & sA^2 - B^2 & 2AB \\ 4AB & 4sAB & 2(B^2 - sA^2) \end{pmatrix}. \tag{4.29}$$

It follows from Eqs. (4.25) and (4.28) that

$$\boldsymbol{\alpha}^{\mathcal{C}} = \left(\sum_{i=0}^{\infty} \left[\mathcal{O}^{\mathcal{C}}\right]^i\right) \boldsymbol{\alpha}^{\mathcal{C}}_0 = \frac{1}{1-\mathcal{O}^{\mathcal{C}}}\,\boldsymbol{\alpha}^{\mathcal{C}}_0 \tag{4.30}$$

and hence, using Eq. (4.29),

$$\alpha^{\mathcal{C}}_1 = \frac{\Delta}{\Delta - 2\mathcal{C}}\,, \tag{4.31}$$

$$\alpha^{\mathcal{C}}_2 = -\frac{4\mathcal{C}A^2}{\Delta^2 + 2\mathcal{C}(B^2 - sA^2) - 8\mathcal{C}^2}\frac{(\Delta - 4\mathcal{C})}{(\Delta - 2\mathcal{C})}\,, \tag{4.32}$$

$$\alpha^{\mathcal{C}}_3 = -\frac{8\mathcal{C}AB}{\Delta^2 + 2\mathcal{C}(B^2 - sA^2) - 8\mathcal{C}^2}\,. \tag{4.33}$$

With these equations one has a closed form for the dressed-quark-gluon vertex.

It is evident that the momentum dependence of the vertex is completely determined by that of the dressed-quark propagator whose behaviour, however, the vertex itself influences because it appears in the gap equation:

$$S(p)^{-1} = i\gamma\cdot p + m + \gamma_\mu S(p)\Gamma^{\mathcal{C}}_\mu(p)\,. \tag{4.34}$$

Subject to Eq. (4.22), the gap equation expresses two coupled algebraic equations:

$$A(s) = 1 + \frac{1}{sA^2 + B^2}\left[A\left(2\alpha_1^{\mathcal{C}} - s\alpha_2^{\mathcal{C}}\right) - B\,\alpha_3^{\mathcal{C}}\right], \tag{4.35}$$

$$B(s) = m + \frac{1}{sA^2 + B^2}\left[B\left(4\alpha_1^{\mathcal{C}} + s\alpha_2^{\mathcal{C}}\right) - sA\,\alpha_3^{\mathcal{C}}\right]. \tag{4.36}$$

The dressed-quark propagator and -quark-gluon vertex follow from the solution of these equations, which is generally obtained numerically.

In the chiral limit, which here is simply implemented by setting $m = 0$, a realisation of chiral symmetry in the Wigner-Weyl mode is always possible: it corresponds to the $B \equiv 0$ solution of the gap equation. However, since the phenomena of QCD are built on a Nambu-Goldstone realisation of chiral symmetry, we do not consider the Wigner-Weyl mode any further. Its characterisation can be achieved in a straightforward manner by adapting the analysis of Ref. [41] to our improved vertex model.

4.4 *Algebraic results*

At this point some observations are useful in order to establish a context for our subsequent results. To begin we explore the ultraviolet behaviour of the model. It is ultraviolet finite and hence at large spacelike momenta, $s \gg 1$ (in units of $\mathcal{G}^2$)

$$A(s) \approx 1 + \frac{\mathrm{a}_1}{s}, \qquad B(s) \approx m + \frac{\mathrm{b}_1}{s}, \tag{4.37}$$

with m the model's finite current-quark mass. The model is useful because these results persist in asymptotically free theories, up to $\ln p^2/\Lambda_{\rm QCD}^2$-corrections. With this behaviour

it follows from Eqs. (4.31) – (4.37) that

$$\alpha_1^{\mathcal{C}}(s) \approx 1 + \frac{2\mathcal{C}}{s}\,, \tag{4.38}$$

$$\alpha_2^{\mathcal{C}}(s) \approx -\frac{4\mathcal{C}}{s^2}\,, \tag{4.39}$$

$$\alpha_3^{\mathcal{C}}(s) \approx -\,m\,\frac{8\mathcal{C}}{s^2}\,, \tag{4.40}$$

and these results in turn mean that in the ultraviolet the behaviour of the massive dressed-quark propagator is determined by the α_1 term in the vertex, so that

$$\underline{\mathrm{a}}_1 = 2\,,\ \underline{\mathrm{b}}_1 = 4\,m\,. \tag{4.41}$$

The expansion of $\alpha_1(s)$ around $1/s = 0$ reported in Eq. (4.38) is the same as that which arises in QCD, apart from the usual $\ln(s/\Lambda^2_{\rm QCD})$- corrections. However, the leading terms in $\alpha_{2,3}$ are different: on the perturbative domain in QCD these functions both begin with a term of order $(1/s)[\ln(s/\Lambda^2_{\rm QCD})]^d$, with d some combination of anomalous dimensions. The reason for the mismatch is readily understood. At one-loop order in QCD

$$B(p^2) = \hat{m}\,\left[\frac{1}{2}\ln(p^2/\Lambda^2_{\rm QCD})\right]^{\gamma_1^m/\beta_1}\,, \tag{4.42}$$

with $\hat{m}$ the renormalisation point invariant current-quark mass and $\gamma_1^m = (3/2)\,C_2(R)$. (This makes explicit the logarithmic correction to the leading term in Eq. (4.37).) For the purpose of this explanation then, on the perturbative domain, with $\mathcal{F}^g(k^2) \approx 1$ and $B(p,q) \approx 0$, the Slavnov-Taylor identity, Eq. (4.3), is approximately equivalent to the Ward-Takahashi identity. Hence, via Eq. (4.8),

$$\alpha_3(s) \approx \frac{\hat{m}}{s}\,\frac{\gamma_1^m}{\beta_1}\,\left[\frac{1}{2}\ln(p^2/\Lambda^2_{\rm QCD})\right]^{\gamma_1^m/\beta_1 - 1}\,. \tag{4.43}$$

It is thus evident that in QCD, even though they are not themselves divergent, the leading order terms in both $\alpha_{2,3}$ are induced by the momentum-dependent renormalisation of

elements contributing to their evaluation. Such terms are naturally missing in our ultraviolet finite model. The absence of $1/s$ terms in Eqs. (4.39) and (4.40) is therefore a model artefact.

We observe in addition that with attraction in the colour-octet channel; namely, for $\mathcal{C} > 0$, $(\alpha_1^{\mathcal{C}} - 1)$ is necessarily positive on the perturbative domain and $\alpha_{2,3}^{\mathcal{C}}$ are negative. These results are also true in QCD ($\alpha_1^{\mathcal{C}} > 1$ up to logarithmic corrections). It would be an exceptional result if these statements were not also true on the nonperturbative domain.

We now turn to the infrared domain and focus on $s = 0$ but consider $0 < m \ll 1$, in which case

$$A(s=0,m) \approx a_0^0 + a_0^1\, m\,,\; B(s=0,m) \approx b_0^0 + b_0^1\, m\,. \tag{4.44}$$

Upon insertion of these expressions into the gap equation one obtains

$$a_0^0 = 2\,\frac{2+3\mathcal{C}}{2+\mathcal{C}}\,,\; a_0^1 = -\sqrt{2}\,\frac{4+20\mathcal{C}+15\mathcal{C}^2}{(2+\mathcal{C})^{5/2}}\,, \tag{4.45}$$

$$b_0^0 = \sqrt{4+2\,\mathcal{C}}\,,\; b_0^1 = \frac{2}{(b_0^0)^2} = \frac{1}{2+\mathcal{C}}\,; \tag{4.46}$$

viz., results which show that in the neighbourhood of $s = 0$ and with attraction in the colour-octet channel, $A(s)$ decreases with increasing current-quark mass while $B(s)$ increases. At this order the mass function is

$$M(s=0,m) = \frac{B(0,m)}{A(0,m)} = \mu_0^0 + \mu_0^1\, m \tag{4.47}$$

with

$$\mu_0^0 = \frac{b_0^0}{a_0^0} \;=\; \frac{\sqrt{2}\,(2+\mathcal{C})^{\frac{3}{2}}}{4+6\,\mathcal{C}}\,, \tag{4.48}$$

$$\mu_0^1 = \frac{b_0^1}{a_0^0} - \frac{b_0^0\, a_0^1}{(a_0^0)^2} \;=\; \frac{6+23\,\mathcal{C}+15\,\mathcal{C}^2}{2\,(2+3\,\mathcal{C})^2}\,. \tag{4.49}$$

For $\mathcal{C} > -(1/3)$ the mass function also increases with rising m.

The infrared behaviour of the dressed-quark-gluon vertex follows immediately via Eqs. (4.31) – (4.33); using which one finds

$$\alpha_i^{\mathcal{C}}(s=0,m) \;\approx\; \mathrm{a}_{i,0}^{\mathcal{C}} + \mathrm{a}_{i,1}^{\mathcal{C}}\, m\,,\; i=1,2,3, \tag{4.50}$$

with

$$\mathrm{a}_{1,0}^{\mathcal{C}} = 1+\frac{\mathcal{C}}{2}\,, \tag{4.51}$$

$$\mathrm{a}_{1,1}^{\mathcal{C}} = -\frac{1}{\sqrt{8}}\,\frac{\mathcal{C}}{\sqrt{2+\mathcal{C}}}\,, \tag{4.52}$$

$$\mathrm{a}_{2,0}^{\mathcal{C}} = -\,\frac{\mathcal{C}(2-\mathcal{C})(2+3\mathcal{C})}{(2+\mathcal{C})^2}\,, \tag{4.53}$$

$$\mathrm{a}_{2,1}^{\mathcal{C}} = \frac{2\sqrt{2}\,\mathcal{C}\,\left(8+20\,\mathcal{C}+2\,\mathcal{C}^2-9\,\mathcal{C}^3\right)}{(2+\mathcal{C})^{7/2}}\,, \tag{4.54}$$

$$\mathrm{a}_{3,0}^{\mathcal{C}} = -\,\frac{\sqrt{8}\,\mathcal{C}}{\sqrt{2+\mathcal{C}}}\,, \tag{4.55}$$

$$\mathrm{a}_{3,0}^{\mathcal{C}} = \frac{2\,\mathcal{C}\,\left(5+6\,\mathcal{C}\right)}{\left(2+\mathcal{C}\right)^2}\,. \tag{4.56}$$

These algebraic formulae provide a clear indication of the effect on the dressed-quark-gluon vertex of attraction in the projection of the quark-antiquark scattering kernel onto the colour-octet channel. Attraction causes $\hat{\Gamma}_1(p,p)$ to be enhanced in the infrared cf. the bare vertex; and it drives $\hat{\Gamma}_{2,3}(p,p)$ to magnified, negative values. These results also signal that there are no surprises in the evolution into the infrared of the ultraviolet behaviour expressed in Eqs. (4.38) – (4.40): in each case attraction ensures that a current-quark mass acts to reduce the vertex function in magnitude.

4.5 ***Numerical results***

4.5.1 Numerical results

In choosing a value for $\mathcal{C}$ we elect to be guided by results from quenched lattice-QCD simulations of the dressed-quark propagator [88] and dressed-quark gluon vertex [37]. We focus on a current-quark mass common to both simulations; namely, 60 MeV, at which

value the lattice dressed-quark propagator has [38]: $Z_{\rm qu}(0) \approx 0.7$, $M_{\rm qu}(0) \approx 0.42$. Then, so as to work with dimensionless quantities, we set $m_{60} = 0.06/M_{\rm qu}(0)$ and, using Eqs. (4.44) – (4.56), require a least-squares fit to[4]

$$A(m_{60}) = 1.4\,, \tag{4.57}$$

$$\alpha_1^{\mathcal{C}}(0, m_{60}) = 2.1\,, \tag{4.58}$$

$$-M(0, m_{60})^2\, \alpha_2^{\mathcal{C}}(0, m_{60}) = 7.1\,, \tag{4.59}$$

$$-M(0, m_{60})\, \alpha_3^{\mathcal{C}}(0, m_{60}) = 1.0\,. \tag{4.60}$$

This procedure yields

$$\mathcal{C} = \bar{\mathcal{C}} = 0.51 \tag{4.61}$$

with an average relative error $\bar{r} = 25\%$ and standard deviation $\sigma_r = 70\%$. We note that for $\mathcal{C} = 0.6$: $\bar{r} = 21\%$, $\sigma_r = 72\%$, while for $\mathcal{C} = 0.4$: $\bar{r} = 31\%$, $\sigma_r = 67\%$. If one omits Eq. (4.59) from the fitting requirements then $\bar{\mathcal{C}} = 0.49$ with $\bar{r} = 2.5\,\%$ and $\sigma_r = 63\%$. It is evident that competing requirements bound the amount of attraction necessary in the kernel. We can now illustrate the results for the dressed-quark propagator and dressed-quark-gluon vertex.

A comparison of the curves in the upper panel of Fig. 7 shows clearly that the presence of net attraction in the colour-octet quark-antiquark scattering kernel uniformly increases the magnitude of $A(p^2)$ at all momenta. This effect is pronounced at infrared spacelike momenta and particularly on the timelike domain, $s < 0$. In this and the following figures $\mathcal{C} = 0$ corresponds to the rainbow-ladder DSE truncation; i.e., the leading order term of the truncation scheme introduced in Ref. [40].

In the lower panel one sees that on the spacelike domain, $s > 0$, the one-, two-, three- and four-loop corrected vertices yield a result for $A(p^2)$ that is little different from

[4] There is a confusion of positive and negative signs in Ref. [37] concerning λ_2, λ_3, as defined therein. Our signs are correct. With the conventions expressed in Eq. (4.22): $4\lambda_2 = -\alpha_2$ and $2\lambda_3 = \alpha_3$.

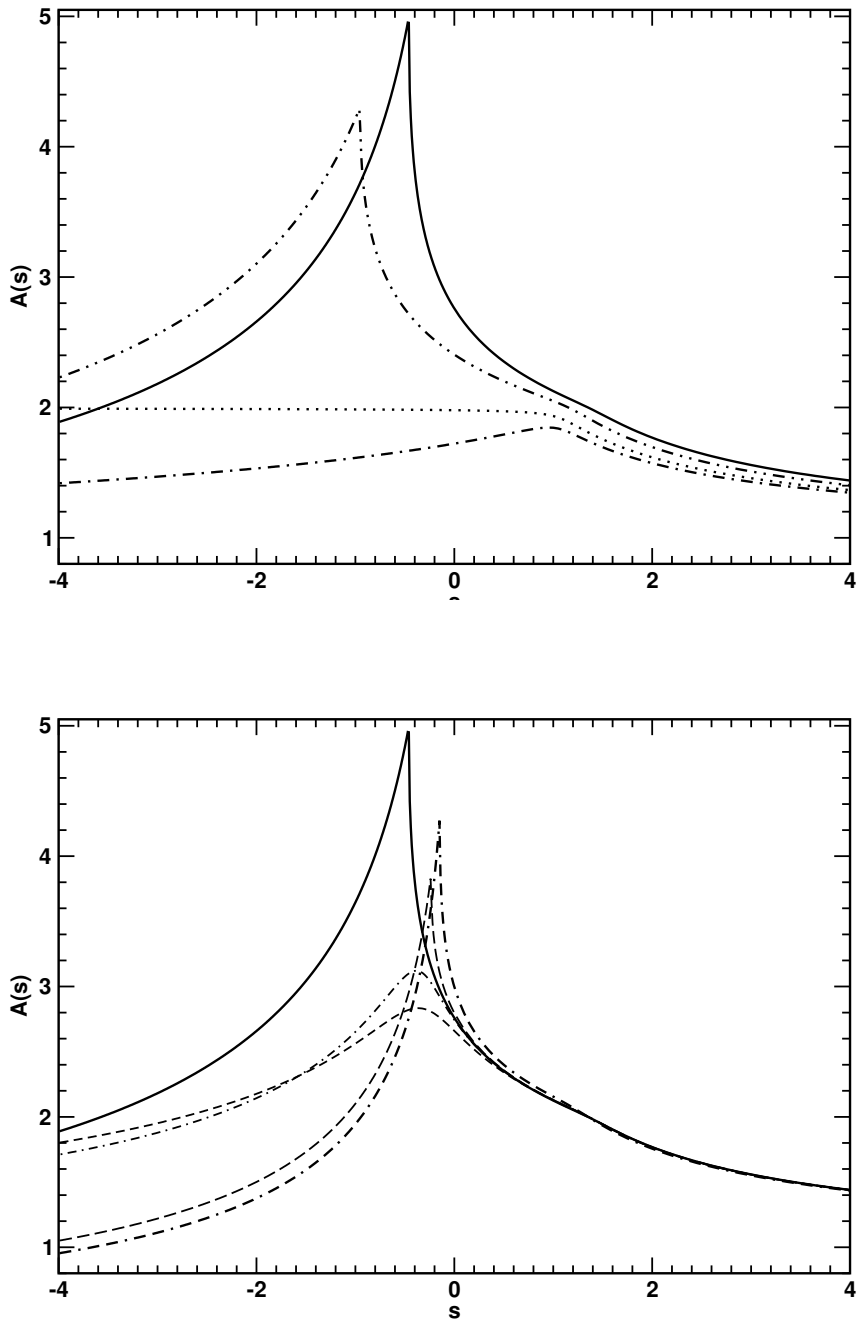

Figure 7: *Upper panel* – $\mathcal{C}$-dependence of $A(s)$. For all curves $m = 0.015$. Solid line: $\mathcal{C} = \bar{\mathcal{C}} = 0.51$; dash-dot-dot line: $\mathcal{C} = 1/4$; dotted line: $\mathcal{C} = 0$; and dash-dot curve: $\mathcal{C} = -1/8$. *Lower panel* – Truncation-dependence of $A(s)$, $\mathcal{C} = \bar{\mathcal{C}}$. Solid line: complete solution; dash-dash-dot line - result obtained with only the $i = 0, 1$ terms retained in Eq. (4.24), the one-loop corrected vertex; short-dash line - two-loop corrected; long-dash line - three-loop corrected; and short-dash-dot line: four-loop corrected. In this and subsequent figures, unless otherwise noted, dimensioned quantities are measured in units of $\mathcal{G}$ in Eq. (4.21). A fit to meson observables requires $\mathcal{G} = 0.69\,\mathrm{GeV}$ and hence $m = 0.015$ corresponds to 10 MeV.

that produced by the completely resummed vertex. However, that is not true on the timelike domain, whereupon confinement is expressed and hence nonperturbative effects become important. In our model confinement is realised via the absence of a particle-like singularity in the dressed-quark propagator [11]. The cusp displayed by $A(p^2)$ in the timelike domain is one manifestation of this feature. The figure shows that convergence to the solution obtained with the completely resummed vertex proceeds via two routes: one followed by solutions obtained with an odd number of loop corrections to the vertex; and another by those obtained using a vertex with an even number of corrections. This effect is absent with net repulsion in the colour-octet projection of the quark-antiquark scattering kernel.

We remark that $A(p^2)$ evolves slowly with the current-quark mass when that mass is significantly smaller than the model's mass-scale. However, when the current-quark mass becomes commensurate with or exceeds that mass-scale, it acts to very effectively dampen this function's momentum dependence so that $A(p^2) \approx 1$. This is also true in QCD.

We plot the dressed-quark mass function in Fig. 8. The existence of a nontrivial solution in the chiral limit is the realisation of DCSB, in our model and QCD. For current-quark masses less than the model's mass-scale, $\mathcal{G}$, the dynamically generated mass determines the scale of observables. However, for $m \gtrsim \mathcal{G}$, this explicit chiral symmetry breaking mass-scale overwhelms that generated dynamically and enforces $M(p^2) \approx m$. This is the behaviour of the b-quark mass function in QCD [44].

From a comparison of the rainbow-ladder result, $\mathcal{C} = 0$, in the lower panel with the $\mathcal{C} = -1/8$ and $\bar{\mathcal{C}} = 0.51$ results, it is apparent that vertex dressing driven by net attraction in the colour-octet scattering kernel reduces the magnitude of the mass function at infrared momenta, a trend which is reversed for spacelike momenta $s \gtrsim \mathcal{G}$. [5] This effect has an

[5] This pattern of behaviour is familiar from explorations [15, 17] of the effect in the gap equation of vertex *Ansätze* [5, 95]; i.e., vertex models whose diagrammatic content is unknown but which exhibit

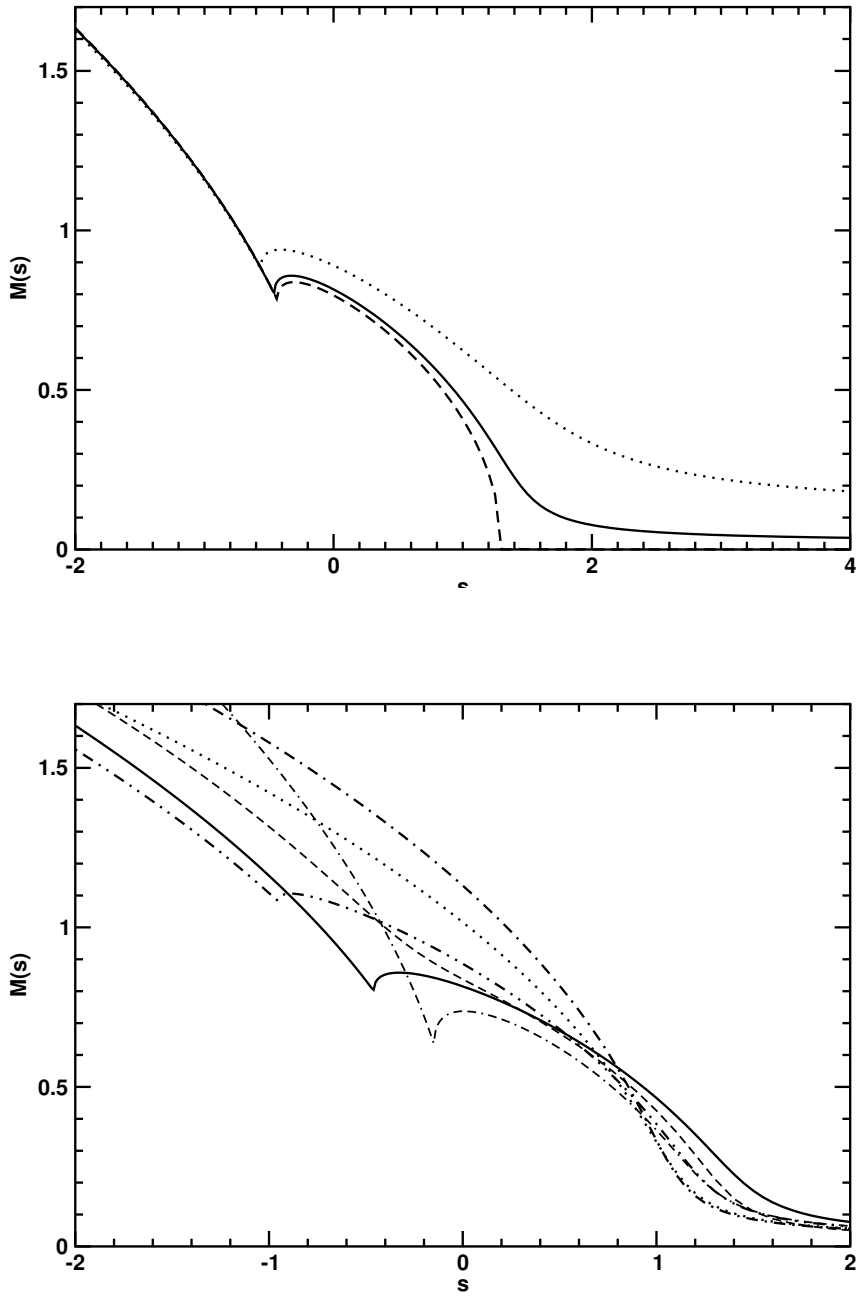

Figure 8: *Upper panel* – Current-quark-mass-dependence of the dressed-quark mass function. For all curves $\mathcal{C} = \bar{\mathcal{C}} = 0.51$. Dotted line: $m = m_{60}$; solid line: $m = 0.015$; dashed line: chiral limit, $m = 0$. *Lower panel* – $\mathcal{C}$-dependence of $M(s)$. For all curves $m = 0.015$. Solid line: $\mathcal{C} = \bar{\mathcal{C}} = 0.51$; dash-dot-dot line: $\mathcal{C} = 1/4$; dotted line: $\mathcal{C} = 0$; and dash-dot curve: $\mathcal{C} = -1/8$. In addition, for $\mathcal{C} = 0.51$: dash-dash-dot line - $M(s)$ obtained with one-loop corrected vertex; and short-dash line - with two-loop-corrected vertex.

impact on the magnitude of the vacuum quark condensate. For example, the mapping of Eq. (3.22) into our model is:

$$-\langle\bar{q}q\rangle^0 = \frac{3}{4\pi^2}\int_0^{s_0} ds\, s\, \frac{Z(s)\,M(s)}{s+M(s)^2}\,, \tag{4.62}$$

where s_0 is the spacelike point at which the model's mass function vanishes in the chiral limit, and we find

$$-\langle\bar{q}q\rangle^0_{\mathcal{C}=\bar{\mathcal{C}}} \;=\; (0.231\,\mathcal{G})^3 = (0.16\,\mathrm{GeV})^3 \tag{4.63}$$

with $\mathcal{G} = 0.69\,\mathrm{GeV}$. The rainbow-ladder result is $-\langle\bar{q}q\rangle^0_{\mathcal{C}=0} = \mathcal{G}^3/(10\pi^2) = (0.15\,\mathrm{GeV})^3$ so that

$$\frac{\langle\bar{q}q\rangle^0_{\mathcal{C}=0}}{\langle\bar{q}q\rangle^0_{\mathcal{C}=\bar{\mathcal{C}}}} = 0.82\,. \tag{4.64}$$

This ratio drops to 0.50 when $\mathcal{C} = 1.0$ is used to calculate the denominator.

It is thus evident that with attraction in the scattering kernel and at a common mass-scale, the condensate is significantly larger than that produced by a ladder vertex owing to an expansion of the domain upon which the dressed-quark mass function has nonzero support.

It is natural to ask for the pattern of behaviour in the presence of repulsion. In this case Fig. 8 indicates that with $\mathcal{C} = -1/8$ the value of the mass function is enhanced at $s = 0$. The magnitude of the mass function grows larger still with a further decrease in $\mathcal{C}$ and its domain of nonzero support expands. Therefore here, too, the condensate is larger than with the ladder vertex; e.g.,

$$\frac{\langle\bar{q}q\rangle^0_{\mathcal{C}=0}}{\langle\bar{q}q\rangle^0_{\mathcal{C}=-\frac{1}{8}}} = 0.92\,, \tag{4.65}$$

and the ratio drops to 0.49 when $\mathcal{C} = -3/8$ is used to evaluate the denominator.

properties in common with our calculated $\mathcal{C} > 0$ result.

The implication of these results is that in general, with a given mass-scale and a common model dressed-gluon interaction, studies employing the rainbow-ladder truncation will materially underestimate the magnitude of DCSB relative to those that employ a well-constrained dressed-quark-gluon vertex. Naturally, in practical phenomenology, alterations of the mass-scale can compensate for this [15].

In Fig. 9 we portray the $\mathcal{C}$-dependence of the scalar function associated with γ_μ in the dressed-quark-gluon vertex, $\alpha_1^{\mathcal{C}}(p^2)$. It is particularly useful here to employ the rainbow-ladder result, $\mathcal{C} = 0$, as our reference point because this makes the contrast between the effect of attraction and repulsion in the colour-octet quark-antiquark scattering kernel abundantly clear. Attraction uniformly increases the magnitude of $\alpha_1^{\mathcal{C}}(p^2)$, while the opposite outcome is produced by omitting the effect of the three-gluon-vertex in the DSE for the dressed-quark-gluon vertex. We remark that, as with $A(p^2)$, $\alpha_1^{\mathcal{C}}(p^2)$ evolves slowly with the current-quark mass but again, when the current-quark mass becomes commensurate with or exceeds the theory's mass-scale, it acts to very effectively dampen the momentum dependence of this function so that $\alpha_1^{\mathcal{C}}(p^2) \approx 1$. This effect is apparent in the rainbow vertex model employed in Ref. [38] to explain quenched-QCD lattice data.

Figure 10 illustrates the $\mathcal{C}$-dependence of $\alpha_2^{\mathcal{C}}(p^2)$, the scalar function modulating the subleading Dirac vector component of the dressed-quark-gluon vertex. The qualitative features of the completely resummed result for $\alpha_1^{\mathcal{C}}(p^2)$ are also manifest here. However, for this component of the vertex, which is purely dynamical in origin, there is a marked difference at timelike momenta between the result obtained with an odd number of loop corrections in the vertex and that obtained with an even number. We note that the magnitude of this function also decreases with increasing current-quark mass.

It is notable that the size of our complete result for $\alpha_2^{\mathcal{C}}(p^2)$ is an order of magnitude smaller than that reported in Ref. [37]. This is an isolated case, however. The calculated

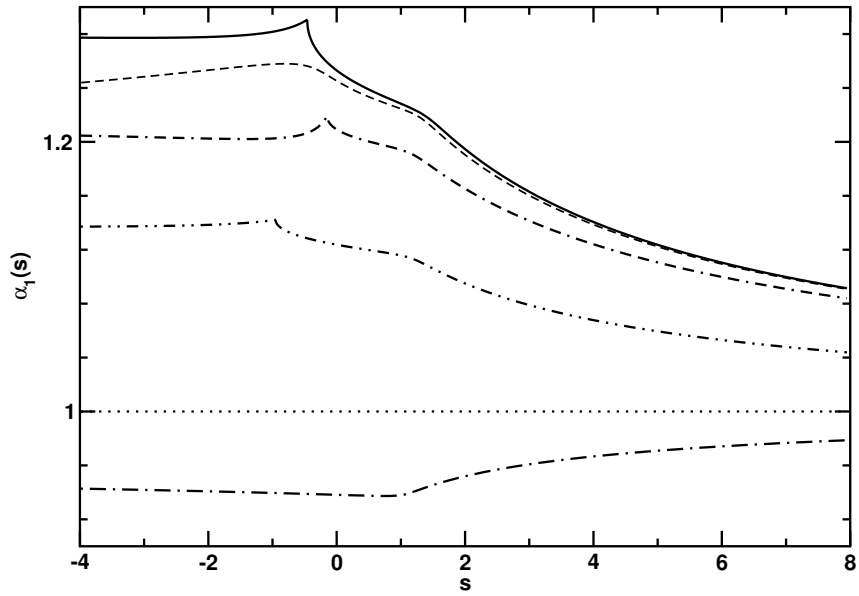

Figure 9: $\mathcal{C}$-dependence of $\alpha_1^{\mathcal{C}}(s)$ in Eq. (4.22). For all curves $m = 0.015$. Solid line: $\mathcal{C} = \bar{\mathcal{C}} = 0.51$; dash-dot-dot line: $\mathcal{C} = 1/4$; dotted line: $\mathcal{C} = 0$; and dash-dot curve: $\mathcal{C} = -1/$ nd short-da

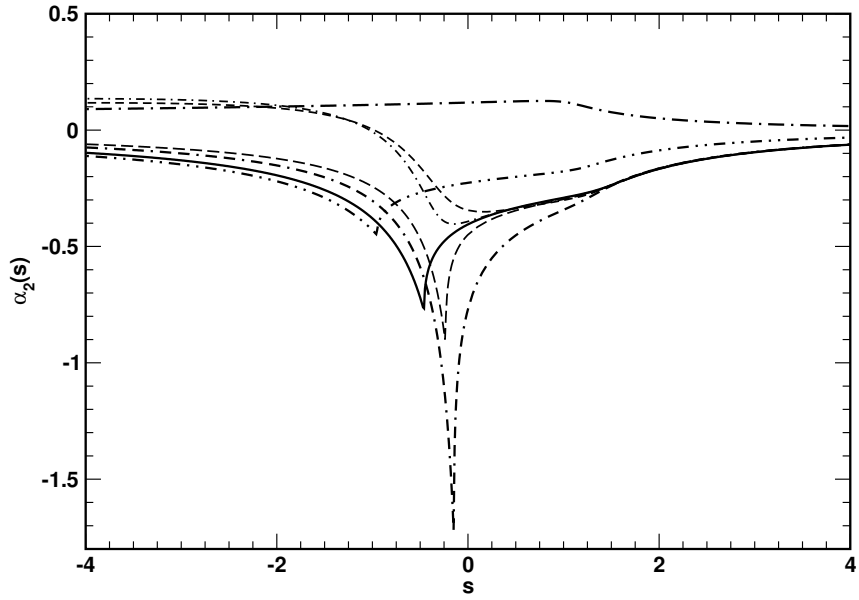

Figure 10: $\mathcal{C}$-dependence of of $\alpha_2^{\mathcal{C}}(s)$. For all curves $m = 0.015$. Solid line: $\mathcal{C} = \bar{\mathcal{C}} = 0.51$; dash-dot-dot line: $\mathcal{C} = 1/4$; and dash-dot curve: $\mathcal{C} = -1/8$. Moreover, for $\mathcal{C} = 0.51$: dash-dash-dot line - one-loop result for $\alpha_2^{\mathcal{C}}(s)$; short-dash line - two-loop result; long-dash line - three-loop; and short-dash-dot line: four-loop. For $\mathcal{C} = 0$, $\alpha_2^{\mathcal{C}}(s) \equiv 0$.

magnitudes of the other functions in the dressed-quark propagator and -quark-gluon vertex are commensurate with those obtained in quenched lattice-QCD. We remark in addition that the lattice result is an order of magnitude larger than that obtained with a commonly used vertex *Ansatz* [95]. This discrepancy deserves study in more sophisticated models.

In Fig. 11 we display what might be called the scalar part of the dressed-quark-gluon vertex; viz., $\alpha_3^{\mathcal{C}}(p^2)$. This is the piece of the vertex whose ultraviolet behaviour is most sensitive to the current-quark mass. The figure demonstrates that at infrared momenta $\alpha_3^{\mathcal{C}}(p^2)$, too, is materially affected by the scale of DCSB, Eq. (4.63): at $s = 0$ the deviation from its rainbow-truncation value is approximately four times that exhibited by $\alpha_1^{\mathcal{C}}(p^2)$. Hence, this term can be important at infrared and intermediate momenta.

Finally, since they are absent in rainbow truncation, it is illuminating to unfold the different roles played by $\alpha_2^{\mathcal{C}}(s)$ and $\alpha_3^{\mathcal{C}}(s)$ in determining the behaviour of the gap equation's self-consistent solution. Some of these effects are elucidated in Fig. 12. The key observation is that $\alpha_3^{\mathcal{C}}(s)$ alone is the source of all coupling between Eqs. (4.35) and (4.36) that is not already present in rainbow-ladder truncation: $\alpha_3^{\mathcal{C}}\, B$ appears in the equation for $A(s)$ and $\alpha_3^{\mathcal{C}}\, s\, A$ appears in the equation for $B(s)$. The action of $\alpha_2^{\mathcal{C}}$ is merely to modify the rainbow-ladder coupling strengths.

A consideration of Eqs. (4.35), (4.36) suggests that omitting $\alpha_3^{\mathcal{C}}(s)$ will affect $A(s)$ at infrared momenta but not $B(s)$. That is easily substantiated by repeating the analysis that gave Eqs. (4.45), (4.46), and is apparent in the figure. It will readily be appreciated that neither $\alpha_2^{\mathcal{C}}(s)$ nor $\alpha_3^{\mathcal{C}}(s)$ can affect the deep ultraviolet behaviour of the gap equation's solution, Eqs. (4.37), (4.41), because they vanish too rapidly as $1/s \to 0$. This is plain in Fig. 12.

At intermediate spacelike momenta both $\alpha_2^{\mathcal{C}}(s)$ and $\alpha_3^{\mathcal{C}}(s)$ are negative and hence act to

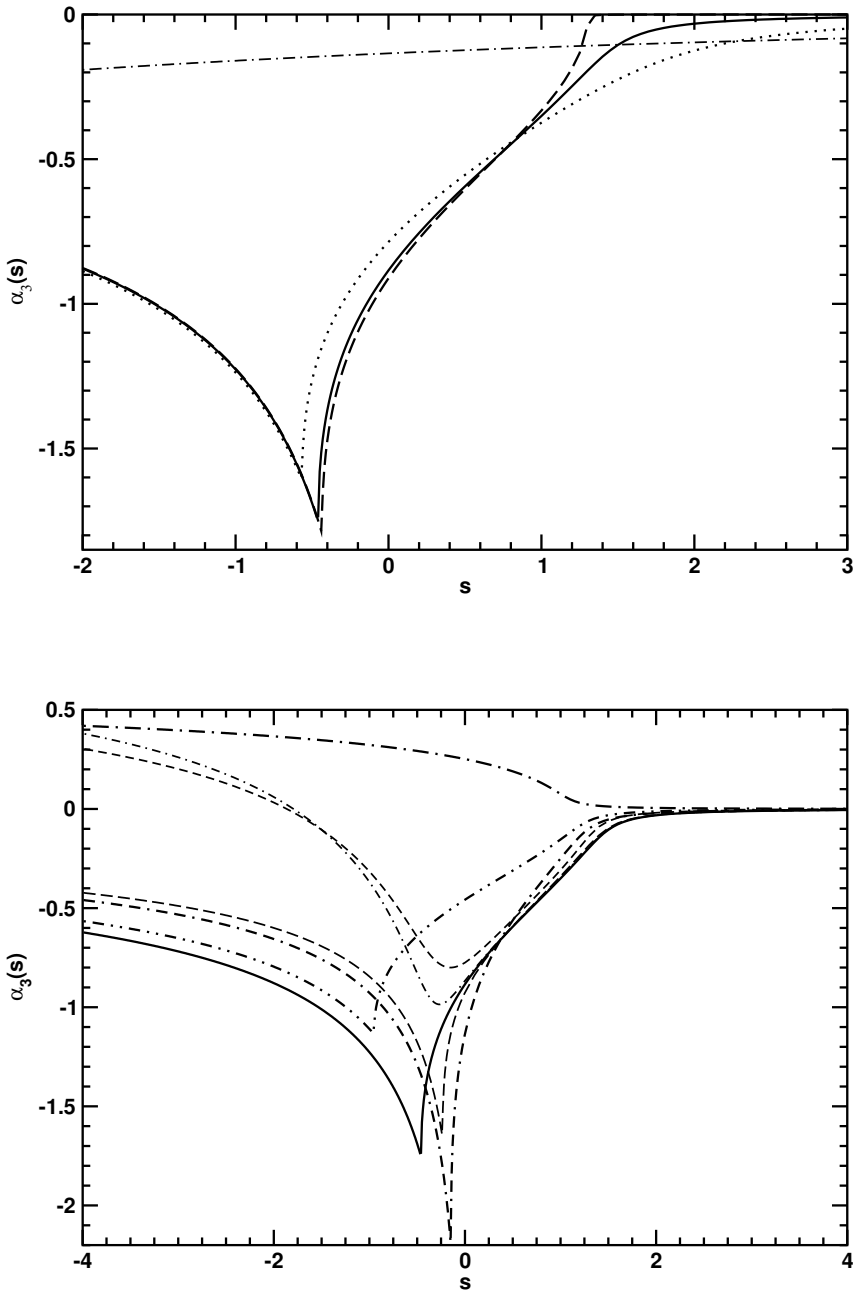

Figure 11: *Upper panel* – Current-quark-mass-dependence of $\alpha_3^{\mathcal{C}}(s)$. For all curves $\mathcal{C} = \bar{\mathcal{C}} = 0.51$. Dash-dot line: $m = 2$; dotted line: $m = m_{60}$; solid line: $m = 0.015$; dashed line: chiral limit, $m = 0$. *Lower panel* – $\mathcal{C}$-dependence of $\alpha_3^{\mathcal{C}}(s)$. For all curves $m = 0.015$. Solid line: $\mathcal{C} = \bar{\mathcal{C}} = 0.51$; dash-dot-dot line: $\mathcal{C} = 1/4$; and dash-dot curve: $\mathcal{C} = -1/8$. Moreover, for $\mathcal{C} = 0.51$: dash-dash-dot line - one-loop result for $\alpha_3^{\mathcal{C}}(s)$; short-dash line - two-loop result; long-dash line - three-loop; and short-dash-dot line: four-loop. For $\mathcal{C} = 0$, $\alpha_3^{\mathcal{C}}(s) \equiv 0$.

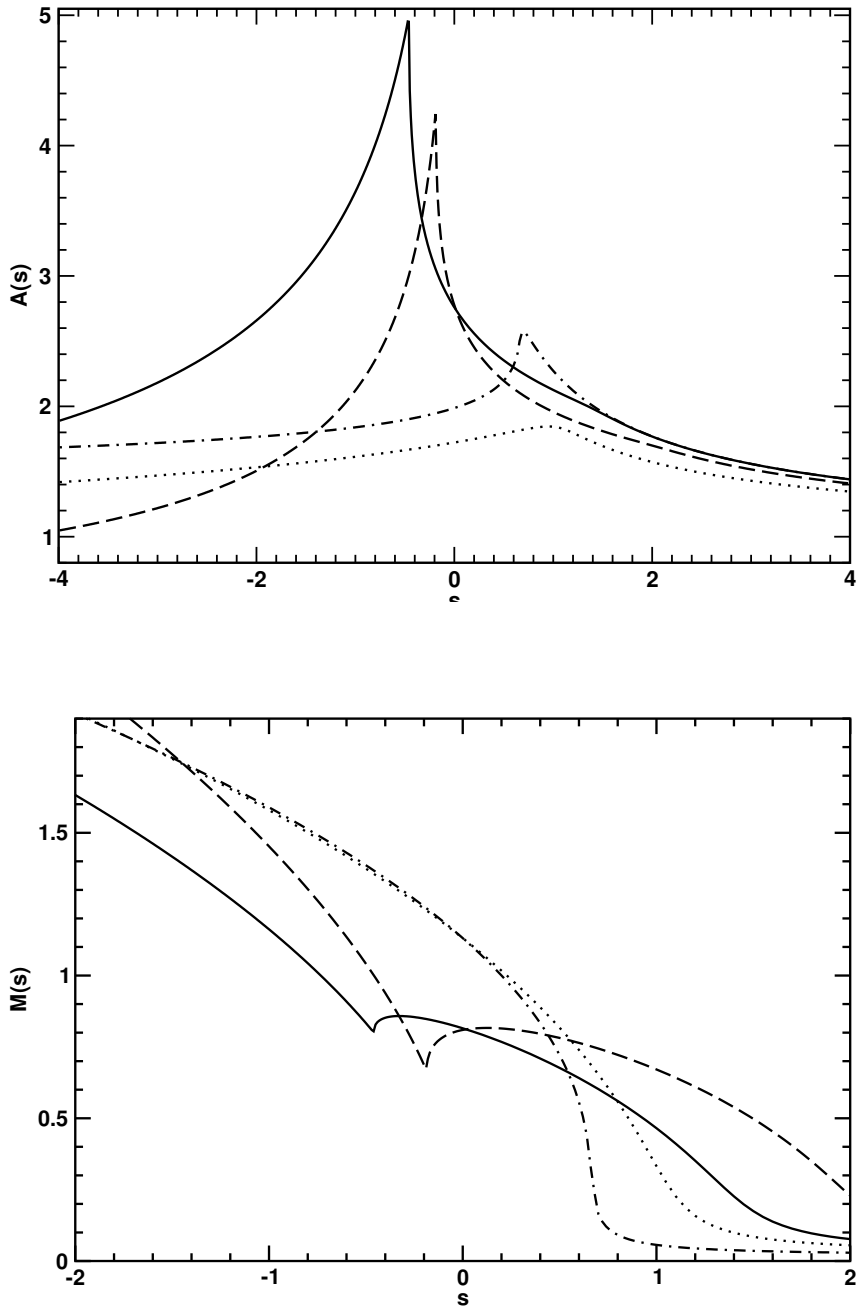

Figure 12: *Upper panel* – Impact of $\alpha_2^{\mathcal{C}}(s)$ and $\alpha_3^{\mathcal{C}}(s)$ on $A(s)$. For $\mathcal{C} = \bar{\mathcal{C}}$, Eq. (4.61), solid line: result obtained with both terms present; dashed-line: $\alpha_2^{\mathcal{C}}(s)$ omitted; dash-dot line: $\alpha_3^{\mathcal{C}}(s)$ omitted. The dotted line is the result obtained with both terms present in the vertex but $\mathcal{C} = -1/8$. *Lower panel* – Impact of $\alpha_2^{\mathcal{C}}(s)$ and $\alpha_3^{\mathcal{C}}(s)$ on $M(s)$. In all cases $m = 0.015$.

magnify $A(s)$ with respect to the value obtained using a bare vertex. However, they compete in Eq. (4.36): $\alpha_2^{\mathcal{C}}(s)$ works to diminish $B(s)$ and $\alpha_3^{\mathcal{C}}(s)$ acts to amplify it. Therefore in the absence of $\alpha_3^{\mathcal{C}}(s)$ one should expect $M(s) = B(s)/A(s)$ to be suppressed at intermediate momenta, and consequently a condensate much reduced in magnitude. Omitting $\alpha_2^{\mathcal{C}}(s)$ should yield the opposite effect. This is precisely the outcome of our numerical studies:

$$\left.\frac{\langle\bar{q}q\rangle^0_{\mathcal{C}=0}}{\langle\bar{q}q\rangle^0_{\mathcal{C}=\bar{\mathcal{C}}}}\right|_{\alpha_3^{\mathcal{C}}\equiv 0} = 1.97\,; \quad \text{and} \quad \left.\frac{\langle\bar{q}q\rangle^0_{\mathcal{C}=0}}{\langle\bar{q}q\rangle^0_{\mathcal{C}=\bar{\mathcal{C}}}}\right|_{\alpha_2^{\mathcal{C}}\equiv 0} = 0.40\,. \tag{4.66}$$

These aspects of our model provide an algebraic illustration of results obtained with more sophisticated *Ansätze*, as apparent from a comparison with, for example, Refs. [15, 17].

4.6 ***Bethe-Salpeter Equation***

4.7 Bethe-Salpeter Equation

The renormalised homogeneous Bethe-Salpeter equation (BSE) for the quark-antiquark channel denoted by M can be compactly expressed as

$$[\Gamma_M(k;P)]_{EF} = \int_q^\Lambda [K(k,q;P)]^{GH}_{EF}\,[\chi_M(q;P)]_{GH} \tag{4.67}$$

where: k is the relative momentum of the quark-antiquark pair and P is their total momentum; $E,\ldots,H$ represent colour, flavour and spinor indices; and

$$\chi_M(k;P) = S(k_+)\,\Gamma_M(k;P)\,S(k_-)\,, \tag{4.68}$$

with $\Gamma_M(q;P)$ the meson's Bethe-Salpeter amplitude. In Eq. (4.67), K is the fully-amputated dressed-quark-antiquark scattering kernel.

4.7.1 Vertex consistent kernel

The preservation of Ward-Takahashi identities in those channels related to hadron observables requires a conspiracy between the dressed-quark-gluon vertex and the Bethe-Salpeter kernel [40, 96]. The manner in which these constraints are realised for vertices of the class considered herein was made explicit in Ref. [41]. In that systematic and nonperturbative truncation scheme the rainbow gap equation and ladder Bethe-Salpeter equation represent the lowest-order Ward-Takahashi identity preserving pair. Beyond this, each additional term in the vertex generates a unique collection of terms in K, a subset of which are always nonplanar.

For any dressed-quark-gluon vertex in the gap equation, which can be represented expressly by an enumerable series of contributions, the Bethe-Salpeter kernel that guarantees the validity of all Ward-Takahashi identities is realised in

$$\begin{aligned}\Gamma_M(k;P) = &\int_q^\Lambda \mathcal{D}_{\mu\nu}(k-q)\, l^a \gamma_\mu \\ &\times \left[\chi_M(q;P)\, l^a\, \Gamma_\nu(q_-,k_-) + S(q_+)\, \Lambda^a_{M\nu}(q,k;P)\right],\end{aligned} \tag{4.69}$$

where

$$\Lambda^a_{M\nu}(q,k;P) = \sum_{n=0}^{\infty} \Lambda^{a;n}_{M\nu}(q,k;P)\,, \tag{4.70}$$

with herein

$$
\begin{aligned}
-\frac{1}{8\mathcal{C}}\,\Lambda^{a;n}_{M\nu}(\ell,k;P) &= \int_q^\Lambda \mathcal{D}_{\rho\sigma}(\ell-q)\,l^b\gamma_\rho\,\chi_M(q;P) \\
&\quad \times l^a\Gamma^{\mathcal{C}}_{\nu,n-1}(q_-,q_-+k-\ell)\,S(q_-+k-\ell)\,l^b\gamma_\sigma \\
&+ \int_q^\Lambda \mathcal{D}_{\rho\sigma}(k-q)\,l^b\gamma_\rho\,S(q_++\ell-k) \\
&\quad \times l^a\Gamma^{\mathcal{C}}_{\nu,n-1}(q_++\ell-k,q_+)\,\chi_M(q;P)\,l^b\gamma_\sigma \\
&+ \int_{q'}^\Lambda \mathcal{D}_{\rho\sigma}(\ell-q')l^b\gamma_\rho\,S(q'_+) \\
&\quad \times \Lambda^{a;n-1}_\nu(q',q'+k-\ell;P)\,S(q'_-+k-\ell)\,l^b\gamma_\sigma.
\end{aligned}
\tag{4.71}
$$

This last equation is a recursion relation, which is to be solved subject to the initial condition $\Lambda^{a;0}_{M\nu}\equiv 0$.

The Bethe-Salpeter amplitude for any meson can be written in the form

$$
\Gamma_M(k;P) = \boldsymbol{I}_c \sum_{i=1}^{N_M} \mathcal{G}^i(k;P)\,f^i_M(k^2,k\cdot P;P^2) =: [\boldsymbol{G}]\ \boldsymbol{f}_M\,, \tag{4.72}
$$

where $\mathcal{G}^i(k;P)$ are those independent Dirac matrices required to span the space containing the meson under consideration. It then follows upon substitution of this formula that Eq. (4.71) can be written compactly as

$$
\Lambda^{a;n}_{M\nu} = \left\{ \left[\mathcal{K}^i_{M\nu}\,\alpha^{\mathcal{C}}_{i;n-1}\right] + \left[\mathcal{L}\,\Lambda^{a;n-1}_{M\nu}\right] \right\} \boldsymbol{f}_M\,. \tag{4.73}
$$

This states that $\Lambda^{a;n}_{M\nu}$ can be considered as a matrix operating in the space spanned by the independent components of the Bethe-Salpeter amplitude, with its Dirac and Lorentz structure projected via the contractions in the BSE. The first term ($\mathcal{K}_M$) in Eq. (4.73) represents the contribution from the first two integrals on the right-hand-side (r.h.s.) of Eq. (4.71). This is the driving term in the recursion relation. The second term ($\mathcal{L}$) represents the last integral, which enacts the recursion.

4.7.2 Solutions of the vertex-consistent meson Bethe-Salpeter equation

π-meson

With the model of the dressed-gluon interaction in Eq. (4.21) the relative momentum between a meson's constituents must vanish. It follows that the general form of the Bethe-Salpeter amplitude for a pseudoscalar meson of equal-mass constituents is ($\hat{P}^2 = 1$)

$$\Gamma_\pi(P) = \gamma_5 \left[i f_1^\pi(P^2) + \gamma \cdot \hat{P}\, f_2^\pi(P^2) \right]. \tag{4.74}$$

To obtain the vertex-consistent BSE one must first determine $\Lambda^{a;1}_{\pi\nu}$. That is obtained by substituting Eq. (4.74) into the r.h.s. of Eq. (4.71). Only the first two integrals contribute because of the initial condition and they are actually algebraic expressions when Eq. (4.21) is used. This gives $\mathcal{K}^i_{\pi\nu}$ in Eq. (4.73). Explicit calculation shows this to be identically zero, and hence $\Lambda^{a;1}_{\pi\nu} \equiv 0$. Since this is the driving term in the recursion relation then

$$\Lambda^a_{\pi\nu}(k,k;P) \equiv 0\,. \tag{4.75}$$

While this result is not accidental [41], it is not a general feature of the vertex-consistent Bethe-Salpeter kernel.

One thus arrives at a particularly simple vertex-consistent BSE for the pion (Q=P/2):

$$\Gamma_\pi(P) = -\,\gamma_\mu\, S(Q)\, \Gamma_\pi(P)\, S(-Q)\, \Gamma^{\mathcal{C}}_\mu(-Q)\,. \tag{4.76}$$

Consider the matrices

$$\mathcal{P}_1 = -\frac{i}{4}\,\gamma_5\,,\ \mathcal{P}_2 = \frac{1}{4}\,\gamma\cdot\hat{P}\,\gamma_5\,, \tag{4.77}$$

which satisfy

$$f_i^\pi(P) = \mathrm{tr}_{\mathrm{D}} \mathcal{P}_i\, \Gamma_\pi(P)\,. \tag{4.78}$$

They may be used to rewrite Eq. (4.76) in the form

$$\boldsymbol{f}_\pi(P) = \mathcal{H}_\pi(P^2)\boldsymbol{f}_\pi(P)\,, \tag{4.79}$$

Table 2: Calculated π and ρ meson masses, in GeV. ($\mathcal{G} = 0.69$ GeV, in which case $m = 0.015\,\mathcal{G} = 10\,$MeV. In the notation of Ref. [40], this value of $\mathcal{G}$ corresponds to $\eta = 1.39\,$GeV.) n is the number of loops retained in dressing the quark-gluon vertex, see Eq. (4.24), and hence the order of the vertex-consistent Bethe-Salpeter kernel. NB. $n = 0$ corresponds to the rainbow-ladder truncation, in which case $m_\rho = \sqrt{2}\,\mathcal{G}$, and that is why this column's results are independent of $\mathcal{C}$.

		$M_H^{n=0}$	$M_H^{n=1}$	$M_H^{n=2}$	$M_H^{n=\infty}$
$\mathcal{C} = -(1/8)$	π, $m = 0$	0	0	0	0
	π, $m = 0.01$	0.149	0.153	0.154	0.154
	ρ, $m = 0$	0.982	1.074	1.089	1.091
	ρ, $m = 0.01$	0.997	1.088	1.103	1.105
$\mathcal{C} = (1/4)$	π, $m = 0$	0	0	0	0
	π, $m = 0.01$	0.149	0.140	0.142	0.142
	ρ, $m = 0$	0.982	0.789	0.855	0.842
	ρ, $m = 0.01$	0.997	0.806	0.871	0.858
$\mathcal{C} = \bar{\mathcal{C}} = 0.51$	π, $m = 0$	0	0	0	0
	π, $m = 0.01$	0.149	0.132	0.140	0.138
	ρ, $m = 0$	0.982	...	0.828	0.754
	ρ, $m = 0.01$	0.997	...	0.844	0.770

wherein $\mathcal{H}_\pi(P^2)$ is a 2×2 matrix

$$\mathcal{H}_\pi(P^2)_{ij} = \\ -\frac{\delta}{\delta f_j^\pi} \mathrm{tr}_{\mathrm{D}} \mathcal{P}_i \, \gamma_\mu \, S(Q) \, \Gamma_\pi(P) \, S(-Q) \, \Gamma_\mu^{\mathcal{C}}(-Q) \,. \tag{4.80}$$

Equation (4.79) is a matrix eigenvalue problem in which the kernel $\mathcal{H}$ is a function of P^2. This equation has a nontrivial solution if, and only if, at some M^2

$$\det \left[\mathcal{H}_\pi(P^2) - \boldsymbol{I} \right] \big|_{P^2 + M^2 = 0} = 0 \,. \tag{4.81}$$

The value of M for which this characteristic equation is satisfied is the bound state's mass. In the absence of a solution there is no bound state in this channel.

We have solved Eq. (4.81) for the pion and the results are presented in Table 2. That the vertex-consistent Bethe-Salpeter kernel ensures the preservation of the axial-vector Ward-Takahashi identity, and hence guarantees the pion is a Goldstone boson in the chiral

limit, is abundantly clear: irrespective of the value of $\mathcal{C}$ and the order of the truncation, $m_\pi = 0$ for $m = 0$. Away from this symmetry-constrained point the results indicate that, with net attraction in the colour-octet quark-antiquark scattering kernel, the rainbow-ladder truncation overestimates the mass; i.e., it yields a value greater than that obtained with the fully resummed vertex ($n = \infty$). Moreover, the approach to the exact result for the mass is not monotonic. On the other hand, given two truncations for which solutions exist, characterised by n_1- and n_2-loop insertions, respectively, then

$$|M_H^{n=\infty} - M_H^{n_2}| < |M_H^{n=\infty} - M_H^{n_1}|\,,\ n_2 > n_1\,; \tag{4.82}$$

viz., correcting the vertex improves the accuracy of the mass estimate.

***ρ*-meson**

In our algebraic model the complete form of the Bethe-Salpeter amplitude for a vector meson is

$$\Gamma_\rho^\lambda(P) = \gamma\cdot\epsilon^\lambda(P)\, f_1^\rho(P^2) + \sigma_{\mu\nu}\,\epsilon_\mu^\lambda(P)\,\hat{P}_\nu\, f_2^\rho(P^2)\,. \tag{4.83}$$

This expression, which has only two independent functions, is simpler than that allowed by a more sophisticated interaction, wherein there are eight terms. Nevertheless, Eq. (4.83) retains the amplitudes that are found to be dominant in more sophisticated studies [30]. In Eq. (4.83), $\{\epsilon_\mu^\lambda(P);\, \lambda = -1, 0, +1\}$ is the polarisation four-vector:

$$P\cdot\epsilon^\lambda(P) = 0\,,\ \forall\lambda\,;\ \ \epsilon^\lambda(P)\cdot\epsilon^{\lambda'}(P) = \delta^{\lambda\lambda'}. \tag{4.84}$$

The construction of the vertex-consistent ρ-meson BSE for the class of vertices under consideration herein is fully described in Ref. [41]. The pion case illustrates the key modification. Brevity requires that we omit further details. Suffice to say, one arrives via a mechanical procedure at the characteristic equation for the ρ-meson, which we solved.

The results are presented in Table 2. With increasing net attraction in the quark-antiquark scattering kernel the amount by which the rainbow-ladder truncation overestimates the exact mass also increases: with the amount of attraction suggested by lattice data the $n = 0$ mass is 27% too large. A related observation is that the bound state's mass decreases as the amount of attraction between its constituents increases. Furthermore, with increasing attraction, even though the fully resummed vertex and consistent kernel always yield a solution, there is no guarantee that a given truncated system supports a bound state: the one-loop corrected vertex and consistent kernel ($n = 1$) do not have sufficient binding to support a ρ-meson. This is overcome at the next order of truncation, which yields a mass 9.7% too large. The observation that a given beyond-rainbow-ladder truncation may not support a bound state, even though one is present in the solution of the complete and consistent system, provides a valuable and salutary tip for model building and hadron phenomenology.

Finally, as has often been observed, and independent of the truncation, bound state solutions of gap-equation-consistent BSEs always yield the full amount of π-ρ mass splitting, even in the chiral limit. This splitting is driven by the DCSB mechanism. Its true understanding therefore requires a veracious realisation of that phenomenon.

Dependence on the current-quark mass

In connection with this last observation it is relevant to explore the evolution with current-quark mass of the pseudoscalar and vector meson masses, and of the difference between them. The results for pseudoscalar mesons should be interpreted with the following caveat in mind. In constructing the vertex and kernel we omitted contributions from gluon vacuum polarisation diagrams. These contribute only to flavour diagonal meson channels. Hence, for light-quarks in the pseudoscalar channel, wherewith such effects may

Table 3: Current-quark masses required to reproduce the experimental masses of the vector mesons. The values of m_{η_c}, m_{η_b} are predictions. Experimentally [100], $m_{\eta_c} = 2.9797 \pm 0.00015$ and $m_{\eta_b} = 9.30 \pm 0.03$. NB. $0^-_{s\bar{s}}$ is a fictitious pseudoscalar meson composed of unlike-flavour quarks with mass m_s, which is included for comparison with other nonperturbative studies. All masses are listed in GeV.

$m_{u,d} = 0.01$	$m_s = 0.166$	$m_c = 1.33$	$m_b = 4.62$
$m_\rho = 0.77$	$m_\phi = 1.02$	$m_{J/\psi} = 3.10$	$m_{\Upsilon(1S)} = 9.46$
$m_\pi = 0.14$	$m_{0^-_{s\bar{s}}} = 0.63$	$m_{\eta_c} = 2.97$	$m_{\eta_b} = 9.42$

be important [99, 98], our results should be understood to apply only to flavour nonsinglets. In principle, the same is true for light vector mesons. However, experimentally, the ω and ϕ mesons are almost ideally mixed; i.e., the ω exhibits no $\bar{s}s$ content whereas the ϕ is composed almost entirely of this combination. We therefore assume that the vacuum polarisation diagrams we have omitted are immaterial in the study of vector mesons. (NB. It is an artefact of Eq. (4.21) that this model supports neither scalar nor axial-vector meson bound states [42, 41].)

We fix the model's current-quark masses via a fit to vector meson masses and the results are presented in Table 3. The model we're employing is ultraviolet finite and hence our current-quark masses cannot be directly compared with QCD's current-quark mass-scales. Nevertheless, the values are quantitatively consistent with the pattern of flavour-dependence in the explicit chiral symmetry breaking masses of QCD.

Our calculated results for the current-quark mass-dependence of pseudoscalar and vector meson masses are presented in Fig. 13. In the neighbourhood of the chiral limit the vector meson mass is approximately independent of the current-quark mass whereas the pseudoscalar meson mass increases rapidly, according to (in GeV)

$$m^2_{0^-} \approx 1.33\, m \quad m \ll \mathcal{G}\,, \tag{4.85}$$

thereby reproducing the pattern predicted by QCD [43].

With the model's value of the vacuum quark condensate, Eq. (4.63), this result allows

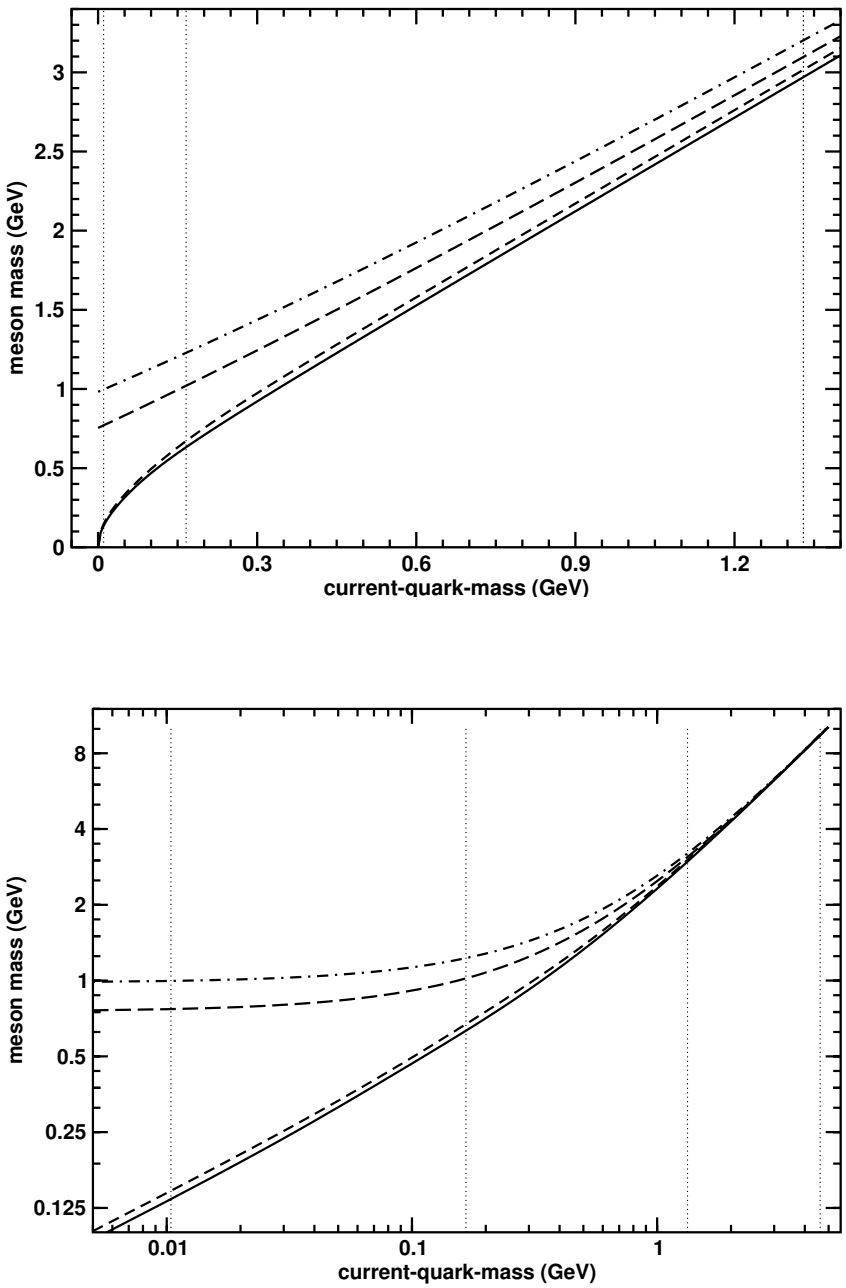

Figure 13: Evolution of pseudoscalar and vector $q\bar{q}$ meson masses with the current-quark mass. Solid line: pseudoscalar meson trajectory obtained with $\mathcal{C} = \bar{\mathcal{C}} = 0.51$, Eq. (4.61), using the completely resummed dressed-quark-gluon vertex in the gap equation and the vertex- consistent Bethe-Salpeter kernel; short-dash line: this trajectory calculated in rainbow-ladder truncation. Long-dash line: vector meson trajectory obtained with $\bar{\mathcal{C}}$ using the completely resummed vertex and the consistent Bethe-Salpeter kernel; dash-dot line: rainbow-ladder truncation result for this trajectory. The dotted vertical lines mark the current-quark masses in Table 3.

one to infer the chiral-limit value of $f_\pi^0 = 0.079\,\mathrm{GeV}$ via the Gell-Mann–Oakes–Renner relation. It is a model artefact that the relative-momentum-dependence of Bethe-Salpeter amplitudes is described by $\delta^4(p)$ and so a direct calculation of this quantity is not realistic. The value is low, as that of the condensate is low, because the model is ultraviolet finite. In QCD the condensate and decay constant are influenced by the high-momentum tails of the dressed-quark propagator and Bethe-Salpeter amplitudes [29, 30].

The curvature in the pseudoscalar trajectory persists over a significant domain of current-quark mass. For example, consider two pseudoscalar mesons, one composed of unlike-flavour quarks each with mass $2m_s$ and another composed of such quarks with mass m_s. In this case

$$\frac{m^2_{0^-_{2m_s}}}{m^2_{0^-_{m_s}}} = 2.4\,, \tag{4.86}$$

which indicates that the nonlinear evolution exhibited in Eq. (4.85) is still evident for current-quark masses as large as twice that of the s-quark. With this result we reproduce a feature of more sophisticated DSE studies [101, 102, 103] and a numerical simulation of quenched lattice-QCD [104].

The mode of behaviour just described is overwhelmed when the current-quark mass becomes large: $m \gg \mathcal{G}$. In this limit the vector and pseudoscalar mesons become degenerate, with the mass of the ground state pseudoscalar meson rising monotonically to meet that of the vector meson. In our model

$$\left.\frac{m_{1^-}}{m_{0^-}}\right|_{m=m_c} = 1.04\,, \tag{4.87}$$

with a splitting of 130 MeV, and this splitting drops to just 40 MeV at m_b; viz., only 5% of its value in the chiral limit. In addition to the calculated value, the general pattern of our results argues for the mass of the pseudoscalar partner of the $\Upsilon(1S)$ to lie above 9.4 GeV. Indeed, we expect the mass splitting to be less than $m_{J/\psi} - m_{\eta_c}$, not more. (See

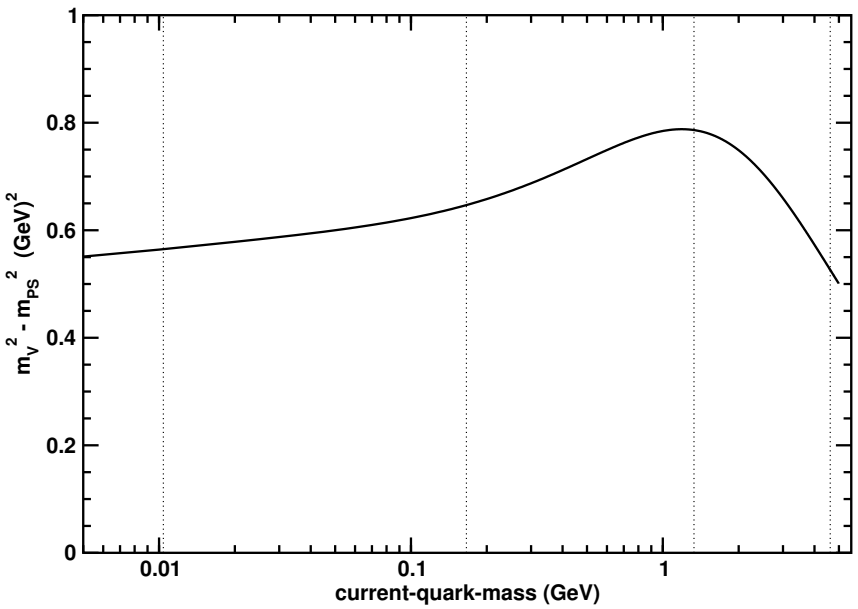

Figure 14: Evolution with current-quark mass of the difference between the squared-masses of vector and pseudoscalar mesons ($\bar{\mathcal{C}} = 0.51$) using the completely resummed dressed-quark-gluon vertex in the gap equation and the vertex-consistent Bethe-Salpeter kernel. The dotted vertical lines mark the current-quark masses in Table 3.

also; e.g., Ref. [105].)

In Fig. 14 one observes that on a material domain of current-quark masses: $m_{1^-}^2 - m_{0^-}^2 \approx 0.56\,\mathrm{GeV}^2$, an outcome consistent with experiment that is not reproduced in numerical simulations of quenched lattice-QCD [104]. The difference is maximal in the vicinity of m_c, a result which re-emphasises that heavy-quark effective theory is not an appropriate tool for the study of c-quarks [44].

Figure 15 is instructive. It shows that with growing current-quark mass the rainbow-ladder truncation provides an increasingly accurate estimate of the ground state vector meson mass. At the s-quark mass the relative error is 20% but that has fallen to $< 4\%$ at the c-quark mass.

Similar statements are true in the valid pseudoscalar channels. In fact, in this case

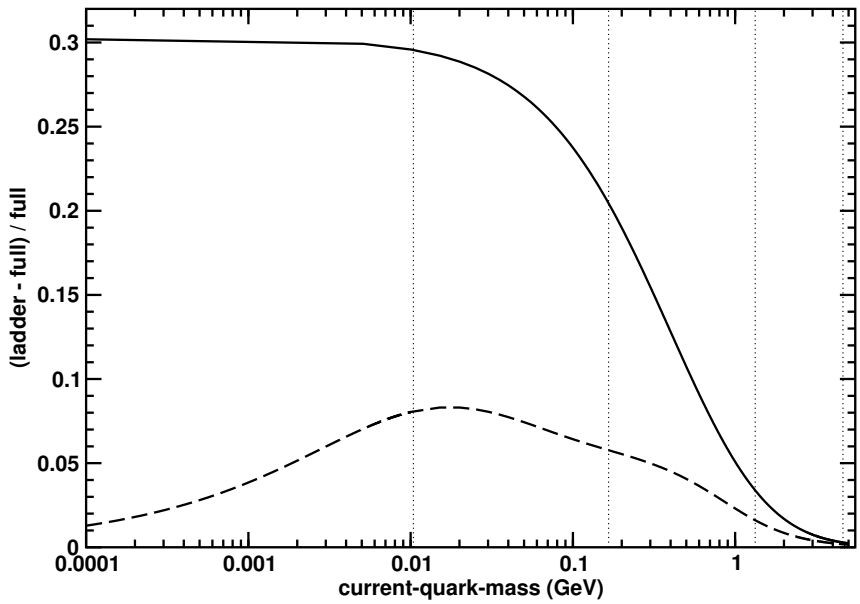

Figure 15: Evolution with current-quark mass of the relative difference between the meson mass calculated in the rainbow-ladder truncation and the exact value. Solid lines: vector meson trajectories; and dashed-lines; pseudoscalar meson trajectories. The dotted vertical lines mark the current-quark masses in Table 3. We used $\bar{\mathcal{C}} = 0.51$.

the agreement between the truncated and exact results is always better; e.g., the absolute difference reaches its peak of $\approx 60\,\mathrm{MeV}$ at $m \sim 4\,m_s$ whereat the relative error is only 3%. This behaviour is fundamentally because of Goldstone's theorem, which requires that all legitimate truncations preserve the axial-vector Ward-Takahashi identity and hence give a massless pseudoscalar meson in the chiral limit. It is practically useful, too, because it indicates that the parameters of a model meant to be employed in a rainbow-ladder truncation study of hadron observables may reliably be fixed by fitting to the values of quantities calculated in the neighbourhood of the chiral limit.

The general observation suggested by Fig. 15 is that with increasing current-quark mass the contributions from nonplanar diagrams and vertex corrections are suppressed in both the gap and Bethe-Salpeter equations. Naturally, they must still be included in precision

spectroscopic calculations. It will be interesting to reanalyse this evolution in a generalisation of our study to mesons composed of constituents with different current-quark masses, and thereby extend and complement the limited such trajectories in Refs. [101, 102].

Chapter 5

Quark-gluon vertex model and lattice-QCD data

In the absence of well-constrained nonperturbative models for the vertex, it has often been assumed that a reasonable beginning is the Ball-Chiu [95] or Curtis-Pennington [5] Abelian Ansatz times the appropriate color matrix. An example is provided by the recent results from a truncation of the gluon-ghost-quark DSEs where this vertex dressing contributes materially to a reasonable quark condensate value [18]. However, there is no known way to develop a Bethe-Salpeter (BSE) kernel that is dynamically matched to a quark self-energy defined in terms of such a phenomenological dressed vertex in the sense that chiral symmetry is preserved through the axial-vector Ward-Takahashi identity. The latter implementation of chiral symmetry guarantees the Goldstone boson nature of the flavor non-singlet pseudoscalars independently of model details [43]. There is a known constructive scheme [40] that defines a diagrammatic expansion of the BSE kernel corresponding to any diagrammatic expansion of the quark self-energy such that the axial-vector Ward-Takahashi identity is preserved. For this reason, recent nonperturbative vertex models have employed simple diagrammatic representations [19, 20, 110, 111].

It is only recently that lattice-QCD has begun to provide information on the infrared structure of the dressed quark-gluon vertex [37, 112]. In this work we generate a model dressed vertex, for zero gluon momentum, based on an Ansatz for non-perturbative extensions of the only two diagrams that contribute at 1-loop order in perturbation theory. An existing ladder-rainbow model kernel is the only required input. We compare to the recent lattice-QCD data without parameter adjustment.

5.1 *One-loop perturbative vertex*

In Euclidean metric we denote the dressed-quark-gluon vertex for gluon momentum k and quark momentum p by $ig\,t^c\,\Gamma_\sigma(p+k,p)$, where $t^c=\lambda^c/2$ and λ^c is an SU(3) color matrix. Through $\mathcal{O}(g^2)$, i.e., to 1-loop, the amplitude Γ_σ is given, in terms of Fig. 16, by[i]

$$\Gamma_\sigma(p+k,p) = Z_{1\rm F}\,\gamma_\sigma + \Gamma^{\rm A}_\sigma(p+k,p) + \Gamma^{\rm NA}_\sigma(p+k,p) + \ldots \quad , \tag{5.1}$$

with

$$\begin{aligned}\Gamma^{\rm A}_\sigma(p+k,p) &= -(C_{\rm F}-\frac{C_{\rm A}}{2})\int_q^\Lambda g^2 D_{\mu\nu}(p-q)\gamma_\mu \\ &\quad \times S_0(q+k)\,\gamma_\sigma\,S_0(q)\gamma_\nu \quad ,\end{aligned} \tag{5.2}$$

and

$$\begin{aligned}\Gamma^{\rm NA}_\sigma(p+k,p) &= -\frac{C_{\rm A}}{2}\int_q^\Lambda g^2\,\gamma_\mu S_0(p-q)\gamma_\nu\,D_{\mu\mu'}(q+k) \\ &\quad \times i\Gamma^{3g}_{\mu'\nu'\sigma}(q+k,q)\,D_{\nu'\nu}(q) \quad ,\end{aligned} \tag{5.3}$$

Here $Z_{1\rm F}(\mu^2,\Lambda^2)$ is the vertex renormalization constant to ensure $\Gamma_\sigma=\gamma_\sigma$ at renormalization scale μ. The following quantities are bare: the three-gluon vertex $ig\,f^{\rm abc}\,\Gamma^{3g}_{\mu\nu\sigma}(q+k,q)$, the quark propagator $S_0(p)$, and the gluon propagator $D_{\mu\nu}(q)=T_{\mu\nu}(q)D_0(q^2)$, where $T_{\mu\nu}(q)$ is the transverse projector. The next order terms in Eq. (5.1) are $\mathcal{O}(g^3)$: the contribution involving the four-gluon vertex, and $\mathcal{O}(g^4)$: contributions from crossed-box and two-rung gluon ladder diagrams, and 1-loop dressing of the triple-gluon vertex, etc.

The color factors in Eqs. (5.2) and (5.3), given by

$$\begin{aligned} t^a\,t^b\,t^a &= (C_{\rm F}-\frac{C_{\rm A}}{2})\,t^b = -\frac{1}{2N_c}\,t^b \\ t^a\,f^{abc}\,t^b &= \frac{C_{\rm A}}{2}i\,t^c = \frac{N_c}{2}i\,t^c \quad ,\end{aligned} \tag{5.4}$$

reveal two important considerations. The color factor of the (Abelian-like) term $\Gamma^{\rm A}_\sigma$ would be given by $t^a\,t^a=C_{\rm F}=(N_c^2-1)/2N_c$ for the strong dressing of the photon-quark vertex,

i.e., in the color singlet channel. The octet $\Gamma^{\rm A}_\sigma$ is of opposite sign and is suppressed by a factor $1/(N_c^2-1)$: single gluon exchange between a quark and antiquark has relatively weak repulsion in the color-octet channel, compared to strong attraction in the color-singlet channel. Net attraction for the gluon vertex (at least to this order) is provided by the non-Abelian $\Gamma^{\rm NA}_\sigma$ term, which involves the three-gluon vertex: the color factor is amplified by $-N_c^2$ over the $\Gamma^{\rm A}_\sigma$ term.

Figure 16: The quark-gluon vertex at one loop. The left diagram labelled A is the Abelian-like term $\Gamma^{\rm A}_\sigma$, and the right diagram labelled NA is the non-Abelian term $\Gamma^{\rm NA}_\sigma$.

The specific form of the bare triple-gluon vertex is conveniently expressed in terms of three momenta $p_1 = q+k$, $p_2 = -q$ and $p_3 = -k$, that are outgoing. Thus with $\Gamma^{3g}_{\mu\nu\sigma}(q+k,q) \equiv \tilde{\Gamma}^{3g}_{\mu\nu\sigma}(p_1,p_2,p_3)$, we have

$$\begin{aligned}\tilde{\Gamma}^{3g}_{\mu\nu\sigma}(p_1,p_2,p_3) &= -\big\{(p_1-p_2)_\sigma\,\delta_{\mu\nu} + (p_2-p_3)_\mu\,\delta_{\nu\sigma} \\ &\quad + (p_3-p_1)_\nu\,\delta_{\sigma\mu}\big\} \quad , \end{aligned} \tag{5.5}$$

and the complete vertex is symmetric under permutations of all gluon coordinates. In Landau gauge $\Gamma^{3g}_{\mu\nu\sigma}$ obeys the Slavnov-Taylor identity

$$k_\sigma\,\Gamma^{3g}_{\mu\nu\sigma}(q+k,q) = D_0^{-1}(q)\,T_{\mu\nu}(q) - D_0^{-1}(q+k)\,T_{\mu\nu}(q+k)\ . \tag{5.6}$$

Our nonperturbative model addresses the $k=0$ case and makes an extension of the bare result

$$\Gamma^{3g}_{\mu\nu\sigma}(q,q) = -\frac{\partial}{\partial q_\sigma} D_0^{-1}(q)\,T_{\mu\nu}(q) \quad , \tag{5.7}$$

which allows the amplitude for the non-Abelian diagram at $k = 0$ to take the form

$$\begin{aligned}\Gamma^{\rm NA}_\sigma(p,p) &= -i\,\frac{C_{\rm A}}{2}\int_q^\Lambda \gamma_\mu S_0(p-q)\gamma_\nu \\ &\quad\times\left\{\frac{\partial}{\partial q_\sigma}g^2\,D_0(q^2)\right\}T_{\mu\nu}(q) \quad . \end{aligned} \tag{5.8}$$

It is easy to verify that the Abelian diagram gives

$$\Gamma^{\rm A}_\sigma(p,p) = -i[1-\frac{C_{\rm A}}{2}\,C_{\rm F}^{-1}]\,\frac{\partial}{\partial p_\sigma}\Sigma^{(1)}(p) \quad , \tag{5.9}$$

in terms of the 1-loop self-energy.

The dressing provided by the combination $\Gamma^{\rm A}_\sigma + \Gamma^{\rm NA}_\sigma$ yields a vertex that satisfies the Slavnov-Taylor identity (STI) through $\mathcal{O}(g^2)$ [94]. This identity expresses the divergence of the vertex in terms of the bare and 1-loop contributions to three objects: $S(p)^{-1}$, the ghost propagator dressing function, and the ghost-quark scattering amplitude. The 1-loop $S(p)^{-1}$ part of this relation is generated partly from $\Gamma^{\rm A}_\sigma$ (with a weak repulsive color strength) and partly from $\Gamma^{\rm NA}_\sigma$ (with the complementary strongly attractive color strength). The $\Gamma^{\rm NA}_\sigma$ term also provides the explicitly non-Abelian terms of the $\mathcal{O}(g^2)$ STI.

5.2 *Nonperturbative vertex model*

Our nonperturbative model for the dressed quark-gluon vertex is defined by extentions of Eqs. (5.2) and (5.3) into dressed versions determined solely from an existing ladder-rainbow model DSE kernel. The bare quark propagators in Eqs. (5.2) and (5.3) are replaced by solutions of the quark DSE in rainbow truncation, namely,

$$\begin{aligned}S(p)^{-1} &= Z_2\,i\not{p} + Z_4\,m(\mu) \\ &\quad + C_{\rm F}\int_{p'}^\Lambda \frac{\mathcal{G}(q^2)}{q^2}\,T_{\mu\nu}(q)\,\gamma_\mu\,S(p')\,\gamma_\nu \ , \end{aligned} \tag{5.10}$$

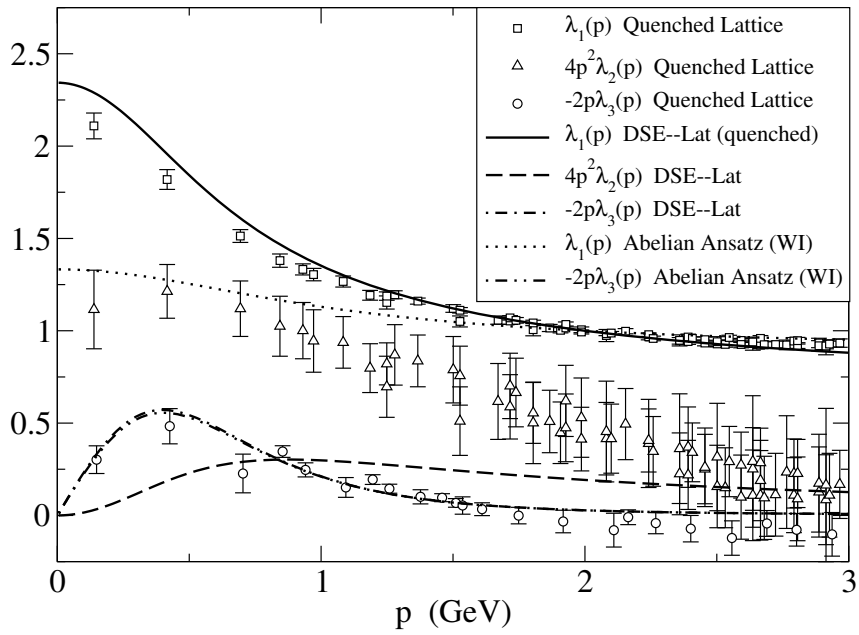

Figure 17: The amplitudes of the dressed quark-gluon vertex at zero gluon momentum and for quark current mass $m(\mu = 2 \text{ GeV}) = 60$ MeV. Quenched lattice data [37] is compared to the results of the DSE-Lat model [38]. The Abelian Ansatz (Ward identity) is also shown except for $\lambda_2(p)$ which is almost identical to the DSE-Lat model.

where $q = p - p'$. A particular ladder-rainbow kernel is specified by the effective quark-quark coupling $\mathcal{G}(q^2)$. Two different DSE models are employed and both have the ultraviolet behavior specified by QCD with 1-loop renormalization group improvement, i.e., the 1-loop renormalizations of the quark and gluon propagators and the pair of quark-gluon vertices have been absorbed so that $\mathcal{G}(q^2)$ matches $4\,\pi\,\alpha_s^{1-\text{loop}}(q^2) = 4\pi^2\gamma_m/\ln(q^2/\Lambda^2_{\text{QCD}})$ [29]. Here $\gamma_m = 12/(33 - 2N_f)$ is the anomalous mass dimension which arises in the leading logarithmic behavior of the quark mass function in the ultraviolet. The two DSE models differ in the infrared content of $\mathcal{G}(q^2)$ specified by parameterization.

The first model (DSE-Lat) [38] is defined by

$$\frac{\mathcal{G}(q^2)}{q^2} = D_{\text{lat}}(q^2)\Gamma_1(q^2, m(\mu)) \quad , \tag{5.11}$$

where $D_{\rm lat}(q^2)$ is a fit to quenched lattice data for the Landau gauge gluon propagator [21] that has the correct 1-loop logarithmic behavior $\sim \ln(q^2/\Lambda^2_{\rm QCD})^{-\frac{13}{22}}$ in the ultraviolet. In the infrared $D_{\rm lat}(q^2)$ is finite and is suppressed with respect to the bare propagator. The vertex factor $\gamma_\nu\,\Gamma_1(q^2, m(\mu))$ represents the remaining 1-loop renormalizations for ultraviolet matching to $4\,\pi\,\alpha_s^{1-\rm loop}(q^2)/q^2$ (with $N_f = 0$) and also contains a parameterized representation of the remaining infrared dressing. Explicit formulas are given in Ref. [38]. Parameters are determined by requiring that the DSE solutions reproduce the quenched lattice data [88] for $S(p)$ in the available domain $p^2 < 10$ GeV^2 and $m(\mu = 2\ {\rm GeV}) < 200$ MeV. In this sense, the DSE-Lat model represents quenched dynamics. It is found that the necessary vertex dressing is a strong but finite enhancement. The model easily reproduces m_π with a current mass that is within acceptible limits. However the resulting chiral condensate $\langle\bar{q}q\rangle^0_{\mu=1\ {\rm GeV}} = (0.19\ {\rm GeV})^3$ is a factor of 2 smaller than the value $(0.24 \pm 0.01\ {\rm GeV})^3$ from a best fit [113] of strong interaction observables [38]. This is attributed to the quenched approximation in the lattice data.

The second model (DSE-MT) [30] implements a one-parameter representation for the infrared sector of $\mathcal{G}(q^2)$ that is fit to the empirical chiral condensate. The explicit form is

$$\begin{aligned}\frac{\mathcal{G}(q^2)}{q^2} &= \frac{4\pi^2\,D\,q^2}{\omega^6}\,{\rm e}^{-q^2/\omega^2} \\ &+ \frac{4\pi^2\,\gamma_m\,\mathcal{F}(q^2)}{\frac{1}{2}\ln\left[\tau + \left(1 + q^2/\Lambda^2_{\rm QCD}\right)^2\right]}\,,\end{aligned} \tag{5.12}$$

Here the first term implements the infrared enhancement necessary to generate the empirical condensate, while the second term, with $\mathcal{F}(s) = (1 - \exp(\frac{-s}{4m_t^2}))/s$, connects smoothly with the 1-loop renormalization group behavior of QCD. Apart from the fixed values $m_t = 0.5\,{\rm GeV}$, $\tau = {\rm e}^2 - 1$, $N_f = 4$, and $\Lambda_{\rm QCD} = 0.234\,{\rm GeV}$, the free parameters, ω and D are not independent. The fitted observables are essentially constant along the trajectory $\omega D = (0.72\ {\rm GeV})^3$ for $\omega = 0.3 - 0.5$ GeV. A standard choice is $\omega = 0.4\,{\rm GeV}$ and $D = 0.93$

GeV^2. The model provides an excellent description of a wide variety of light quark meson physics including the masses and decay constants of the light-quark pseudoscalar and vector mesons [29, 30], the elastic charge form factors $F_\pi(Q^2)$ and $F_K(Q^2)$ [114], and the electroweak transition form factors of the pseudoscalars and vectors [115, 116]. In this sense it represents unquenched dynamics.

In the ultraviolet, the $\bar{q}q$ scattering kernel appearing in the Abelian-like vertex diagram shown in Fig. 16-A coincides with the ladder-rainbow kernel; thus the latter provides a suitable nonperturbative exension. We substitute $g^2\, D_0(q^2) \to \mathcal{G}(q^2)/q^2$ in the integrand for $\Gamma^{\rm A}_\sigma$, in Eq. (5.2). The vertex for the external gluon is taken to be bare.

Even in the ultraviolet, the $\bar{q}q$ scattering kernel does not appear explicitly in the non-Abelian vertex diagram shown in Fig. 16-NA. However at $k = 0$, the expression in Eq. (5.8) for $\Gamma^{\rm NA}_\sigma(p,p)$ has combined the triple gluon vertex and the gluon propagators to produce a form that emphasizes the close connection to the ladder kernel and the self-energy integral. The same nonperturbative extension $g^2\, D_0(q^2) \to \mathcal{G}(q^2)/q^2$ now suggests itself for Fig. 16-NA, and we use it. Justifications for this choice are consistency and simplicity; no new parameters are introduced.

5.3 *Results and discussion*

The general nonperturbative vertex at $k = 0$ has a representation in terms of three invariant amplitudes; here we choose

$$\Gamma_\sigma(p,p) = \gamma_\sigma \lambda_1(p^2) - 4p_\sigma\, \gamma\cdot p\, \lambda_2(p^2) - i2p_\sigma\, \lambda_3(p^2) \quad . \tag{5.13}$$

since the lattice-QCD data [37] is provided in terms of these $\lambda_i(p^2)$ amplitudes. A useful comparison is the corresponding vertex in an Abelian theory like QED; it is given by the Ward identity $\Gamma^{WI}_\sigma(p,p) = -i\partial S^{-1}(p)/\partial p_\sigma$ in terms of the exact propagator $S^{-1}(p)$. With $S^{-1}(p) = i\gamma\cdot p\, A(p^2) + B(p^2)$, this leads to the correspondance $\lambda_1^{\rm WI} = A$, $\lambda_2^{\rm WI} = -A'/2$,

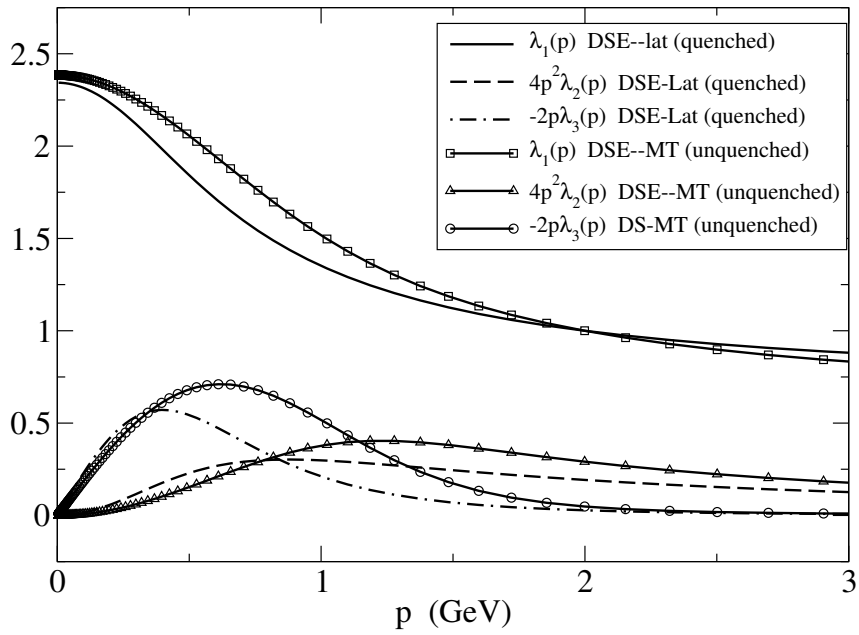

Figure 18: The amplitudes of the dressed quark-gluon vertex at zero gluon momentum, and for quark current mass $m(\mu = 2 \text{ GeV}) = 60$ MeV, from two models: DSE-Lat [38] and DSE-MT [30] that relate to quenched and unquenched content respectively.

and $\lambda_3^{\rm WI} = B'$, where $f' = \partial f(p^2)/\partial p^2$.

In Fig. 17 we display the DSE-Lat model results in a dimensionless form for comparison with the (quenched) lattice data[ii]. The renormalization scale of the lattice data is $\mu = 2$ GeV where $\lambda_1(\mu) = 1$, $A(\mu) = 1$. We compare to the lattice data set for which $m(\mu) = 60$ MeV. The same renormalization scale and conditions have been implemented for both DSE models[iii]. For λ_1 and λ_3 we also compare with the Abelian Ansatz in which the amplitudes are obtained from the quark propagator through the Ward Identity, which is equivalent to the $k = 0$ limit of either the Ball-Chiu [95] or Curtis-Pennington [5] Ansatz. Without parameter adjustment, the model reproduces the lattice data for λ_1 and λ_3 quite

[ii] We note that in Ref. [37] both the lattice data, and the Abelian (Ward identity) Ansatz, for $\lambda_3(p)$ are presented as positive. These two sign errors have been acknowledged [112].

[iii] To facilitate change of the scale μ, we have slightly modified both DSE kernels (both originally defined at fixed scale $\mu_0 = 19$ GeV) by including the additional kernel strength factor $Z_2^2(\mu^2, \Lambda^2)/Z_2^2(\mu_0^2, \Lambda^2)$ recommended by Maris [106]. This does not alter results for observables.

well over the whole momentum range for which data is available. The Abelian Ansatz, while clearly inadequate for λ_1 below 1.5 GeV, reproduces λ_3. The present lattice data for λ_2 has large errors; it suggests infrared strength that is seriously underestimated by the model. (The Abelian Ansatz for λ_2 is very close to the DSE model and for reasons of clarity, is not displayed.)

The relative contributions to the vertex dressing made by $\Gamma_\sigma^{\rm NA}$ and $\Gamma_\sigma^{\rm A}$ are indicated by the following amplitude ratios at $p = 0$: $\lambda_1^{\rm NA}/\lambda_1^{\rm A} = -60$, $\lambda_2^{\rm NA}/\lambda_2^{\rm A} = -14$, and $\lambda_3^{\rm NA}/\lambda_3^{\rm A} = -12$. Thus the non-Abelian term $\Gamma_\sigma^{\rm NA}$ dominates to a greater extent than what the ratio of color factors (-9) would suggest; it also distributes its infrared strength to favor λ_1 more so than does $\Gamma_\sigma^{\rm A}$. Since the momentum-dependent shapes of the $\lambda_i^{\rm NA}(p)$ and $\lambda_i^{\rm A}(p)$ are quite similar, the present model results could be summarized quite effectively by ignoring $\Gamma_\sigma^{\rm A}$ and scaling $\Gamma_\sigma^{\rm NA}$ up by about 10%.

Due to the definition of the two DSE models, their comparison in Fig. 18 provides an estimate of the effects of the quenched approximation. The effects are moderate within the present DSE model framework. Fig. 18 also suggests that a model including the four gluon vertex as well as the two diagrams of Fig. 16 should be considered, especially for amplitude λ_2. The question of the importance of the iterations of the diagrams of Fig. 16 also arises. We have estimated such effects by iteration to all orders based on the ladder-rainbow kernel. This amounts to solution of a ladder Bethe-Salpeter integral equation in which the inhomogeneity is our dressed extension of $Z_{1\rm F}\,\gamma_\sigma + \Gamma_\sigma^{\rm NA}(p,p)$ and the kernel term is the dressed extension of $\Gamma_\sigma^{\rm A}(p,p)$ with the internal γ_σ replaced by $\Gamma_\sigma(q,q)$. This generates very little change—significantly less than the quenching effect evident in Fig. 18. This is due to the small color factor of the kernel term. We have not explored the consequences of using the dressed vertex self-consistently for the internal quark-gluon vertices of $\Gamma_\sigma^{\rm NA}$ in Fig. 16-NA.

The nonperturbative Ansatz we have applied to Eq. (5.8) for the non-Abelian diagram, Fig. 16-NA, effectively includes dressing of the triple-gluon vertex $\Gamma^{3g}_{\mu\nu\sigma}$. Some perturbative studies of $\Gamma^{3g}_{\mu\nu\sigma}$ have been made at 1-loop [107, 108] but they provide no guidance for extension to infrared scales. The nonperturbative Ansätze for $\Gamma^{3g}_{\mu\nu\sigma}$ suggested in Refs. [3] and [109] for use within truncated gluon-ghost-quark DSEs require explicit models for the ghost dressing function and the ghost-gluon vertex that appear in the STI for $\Gamma^{3g}_{\mu\nu\sigma}$. Such considerations are beyond the scope of the present work; they would entail additional parameters that are not warranted at this stage.

A different approach to the nonperturbative extension of the non-Abelian diagram, Fig. 16-NA, has recently been explored in Refs. [110] and [111]. That approach employs a bare triple-gluon vertex and dressed gluon two-point functions resulting from previous solution of a truncation of the coupled ghost-gluon-quark DSEs [18]. (The quark-gluon vertex within that calculation was described by the Curtis-Pennington [5] Abelian Ansatz times the square of the infrared enhanced ghost dressing function.) The strong infrared suppression inherent in such gluon propagator solutions produces a very weak quark-gluon vertex unless the internal quark-gluon vertices of Fig. 16-NA are also enhanced. Refs. [110] and [111] proceed by assuming that attachment of a single ghost dressing function to each vertex is appropriate for this. The results are similar to the present work, except that the $m(\mu) = 115$ MeV case is considered [110, 111].

The infrared content of QCD 2-point and 3-point functions is not a settled subject and there is much to be gained from comparison of a variety of modeling strategies. Our approach to the vertex differs from Refs. [110] and [111] in the following respect. We exploit the similarity betwen Eq. (5.8) for $\Gamma^{\rm NA}_{\sigma}(p,p)$ and a zero momentum gluon insertion into the lowest order $\bar{q}q$ scattering kernel appearing in the rainbow diagram for the quark self-energy. Note that if the derivative in Eq. (5.8) were to act also on the transverse projector,

then result would be an Abelian-like derivative of the self-energy. The correction terms to this are evidently small for the resulting amplitudes λ_2 and λ_3 but they are large for λ_1. Since the renormalization group improved DSE-Lat kernel has infrared content that supplements quenched lattice data for the gluon 2-point function to get a precise fit to the quenched-lattice quark propagator mass-function, it is not surprizing that our result for λ_3 is a closer representation of the lattice data than the corresponding result from Refs. [110] and [111]. The latter works do not determine parameters by fitting the quark propagator.

Our approach induces effective dressing of the gluon propagators, internal quark vertices and the triple-gluon vertex in one quantity that is tightly constrained by quenched lattice data for 2-point functions. There is no well-defined and consistent way to separate the various contributions. If we assume this $\bar{q}q$ kernel can be used for each quark-gluon interaction in Fig. 16-NA then our Ansatz is equivalent to corresponding use of a dressed triple-gluon vertex $\Gamma^{3g}_{\mu\nu\sigma}$ satisfying Eqs. (5.6) and (5.7) with the substitution $D_0(q^2) \to [\mathcal{G}(q^2)/g^2(\mu^2)]/q^2$. If one were to replace this by the bare vertex, leaving other factors unchanged, then the final vertex amplitudes increase by at least an order of magnitude; the infrared dressing enhancements have been treated inconsistently. An opposite extreme, that is at least consistent, is to use the bare limit for all elements of Fig. 16-NA except for the quark propagator. That is, use $D_0(q^2) \to 1/q^2$ in Eq. (5.8). This underestimates the quark-gluon vertex amplitudes by an order of magnitude. In the absence of clear guidance for the infrared content of each of the 2-point and 3-point functions involved, the consistent use of an empirical ladder-rainbow kernel representation of the $\bar{q}q$ scattering amplitude recommends itself.

An issue of consistency that requires future attention is the following. Both lattice data and the present model calculation indicate that vertex amplitude λ_1 is infrared enhanced to

about 2.5 times the bare value. However the phenomenological vertex enhancement found in the DSE-Lat model (assumed to be concentrated solely in that single amplitude) is about 6 times this at a typical infrared point $p^2 \sim 0.04$ GeV^2 [117]. The proper distribution of vertex strength over the many amplitudes available at finite momenta may be part of resolution. On a more general note, it would be desirable to replace the phenomenological aspects of the dressing effects implicitly included for the internal quark-gluon vertices by the results of explicit model calculations.

Chapter 6

Summary and Conclusions

We studied quenched-QCD using a rainbow-ladder truncation of the Dyson-Schwinger equations (DSEs) and demonstrated that existing results from lattice simulations of quenched-QCD for the dressed-gluon and -quark Schwinger functions can be correlated via a gap equation that employs a renormalisation-group-improved model interaction. As usual, the ultraviolet behaviour of this effective interaction is fully determined by perturbative QCD.

For the infrared behaviour we employed an *Ansatz* whose parameters were fixed in a least squares fit of the gap equation's solutions to lattice data on the dressed-quark mass function, $M(p^2)$, at available current-quark masses. With our best-fit parameters the mass functions calculated from the gap equation were indistinguishable from the lattice results. The gap equation simultaneously yields the dressed-quark renormalisation function, $Z(p^2)$, and, without tuning, our results agreed with those obtained in the lattice simulations.

To correlate the lattice's dressed-gluon and -quark Schwinger functions it was necessary for the gap equation's kernel to exhibit infrared enhancement over and above that observed in the gluon function alone. We attributed that to an infrared enhancement of the dressed-quark-gluon vertex. The magnitude of the vertex modification necessary to achieve the correlation is semi-quantitatively consistent with that observed in quenched lattice-QCD estimates of this three-point function.

With a well-defined effective interaction, the gap equation provides a solution for the dressed-quark Schwinger function at arbitrarily small current-quark masses and, in

particular, in the chiral limit: no extrapolation is involved. A kernel that accurately describes dressed-quark lattice data at small current-quark masses may therefore be used as a tool with which to estimate the chiral limit behaviour of the lattice Schwinger function. Our view is that this method is a more reliable predictor than a linear extrapolation of lattice data to the chiral limit. Even failing to accept this perspective, the material difference between results obtained via the lattice-constrained gap equation and those found by linear extrapolation of the lattice data must be cause for concern in employing the latter.

In addition, from a well-defined gap equation it is straightforward to construct symmetry-preserving Bethe-Salpeter equations whose bound state solutions describe mesons. We illustrated this via the pion, and calculated its mass and decay constants in our DSE model of the quenched theory.

Quenched lattice-QCD data on the dressed-quark Schwinger function can be correlated with dressed-gluon data via a rainbow gap equation so long as that equation's kernel possesses enhancement at infrared momenta above that exhibited by the gluon alone. The required enhancement can be ascribed to a dressing of the quark-gluon vertex. The solutions of the rainbow gap equation exhibit dynamical chiral symmetry breaking and are consistent with confinement. The gap equation and related, symmetry-preserving ladder Bethe-Salpeter equation yield estimates for chiral and physical pion observables that suggest these quantities are materially underestimated in the quenched theory: $|\langle\bar{q}q\rangle|$ by a factor of two and f_π by 30%.

Assuming that existing lattice-QCD data are not afflicted by large systematic errors associated with finite volume or lattice spacing, we infer from our analysis that quenched QCD exhibits dynamical chiral symmetry breaking and dressed-quark two-point functions that violate reflection positivity but that chiral and physical pion observables are

significantly smaller in the quenched theory than in full QCD.

We have then explored the character of the dressed-quark-gluon vertex and its role in the gap and Bethe-Salpeter equations.We employed a simple model for the dressed-gluon interaction to build an *Ansatz* for the quark-gluon vertex. The model reduces coupled integral equations to algebraic equations and thus provides a useful intuitive tool. We used this framework to argue that data obtained in lattice simulations of quenched-QCD indicate the existence of net attraction in the colour-octet projection of the quark-antiquark scattering kernel.

We observed that the presence of such attraction can affect the uniformity of pointwise convergence to solutions of the gap and vertex equations. For example, in the timelike region, the vertex obtained by summing an odd number of loop corrections is pointwise markedly different from that obtained by summing an even number of loops. The two sub-series of vertices so defined follow a different pointwise path to the completely resummed vertex. This entails that the solutions of two gap equations that are defined via vertex truncations or vertex *Ansätze* which appear similar at spacelike momenta need not yield qualitatively equivalent results for the dressed-quark propagator. This is especially true in connection with the manifestation of confinement, for which the behaviour of Schwinger functions at timelike momenta is important.

Our study showed that the dependence of the dressed-quark-gluon vertex on the current-quark mass is weak until that mass becomes commensurate in magnitude with the theory's intrinsic mass-scale. For masses of this magnitude and above, all vertex dressing is suppressed and the dressed vertex is well approximated by the bare vertex.

It is critical feature of our study that the diagrammatic content of the model we proposed for the vertex is explicitly enumerable because this enables the systematic construction of quark-antiquark and quark-quark scattering kernels that ensure the preservation of

all Ward-Takahashi identities associated with strong interaction observables. This guaranteed, in particular, that independent of the number of loop corrections incorporated in the dressed-quark-gluon vertex, and thereby in the gap equation, the pion was automatically realised as a Goldstone mode in the chiral limit. Such a result is impossible if one merely guesses a form for the vertex, no matter how sound the motivation. As a consequence we could reliably explore the impact on the meson spectrum of attraction in the colour-octet projection of the quark-antiquark scattering kernel. In accordance with intuition, the mass of a meson decreases with increasing attraction between the constituents.

We found that the fidelity of an approximate solution for a meson's mass increases with the number of loops retained in building the vertex. However, a given consistent truncation need not yield a solution. This fact is tied to a difference between the convergence paths followed by the odd-loop vertex series and the even-loop series. In addition, we observed that with increasing current-quark mass the rainbow-ladder truncation provides an ever more reliable estimate of the exact vector meson mass; i.e., the mass obtained using the completely resummed vertex and the completely consistent Bethe-Salpeter equation. For pseudoscalar mesons, this is even more true because the rainbow-ladder and exact results are forced by the Ward-Takahashi identity to agree in the chiral limit. This is practically useful because it means that the parameters of a model meant to be employed in rainbow-ladder truncation may reliably be fixed by fitting to the values of pseudoscalar meson quantities calculated in the neighbourhood of the chiral limit. Moreover, both in rainbow-ladder truncation and with the complete vertex and kernel, the splitting between pseudoscalar and vector meson masses vanishes as the current-quark mass increases. In our complete model calculation this splitting is 130 MeV at the c-quark mass and only 40 MeV at the b-quark mass, a pattern which suggests that the pseudoscalar partner of the $\Upsilon(1S)$ cannot have a mass as low as that currently ascribed to the $\eta_b(1S)$.

Finally, we have studied the dressed-quark-gluon vertex via the successful rainbow-DSE model developed to analyse the lattice-QCD data for the mass function of the quark propagator in chapter 3. We use the information provided by pQCD to obtain an *Ansatz* for a 1-loop non-perturbative Feynman diagram representation of the vertex. There are two such diagrams, an Abelian one and a non-Abelian one. The color factor of the non-Abelian diagram indicates a clear domination over the Abelian diagram, which is found to be the case on evaluating these diagrams. It is also found that the non-Abelian contribution for λ_1 is about 6 times more than that suggested by the color factor and greater than a factor of 1 for the other 2 amplitudes.

Comparison with quenched lattice-data, without any parameter readjustment, indicates excellent results for λ_1 and λ_3, but significant differences for λ_2, which appears to diverge in the lattice calculations as the momentum $\rightarrow 0$. Lattice data for λ_2 is difficult to extract as it mixes with λ_1 and so has large error bars. We believe that better lattice data is required before reaching final conclusions about our comparison for λ_2.

It is also found that the effects of quenching, after comparing these quenched results with those of the phenomenlogically successful unquenched Maris-Tandy model are moderate.

References

[1] C. D. Roberts and A. G. Williams, Prog. Part. Nucl. Phys. **33**, 477 (1994).

[2] C. D. Roberts and S. M. Schmidt, Prog. Part. Nucl. Phys. **45**, S1 (2000).

[3] R. Alkofer and L. von Smekal, Phys. Rept. **353**, 281 (2001).

[4] P. Maris and C. D. Roberts, Int. J. Mod. Phys. **E12**, 297 (2003), `nucl-th/0301049`.

[5] D.C.Curtis and M.R.Pennington, Phys. Rev. D **42**, 4165 (1990).

[6] A.Bashir and M.R.Pennington, Phys. Rev. D **53**, 4694 (1996).

[7] J.C.R.Bloch, Few Body Syst. **33**, 111 (2003).

[8] C.J.Burden and C.D.Roberts, Phys. Rev. D **44**, 540 (1991).

[9] Z.-h.Dong, H.J.Munczek, and C.D.Roberts, Phys. Lett. B **333**, 536 (1994).

[10] F. T. Hawes, C. D. Roberts, and A. G. Williams, Phys. Rev. D **49**, 4683 (1994).

[11] F. T. Hawes, P. Maris, and C. D. Roberts, Phys. Lett. **B440**, 353 (1998).

[12] J. Papavassiliou and J. M. Cornwall, Phys. Rev. D **44**, 1285 (1991).

[13] D.Atkinson and P.W.Johnson, Phys. Rev. D **41**, 1661 (1990).

[14] A.G.Williams, G.Krein, and C.D.Roberts, Annals Phys. **210**, 464 (1991).

[15] F.T.Hawes and A.G.Williams, Phys. Lett. B **268**, 271 (1991).

[16] H.J.Munczek, Phys. Lett. B **175**, 215 (1986).

[17] C.J.Burden, C.D.Roberts, and A.G.Williams, Phys. Lett. B **285**, 347 (1992).

[18] C. S. Fischer and R. Alkofer, Phys. Rev. **D67**, 094020 (2003), `hep-ph/0301094`.

[19] M. S. Bhagwat, A. Holl, A. Krassnigg, C. D. Roberts, and P. C. Tandy Phys. Rev. C **70**, 035205 (2004).

[20] P. Watson, W. Cassing, and P. C. Tandy Few Body Syst. **35**, 129 (2004).

[21] D. B. Leinweber, J. I. Skullerud, A. G. Williams, and C. Parrinello (UKQCD), Phys. Rev. D **60**, 094507 (1999).

[22] C. Alexandrou, P. De Forcrand, and E. Follana, Phys. Rev. D **65**, 117502 (2002), `and references therein`.

[23] P. O. Bowman, U. M. Heller, D. B. Leinweber, and A. G. Williams, Phys. Rev. D **66**, 074505 (2002a), and references therein.

[24] J. C. R. Bloch, A. Cucchieri, K. Langfeld, and T. Mendes (2002), ‘‘Running coupling constant and propagators in SU(2) Landau gauge,’’ hep-lat/0209040.

[25] P. O. Bowman, U. M. Heller, and A. G. Williams, Phys. Rev. D **66**, 014505 (2002b).

[26] P. O. Bowman, U. M. Heller, D. B. Leinweber, and A. G. Williams (2002c), ‘‘Modelling the quark propagator,’’ hep-lat/0209129.

[27] L. von Smekal, A.Hauck, and R.Alkofer, Annals Phys. **267**, 1 (1998), [Erratum-ibid. **269**, 182 (1998)].

[28] D. Atkinson and J. C. R. Bloch, Mod. Phys. Lett. **A13**, 1055 (1998).

[29] P. Maris and C. D. Roberts, Phys. Rev. C **56**, 3369 (1997), nucl-th/9708029.

[30] P. Maris and P. C. Tandy, Phys. Rev. C **60**, 055214 (1999), nucl-th/9905056.

[31] P. C. Tandy Prog. Part. Nucl. Phys. **50**, 305 (2003).

[32] D. Zwanziger (2003), Phys. Rev. D **69**, 016002 (2004). hep-ph/0303028.

[33] J. C. R. Bloch, Phys. Rev. D **66**, 034032 (2002).

[34] P. Maris, A. Raya, C. D. Roberts, and S. M. Schmidt Eur. Phys. J. A **18**, 231 (2003), nucl-th/0208071.

[35] J. Skullerud and A. Kızılersü, JHEP **09**, 013 (2002).

[36] J. Skullerud, P. Bowman, and A. Kızılersü (2002), ‘‘The nonperturbative quark gluon vertex,’’ hep-lat/0212011.

[37] J. I. Skullerud, P. O. Bowman, A. Kızılersü, D. B. Leinweber, and A. G. Williams, JHEP **04**, 047 (2003), hep-ph/0303176.

[38] M.S.Bhagwat, M.A.Pichowsky, C.D.Roberts, and P.C.Tandy, Phys. Rev. C **68**, 015203 (2003).

[39] R.Alkofer, W.Detmold, C.S.Fischer, and P.Maris, Nucl. Phys. Proc. Suppl. **141**, 122 (2005),hep-ph/0309077.

[40] A. Bender, C. D. Roberts, and L. Von Smekal, Phys. Lett. **B380**, 7 (1996a).

[41] A. Bender, W. Detmold, C. D. Roberts, and A. W. Thomas, Phys. Rev. C **65**, 065203 (2002).

[42] H. J. Munczek and A. M. Nemirovsky, Phys. Rev. D **28**, 181 (1983), and references therein and thereto.

[43] P. Maris, C. D. Roberts, and P. C. Tandy, Phys. Lett. **B420**, 267 (1998).

[44] M. A. Ivanov, Y. L. Kalinovsky, and C. D. Roberts, Phys. Rev. D **60**, 034018 (1999).

[45] S. R. Cotanch and P. Maris, Phys. Rev. D **66**, 116010 (2002).

[46] P.Bicudo, S.Cotanch, F.Llanes-Estrada, P.Maris, E.Ribeiro, and A.Szczepaniak, Phys. Rev. D **65**, 076008 (2002); P.Bicudo, Phys. Rev. C **67**, 035201,(2003).

[47] A.Krassnigg and C.D.Roberts,Nucl. Phys. A **737**, 7 (2004), nucl-th/0308039.

[48] C. Itzykson and J. Zuber (1986), *Quantum Field Theory* (McGraw-Hill).

[49] R. J. Rivers (1987), *Path Integral Methods in Quantum Field Theory* (Cambridge University Press).

[50] K. Huang (1998), *Quantum Field Theory* (Wiley interscience).

[51] J. J. Sakurai (1967), *Advanced Quantum Mechanics* (Addison-Wesley).

[52] M. E. Peskin and D. V. Schroeder (1995), *An Introduction to Quantum Field Theory* (Perseus Books).

[53] P. Pascual and R Tarrach, (1984), *QCD:Renormalisation for the practitioner* (Springer-Verlag).

[54] D.Atkinson and P.W.Johnson, Phys. Rev. D **37**, 2296 (1988).

[55] F. T. Hawes, private communication.

[56] K. D. Lane, Phys. Rev. D **10**, 2605 (1974).

[57] H. D. Politzer, Nucl. Phys. **B117**, 397 (1976).

[58] K. Johnson, M. Baker, and R. Willey, Phys. Rev. **136**, B1111 (1964).

[59] S. Capstick et al. (2000), ''Key issues in hadronic physics,'' hep-ph/0012238.

[60] A. X. El-Khadra, G. Hockney, A. S. Kronfeld, and P. B. Mackenzie, Phys. Rev. Lett. **69**, 729 (1992).

[61] S. Aoki et al., Phys. Rev. Lett. **74**, 22 (1995).

[62] J. Glimm and A. Jaffee (1981), *Quantum Physics. A Functional Point of View* (Springer-Verlag, New York).

[63] K. Osterwalder and R. Schrader, Commun. Math. Phys. **31**, 83 (1973).

[64] K. Osterwalder and R. Schrader, Commun. Math. Phys. **42**, 281 (1975).

[65] J. M. Cornwall, Phys. Rev. D **22**, 1452 (1980), and references therein and thereto.

[66] G. Krein, C. D. Roberts, and A. G. Williams, Int. J. Mod. Phys. **A7**, 5607 (1992).

[67] U. Habel, R. Konning, H. G. Reusch, M. Stingl, and S. Wigard, Z. Phys. **A336**, 435 (1990).

[68] M. Stingl, Z. Phys. **A353**, 423 (1996).

[69] A. Bender, D. Blaschke, Y. Kalinovsky, and C. D. Roberts, Phys. Rev. Lett. **77**, 3724 (1996b).

[70] A. Bender, G. I. Poulis, C. D. Roberts, S. M. Schmidt, and A. W. Thomas, Phys. Lett. **B431**, 263 (1998).

[71] A. Bender and R. Alkofer, Phys. Rev. D **53**, 446 (1996).

[72] P. Maris, Phys. Rev. D **52**, 6087 (1995).

[73] D. Gomez Dumm and N. N. Scoccola, Phys. Rev. D **65**, 074021 (2002).

[74] V. Sauli, JHEP **02**, 001 (2003).

[75] M. Bhagwat, M. A. Pichowsky, and P. C. Tandy, Phys. Rev. D **67**, 054019 (2003).

[76] D. B. Leinweber, Annals Phys. **254**, 328 (1997).

[77] P. Bicudo, Phys. Rev. C **67**, 035201 (2003).

[78] P. Maris (2003), `private communication`.

[79] C. H. Llewellyn-Smith, Ann. Phys. **53**, 521 (1969).

[80] M.B.Hecht, M.Oettel, C.D.Roberts, S.M.Schmidt, P.C.Tandy, and A.W.Thomas, Phys. Rev. C **65**, 055204 (2002).

[81] D.Morel and S.Capstick, nucl-th/0204014.

[82] E.J.Hackett-Jones, D.B.Leinweber, and A.W.Thomas, Phys. Lett. B **489**, 143 (2000a).

[83] E.J.Hackett-Jones, D.B.Leinweber, and A.W.Thomas, Phys. Lett. B **494**, 89 (2000b).

[84] K.Langfeld, H.Markum, R.Pullirsch, C.D.Roberts, and S.M.Schmidt, Phys. Rev. C **67**, 065206 (2003).

[85] D.Atkinson and J.C.R.Bloch, Phys. Rev. D **58**, 094036 (1998);

[86] K.I.Kondo, hep-th/0303251.

[87] D.B.Leinweber, J.I.Skullerud, A.G.Williams, and C. U. Collaboration], Phys. Rev. D **60**, 094507 (1999), [Erratum-ibid. D **61**, 079901 (2000)].

[88] P.O.Bowman, U.M.Heller, D.B.Leinweber, and A.G.Williams, Nucl. Phys. Proc. Suppl. **119**, 323, `hep-lat/0209129`.

[89] W.J.Marciano and H.Pagels, Phys. Rept. **36**, 137 (1978).

[90] C.D.Roberts, Nucl. Phys. A **605**, 475 (1996).

[91] P.Maris and P.C.Tandy, Phys. Rev. C **62**, 055204 (2000a).

[92] P.Maris and P.C.Tandy, Phys. Rev. C **61**, 045202 (2000b).

[93] P.Maris and P.C.Tandy, Phys. Rev. C **65**, 045211 (2002).

[94] A.I.Davydychev, P.Osland, and L.Saks, Phys. Rev. D **63**, 014022 (2001).

[95] J.S.Ball and T.W.Chiu, Phys. Rev. D **22**, 2542 (1980).

[96] H.J.Munczek, Phys. Rev. D **52**, 4736 (1995).

[97] L. Smekal, A.Mecke, and R.Alkofer, hep-ph/9707210.

[98] A.Scarpettini, D. Dumm, and N.N.Scoccola, Phys. Rev. D **69**, 114018 (2004). hep-ph/0311030.

[99] D.Kekez and D.Klabučar, Phys. Rev. D **65**, 057901 (2002).

[100] K. et al., Phys. Rev. D **66**, 010001 (2002).

[101] P.Maris, in *Quark Confinement and the Hadron Spectrum IV*, edited by W.Lucha and K. Maung (World Scientific, Singapore, 2002).

[102] P.C.Tandy, Prog. Part. Nucl. Phys. **50**, 305.

[103] C.D.Roberts, Nucl. Phys. Proc. Suppl. **108**, 227 (2002).

[104] K.C.Bowler *et al.* [UKQCD Collaboration], Phys. Rev. D **62**, 054506 (2000).

[105] F.J.Llanes-Estrada, S.R.Cotanch, A.P.Szczepaniak, and E.S.Swanson,Phys. Rev. C **70**, 035202 (2004), hep-ph/0402253.

[106] P. Maris (2004), private communication.

[107] A. I. Davydychev, P. Osland, and O. V. Tarasov, Phys. Rev. **D54**, 4087 (1996), `hep-ph/9605348`.

[108] A. I. Davydychev, P. Osland, and L. Saks, JHEP **08**, 050 (2001b), `hep-ph/0105072`.

[109] C. S. Fischer, R. Alkofer, and H. Reinhardt, Phys. Rev. **D65**, 094008 (2002), `hep-ph/0202195`.

[110] C. S. Fischer, F. Llanes-Estrada, and R. Alkofer, Nucl. Phys. Proc. Suppl. **141**, 128 (2005), `hep-ph/0407294`.

[111] F. J. Llanes-Estrada, C. S. Fischer, and R. Alkofer (2004), `hep-ph/0407332`.

[112] J.-I. Skullerud, P. O. Bowman, A. Kızılersü, D. B. Leinweber, and A. G. Williams Nucl. Phys. Proc. Suppl. **141**, 244, (2005), `hep-lat/0408032`.

[113] D. B. Leinweber, Annals Phys. **254**, 328 (1997), nucl-th/9510051.

[114] P. Maris and P. C. Tandy, Phys. Rev. **C62**, 055204 (2000), nucl-th/0005015.

[115] P. Maris and P. C. Tandy, Phys. Rev. **C65**, 045211 (2002), nucl-th/0201017.

[116] C.-R. Ji and P. Maris, Phys. Rev. **D64**, 014032 (2001), nucl-th/0102057.

[117] P. C. Tandy Nucl. Phys. Proc. Suppl. **141**, 9, nucl-th/0408037.